UNIVERSITY OF CALIFORNIA SAN DIEGO

Defining the Cellular Consequences of Loss of the Cohesin Complex Subunit STAG2 in Cancer Cells

A dissertation submitted in partial satisfaction of the requirements for the degree Doctor of Philosophy

in

Biomedical Sciences

by

Amelia Katherine Richardson

Committee in charge:

Professor Arshad Desai, Chair
Professor Seth Field
Professor Richard Kolodner
Professor Karen Oegema
Professor Bing Ren

2018

The Dissertation of Amelia Katherine Richardson is approved, and it is acceptable in quality and form for publication on microfilm and electronically:

_____

_____

_____

_____

_____

Chair

University of California San Diego

2018

DEDICATION

To my grandma Robin, for every

encouraging phone call and visit.

TABLE OF CONTENTS

LIST OF FIGURES

LIST OF TABLES

ACKNOWLEDGEMENTS

I would like to acknowledge the many people who have helped me throughout my graduate experience. This project is the culmination of that collaborative process. In particular, I am thankful for the support I received from my mentor, Arshad Desai. Arshad has patiently and expertly guided me through the (sometimes grueling, sometimes confusing) research process, and has helped me to more effectively think over and communicate my scientific findings. He has likewise encouraged my pursuit of science education opportunities, for which I am incredibly grateful. Karen Oegema has also provided enthusiastic feedback and spot-on guidance that have invaluably shaped my dissertation research. It has been a privilege to learn from them both.

I am also indebted to the past and present members of the Oegema-Desai labs. They have generously offered their time, expertise, wisdom, presentation feedback, manuscript comments, encouragement, and reassurance. I couldn't have done this without them.

I would also like to thank the members of the Small-Molecule Discovery group for their training, mentorship, and support. Likewise, I have been fortunate enough to participate in collaborations with members of Bing Ren's and Angelika Amon's labs, and I am grateful for what I have learned through those experiences. To Mark Tomishima and Jeffery Barrow – thank you for believing in me.

I would also like to acknowledge the extended support I have received from my thesis committee: Seth Field, Richard Kolodner, and Bing Ren. I am grateful to my committee members for their expert advice and for pushing me to continually improve as a scientist throughout my graduate experience.

Finally, I could not have done this without the support of my family and my partner, Belinda. STAG2 has been a tough nut to crack, but they have been there for me through it all.

Chapter 2, in part, is currently being prepared for submission for publication. Richardson A, Fang R, Lara-Gonzalez P, Ren B, Oegema K, Desai A. The dissertation author is the primary investigator and author of this material.

Chapter 3, in part, was published under the following citation: Santaguida S, Richardson A, Iyer DR, M'Saad O, Zasadil L, Knouse KA, Wong YL, Rhind N, Desai A, Amon A. Chromosome Mis-segregation Generates Cell-Cycle-Arrested Cells with Complex Karyotypes that Are Eliminated by the Immune System. *Dev Cell*. 2017;41(6):638-651. The dissertation author was one of the primary investigators and the second author of this material.

VITA

2008 BS, Molecular Biology, Brigham Young University

2018 PhD, Biomedical Sciences, University of California San Diego

PUBLICATIONS

Hattersley N, Cheerambathur D, Moyle M, Stefanutti M, **Richardson A**, Lee KY, Dumont J, Oegema K, Desai A. A Nucleoporin Docks Protein Phosphatase 1 to Direct Meiotic Chromosome Segregation and Nuclear Assembly. *Dev Cell*. 2016;38(5):463-477.

Meitinger F, Anzola JV, Kaulich M, **Richardson A**, Stender JD, Benner C, Glass CK, Dowdy SF, Desai A, Shiau AK, Oegema K. 53BP1 and USP28 Mediate p53 Activation and G1 Arrest After Centrosome Loss or Extended Mitotic Duration. *J Cell Biol*. 2016;214(2):155-166.

Santaguida S, **Richardson A**, Iyer DR, M'Saad O, Zasadil L, Knouse KA, Wong YL, Rhind N, Desai A, Amon A. Chromosome Mis-segregation Generates Cell-Cycle-Arrested Cells with Complex Karyotypes that Are Eliminated by the Immune System. *Dev Cell*. 2017;41(6):638-651.

ABSTRACT OF THE DISSERTATION

Defining the Cellular Consequences of Loss of the
Cohesin Complex Subunit STAG2 in Cancer Cells

by

Amelia Katherine Richardson

Doctor of Philosophy in Biomedical Sciences

University of California San Diego, 2018

Professor Arshad Desai, Chair

Inactivating mutations in the cohesin subunit *STAG2* are frequent in many cancers, but the consequences of these mutations have not been clearly defined. STAG2 loss may impair sister chromatid cohesion, but it is not clear if it also increases aneuploidy as initially proposed. Alternatively, STAG2 loss may contribute to cancer through defective DNA repair and genomic instability or

through aberrant transcription, which could dysregulate cancer-regulating genes. The primary goal of this project is to thoroughly define the effects of STAG2 loss on cohesin's cellular functions to better understand why STAG2 is frequently lost in cancers.

To address this goal, I developed a quantitative assay to measure cohesion strength in live cells. Cohesion fatigue timing indicated cohesion strength after STAG1 or STAG2 perturbation. I also measured the effect of STAG1 and STAG2 perturbation on inter-kinetochore stretch and anaphase defects, both indicators of cohesion strength. Surprisingly, collective results suggested that STAG1 and STAG2 are functionally redundant for cohesion strength in immortalized hTERT RPE-1 cells, and that STAG2 loss does not impair cohesion in glioblastoma H4 or colorectal cancer HCT116 cells as previously reported.

I then quantified the effect of STAG2 depletion on DNA repair of localized DSBs using a reporter assay for HR and NHEJ and found that STAG2 depletion does not alter HR or NHEJ frequency in U-2 OS cells. Loss of STAG2 also does not severely sensitize H4 (or hTERT RPE-1 and HCT116) cells to PARP inhibition as previously reported.

Finally, I assessed the effect of STAG1 and STAG2 perturbation on gene expression by RNA-seq in hTERT RPE-1 cells and Ewing sarcoma A673 cells. There, I found the exiting result that STAG1 depletion and STAG2 depletion have differential effects on gene expression in Ewing sarcoma cells, but not in other

tested cell lines. These preliminary results suggest a unique potential role for STAG2 loss in the aberrant gene expression that drives Ewing sarcoma.

A secondary, collaborative goal of this project was to clarify the immediate cellular consequences of aneuploidy. I confirmed, through live imaging of mis-segregating chromatin, that a mitotic timer, and not mis-segregation, is responsible for subsequent cell-cycle arrest.

CHAPTER 1: INTRODUCTION

Inactivating mutations of the cohesin complex subunit Stromal AntiGen 2 (*STAG2*) are frequent in a large subset of cancers, but the consequences of these mutations are not yet clearly defined. STAG2 is known to be essential during development, where it plays a role in cohesin's cellular functions of sister chromatid cohesion, DNA repair, and transcriptional regulation. When I first began the research discussed in this dissertation, STAG2 loss in cancer was proposed to regulate sister chromatid cohesion. Landmark papers from the Heiter and Waldman labs linked cohesin mutations, and then STAG2 loss specifically, to impaired sister chromatid cohesion and subsequent aneuploidy (Barber et al., 2008; Solomon et al., 2011). These and other papers proposed that STAG2 loss led to chromosomal instability (CIN) via impaired cohesion in colorectal, glioblastoma, and Ewing sarcoma tumor samples (Barber et al., 2008; Solomon et al., 2011), and in colorectal, melanoma, Ewing sarcoma, glioblastoma, and bladder cancer cell lines (Barber et al., 2008; Solomon et al., 2011; Solomon et al., 2013; Li et al., 2015). Thus, STAG2 loss and subsequent impaired cohesion was thought to answer a long-standing question of how CIN is generated in cancers.

However, other work in bladder cancer (Balbás-Martínez et al., 2013; Taylor et al., 2014) and acute myeloid leukemia (AML; Welch et al., 2012) failed to find correlations between STAG2 loss and CIN. Additionally, in a follow-up study, the Waldman lab found that while nine tumor-derived *STAG2* null

mutations in colorectal cancer cells impaired cohesion, only a subset of these mutations induced aneuploidy, and only one induced CIN (Kim et al., 2016). These findings suggested that STAG2 loss may not contribute to cancer through impaired sister chromatid cohesion and aneuploidy, at least not in all cases or in all cancers.

Instead, researchers proposed a role for STAG2 in DNA repair. Depletion of cohesin subunits, including STAG2, was shown to sensitize human cells to poly(ADP-ribose) polymerase (PARP) inhibition (McLellan et al., 2012; Bailey et al., 2014), suggesting a role for STAG2 in DNA repair, possibly through replication fork stability. A role was also proposed for STAG2 in maintaining the balance of double-strand break (DSB) repair in favor of homologous recombination (HR) over the less accurate non-homologous end joining (NHEJ) in HeLa cells (Kong et al., 2014). However, *STAG2* mutations have yet to be directly linked to an accumulation of DNA mutations in cancer. Importantly, while *STAG2* is mutated in some cancers high mutational burdens, such as melanoma, bladder and colorectal cancers, *STAG2* is also mutated in cancers with low rates of mutation, such as AML and Ewing sarcoma (Grove and Vassiliou, 2014; Crompton et al., 2014). These results suggest that if *STAG2* mutations contribute to the generation of cancer through defective DNA repair, they may only do so in a subset of cancers. Instead, at least for cancers like AML and Ewing sarcoma, STAG2 loss may contribute to cancer progression through aberrant

transcriptional regulation (Corces-Zimmerman et al., 2014; Mullenders et al., 2015).

Despite a ten-year accumulation of research linking cohesin mutations and cancer, the consequences of STAG2 loss are still not clearly defined. This dissertation aims, through a careful characterization of the effect of STAG2 loss on cohesin's cellular functions, to discover the role(s) of STAG2 loss in cancer.

To this end, in this chapter, I give a general introduction to the cohesin complex and its cellular functions. I also give a general introduction to cancer and its characteristic hallmarks, including aneuploidy. Finally, I expand on published observations that link cohesin mutations to cancer. In the next chapter, I describe the thorough characterization of the cellular consequences of STAG2 loss, including the finding that STAG2 loss has a differential effect on gene expression compared to STAG1 loss in Ewing sarcoma cells. The third chapter focuses on the immediate cellular consequences of aneuploidy, one of the hallmarks of cancer. In the last chapter, my major conclusions are summarized, and the implications for my findings and future directions are discussed.

1.1 Cohesin Complex

Cohesin is a conserved, ring-shaped protein complex comprised of four subunits. Cohesin's tripartite ring is formed by Structural Maintenance of Chromosomes 1 (SMC1), SMC3, and Sister Chromatid Cohesion 1 (SCC1; Michaelis et al., 1997). SMC1 and SMC3 are long, flexible coiled coil containing proteins that dimerize to form cohesin's hinge domain. SCC1 is a kleisin that

completes the tripartite ring by bridging the ATPase domains of SMC1 and SMC3 (Gligoris et al., 2014). A fourth subunit, SCC3, binds directly to SCC1 (Zhang et al., 2013; Fig. 1.1). All four cohesin subunits are required for viability. In mammals, several cohesin subunits are duplicated and are thought to have evolved specialized roles. Meiotic cohesin can also include SMC1B, the kleisins REC8 meiotic recombination protein or RAD21-like protein (RAD21L), and the SCC3 derivative STAG3 (Pezzi et al., 2000; Revenkova et al., 2001; Xu et al., 2005; Ishiguro et al., 2011). Mitotic human cohesin include SMC1A, SMC3, RAD21, and either STAG1 or STAG2. Importantly, the specialized roles of mitotic paralogs STAG1 and STAG2 are not yet well understood. Subsequent sections of this chapter will highlight our current limited understanding of the differential roles for STAG1 and STAG2 in human mitotic cohesin's cellular functions.

1.2 Cohesin Cellular Functions

1.2.1 Sister Chromatid Cohesion

The ring-shaped cohesin complex achieves sister chromatid cohesion by encircling and tethering replicated DNA from S phase to anaphase. Cohesin is essential for cell viability, in part because of its essential role in promoting sister chromatid cohesion, which is required for accurate chromosome segregation. Cohesin promotes proper chromosome segregation in two ways. First, cohesin tethers sister chromatids from the moment they are replicated in S phase, which allows cells to track sister chromatid pairs throughout the cell cycle and to accurately allocate exactly one copy of each chromosome to both daughter cells.

Secondly, cohesin actively resists the outward pulling forces of the spindle during mitosis. This gives cells time to bi-orient their chromosomes, which again allows cells to accurately segregate exactly one copy of each chromosome to both daughter cells (Reviewed in Morales and Losada, 2018).

Cohesin is a dynamic protein complex that undergoes a series of precisely coordinated structural changes throughout the cell cycle. To begin, cohesin is loaded onto DNA in G1 or early S phase, prior to DNA replication. Before DNA replication, the cohesin ring is able to open and close, possibly to make way for replication machinery and to allow cohesin to entrap a second replicated DNA molecule at replication. The exact mechanism by which cohesin encircles replicated DNA is somewhat controversial. Proposed models include a monomeric ring, in which a single cohesin encircles two DNA strands, a bracelet, where multiple open cohesins link to entrap two DNA strands, or dimeric rings, where pairs of linked cohesin molecules each entrap a single DNA molecule (Huang et al., 2005; Zhang et al., 2008b; Nasmyth, 2011; Eng et al., 2015). Cohesin locks and becomes cohesive in a replication-dependent manner, enabling it to tether sister chromatids (Skibbens et al., 1999; Tóth et al., 1999). At prophase, some cohesin removed, primarily from chromatid arms. This process, called the prophase removal pathway, is thought to prepare chromosomes for a more timely and synchronized separation of sister chromatids' remaining centromere cohesin at anaphase. It is important to note that unlike later cohesin removal at anaphase, cohesin removal at prophase is

reversible. Also, intact cohesin that was removed at prophase may be reloaded quickly after mitotic exit after deacetylation of SMC3 by the Histone DeACetylase 8 (HDAC8; Deardorff et al., 2012). Finally, after chromosomes are properly aligned at metaphase and the Spindle Assembly Checkpoint (SAC) is satisfied, cohesin is irreversibly cleaved, and sister chromatids are free to segregate to opposite daughter cells at anaphase.

These four key stages of cohesion regulation are achieved by post-translational protein modifications of the cohesin complex and its related regulatory proteins. In the first stage, cohesin is loaded onto DNA after mitotic exit by the heterodimer of Nipped-B homolog and MAU2 sister chromatid cohesion factor (NIPBL-MAU2; SCC2-SCC4 in budding yeast), which promotes ATP hydrolysis of the ATPase domains on SMC1 and SMC3 (Ciosk et al., 2000; Arumugam et al., 2003; Weitzer et al., 2003). At this point, before DNA replication, cohesin is not locked onto DNA. Instead it is constantly removed by the cohesin regulators Wings apart-like homolog (WAPL) and Regulator of cohesion maintenance homolog (PDS5), through their interaction with RAD21 and STAG1/2, and then re-loaded by NIPBL-MAU2 (Shintomi and Hirano, 2013; Ouyang et al., 2016). Single strands of DNA are thought to enter and exit the cohesin ring through the open SMC3-RAD21 interface (Gligoris et al., 2014; Huis in't Veld et al., 2014), but it has also been proposed that DNA may be loaded through the open SMC1-SMC3 hinge (Gruber et al., 2006).

In the second stage, cohesin is stabilized on DNA and becomes cohesive.

This process requires DNA replication, acetylation of SMC3 by Establishment of Sister Chromatid Cohesion N-Acetyltransferase 1 (ESCO1) and ESCO2 (ECO1 in budding yeast), and cohesin interaction with the cohesin-regulators Sororin Cell division cycle associated 5 (CDCA5) and PDS5 (Ben-Shahar et al., 2008; Lafont et al., 2010; Ladurner et al., 2016). Sororin-PDS5 antagonizes the WAPL-PDS5 binding to RAD21-STAG1/2 interface and promotes cohesion.

In the third stage, cohesin is removed from chromosome arms as part of the prophase removal pathway. Phosphorylation of STAG1/2 by Polo-like kinase 1 (PLK1) and phosphorylation of Sororin by Cyclin Dependent Kinase 1 (CDK1) and Aurora kinase B (AURKB) displaces Sororin from the cohesin complex (Hauf et al., 2005; Nishiyama et al., 2013), leaving room for WAPL to bind the RAD21-STAG1/2 interface. As described previously, WAPL interaction with cohesin opens the SMC3-RAD21 gate and promotes cohesin removal (Gandhi et al., 2006). Cohesin is then primarily removed from chromosome arms, because Shugoshin 1 (SGO1) protects centromeric cohesin; SGO1 does this by preferentially interacting with RAD21-STAG1/2 over WAPL at centromeres (Kitajima et al., 2006; Liu et al., 2013). Once most cohesin is removed from chromosome arms and instead remains primarily at the centromere, condensed chromosomes display their characteristic X shape. It is interesting to note that cohesin-STAG1 and cohesin-STAG2 have been proposed to localize to different regions of condensed mitotic chromosomes. Cohesin-STAG1 is thought to remain at telomeres, while cohesin-STAG2 is thought to persist at the

centromere (Canudas and Smith, 2009). Unique chromosome localization patterns could lead to differential roles for STAG1 and STAG in sister chromatid cohesion.

In the fourth and final stage of cohesion regulation, cohesin is removed at the metaphase to anaphase transition. Prior to anaphase, cohesin continues to tether sister chromatids and resist the outward pulling forces of the mitotic spindle until all chromosomes are properly bioriented at the metaphase plate. Then, and only then, when the SAC is satisfied and the Anaphase Promoting Complex/Clyclosome (APC/C) is subsequently activated, the last remaining cohesin is quickly and synchronously removed (Reviewed by Lara-Gonzalez et al., 2012). APC/C activation activates separase, which irreversibly cleaves RAD21, releasing cohesin (Uhlmann et al., 1999). At this point, sister chromatids can finally segregate to opposite poles.

The careful regulation of cohesin removal after satisfaction of the SAC promotes proper chromosome segregation and genomic stability. Premature cohesin removal results in separation of sister chromatids before they are properly aligned, which can result in inappropriate merotelic attachments, lagging chromosomes, and mis-segregation; mis-segregation can lead to aneuploidy (Cimini et al., 2001; Zhang et al., 2008a). In short, defective cohesion can lead to aneuploidy, which is a hallmark of cancer, and will be discussed again later on in this chapter.

1.2.2 DNA Repair

In addition to maintaining the proper complement of chromosomes, cells must also maintain genome integrity at the DNA sequence level. Cells acquire DNA lesions on a daily basis as a result of normal cellular processes or environmental factors, and the cell must repair these lesions to avoid the accumulation of DNA mutations. (Reviewed in Ciccia and Elledge, 2010). To counter these accumulated mutations, cells have evolved specialized DNA repair mechanisms to fix specific types of DNA damage. Mis-paired DNA bases are repaired by mismatch repair (MMR), and chemical distortions of the DNA bases are repaired by base excision repair (BER) or nucleotide excision repair (NER). SSBs are repaired by single-strand break repair (SSBR), and DSBs are repaired by HR or NHEJ. HR promotes accurate DNA repair through the use of a DNA repair template, whereas NHEJ often introduces small DNA deletions (Reviewed in Ciccia and Elledge, 2010). Repair of DSBs by NHEJ and HR is carried out by an extensive set of proteins that are activated at DSBs in a precisely controlled, spatiotemporal manner (Bekker-Jensen et al., 2006). These proteins form DNA repair foci, which are commonly visualized by immunofluorescence microscopy to indicate the presence of DSBs and DSB repair. Two common markers of DSB repair are phosphorylated histone H2AX (yH2AX) and tumor protein p53 binding protein 1 (53BP1; Rogakou et al., 1998).

The cohesin complex is specifically required for DSB repair by HR. Appropriately, cohesin subunit RAD21 (SCC1) was first discovered in a screen in

fission yeast for genes that promote DSB repair (Birkenbihl et al. 1992). It is now known that cohesin is recruited to DSBs (Kim et al., 2002; Ünal et al., 2004) where it forms cohesin domains that are dependent on recruitment of upstream HR factors, including yH2AX and components of the MRN complex. (Ünal et al., 2004).

Interestingly, a differential role has been suggested for STAG2 in DNA repair compared to STAG1. Loss of STAG2 has been proposed to shift DSB repair in individual cells from HR to NHEJ (Kong et al. 2014). This shift could induce low levels of genomic instability as a result of inaccurate repair through NHEJ. Loss of STAG2 has also been associated with sensitivity to PARP inhibitors in glioblastoma cancer cell lines (McLellan et al., 2012; O'Neil et al. 2013; Bailey et al., 2014). PARP1/2 are involved in repair of SSBs (Caldecott, 2008), and PARP inhibition leads to the accumulation of DSBs (Ashworth, 2008). Cells with defective HR, such as those in BRAC1/2 mutant breast tumors, are known to be sensitive to PARP inhibition (Bryant et al., 2005), suggesting in turn a similar link between HR deficiency and PARP inhibitor-sensitive STAG2 null cancer cells.

1.2.3 Genome Organization and Gene Expression

Cohesin has an emerging role in transcriptional regulation through 3D organization of chromatin. Our understanding of higher-order 3D chromatin arrangement is growing, and so is our understanding of the cohesin complex's role in this organization. Cohesin is thought to participate in two levels of higher-

order chromatin structures. The first level is sub-megabase chromatin looping, which promotes long-range chromatin interactions between genes, promoters, and regulatory units (Kagey et al., 2010; Sanyal et al., 2012). These interactions are sometimes required for transcriptional activation. Hi-C after inducible RAD21 cleavage shows that cohesin is required for chromatin looping (Zuin et al., 2014). Additionally, cohesin frequently co-occurs with CCCTC-binding factor (CTCF) to tether these chromatin loops, although the exact arrangement of cohesin at these loops is not completely understood (Corces and Corces, 2016; Nagy et al., 2016).

The second level of chromatin organization that cohesin participates in is megabase topologically associated domains (TADs). Each TAD consists of a group of chromatin loops that are isolated from neighboring TADs by cohesin, CTCF, insulators, and other factors (Dixon et al., 2012; Zuin et al., 2014; Kojic et al., 2017). Interestingly, although cohesin localizes to TAD boundaries with CTCF, only CTCF is required to maintain those TAD boundaries (Zuin et al., 2014). Because TAD boundaries contain insulators, TADs are thought to influence gene expression by stopping the spread of heterochromatin and by physically restricting promoter-enhancer access to within TADs (Dixon et al., 2012).

Sub-populations of cohesin may carry out different transcriptional roles as part of these chromatin loops and TADs. Chromatin ImmunoPrecipitation (ChIP) experiments reveal that, depending on the cell type, most or approximately 50%

of cohesin co-occurs with CTCF, a known insulator regulator. However, approximately 25% of cohesin co-occurs with the mediator complex, which tends to localize to promoters and enhancers of transcriptionally active genes. (Wendt et al., 2008; Kagey et al., 2010; Schmidt et al., 2010). The existence of differentially localized, chromatin-bound cohesin populations suggests that cohesin's contribution to transcriptional regulation is complex and probably cellular function- and cell type-specific.

Recent work suggests that cohesin-STAG1 and cohesin-STAG2 may define several these differentially localized cohesin sub-populations. ChIP-seq of DNA-bound STAG1 and STAG2 in human epithelial (HMEC, MCF10A) and endothelial (HCAEC) cells reveals three populations: co-occurring cohesin-STAG1 and cohesin-STAG2 (50-55% of cohesin), uniquely localized cohesin-STAG1 (5% of cohesin), and uniquely localized cohesin-STAG2 (40-45% of cohesin; Kojic et al., 2017). Compared to the first two categories, uniquely localized cohesin-STAG2 did not co-occur with CTCF at TAD boundaries, and instead localized within TADs, especially at enhancers. Interestingly, the unique cohesin-STAG2 population localized to different enhancers in each cell type, suggesting that a sub-population of cohesin-STAG2 promotes gene expression in a lineage-specific manner (Kojic et al., 2017).

Cohesin was first linked to the transcriptional regulation of individual genes but has since been linked to global patterns of gene expression. For example, mutations in RAD21 alter Runt Related transcription factor (RUNX)

gene expression in zebrafish (Horsfield et al., 2007), and the cohesin loader, NIPBL, has been shown to alter expression of Cut (CT) and Ultrabithorax (UBX) in drosophila (Rollins et al., 1999; Dorsett and Krantz, 2005) and protocadherin (PCDH) in mice (Kawauchi et al., 2009). Further evidence for cohesin's involvement in transcriptional regulation includes the discovery that cohesin is expressed in post-mitotic Drosophila neural cells where it is required for a cell-type specific process, γ neuron pruning (Pauli et al., 2008; Mönnich et al., 2009); this post-mitotic cellular function suggests a role for cohesin outside of mitotic cohesion, namely in transcriptional regulation.

More recent work has revealed a role for cohesin in regulating stem cell maintenance and differentiation. Cohesin, along with mediator, NIPBL, and other protein complexes, is enriched at super-enhancers, which are a set of approximately 200 enhancers that regulate an undifferentiated, pluripotent state (Hnisz et al., 2013). Strong evidence also points to a role for cohesin in transcriptional regulation of the hematopoietic stem cell (HSC) state. For example, depletion of cohesin subunits (RAD21, SMC3, STAG1, or STAG2) in human HSCs increases stem cell expansion and delays differentiation in cell culture and in cells transplanted into mice (Galeev et al., 2016). Depletion of STAG2 specifically directs differentiation towards a myeloid lineage compared to depletion of SMC3 (Galeev et al., 2016). Similarly, depletion of cohesin in conditional cohesin knock-down mice increases the regenerative ability of plated HSCs, alters gene expression and chromatin organization, and in the long term,

leads to myeloid disorders in the knock-down mice (Mullenders et al., 2015). Finally, inducible cohesin mutations that disrupt expression of RAD21, SMC1A, SMC3, or STAG2 impair myeloid, erythroid, and stem cell differentiation of human hematopoietic stem precursor cells (HSPCs), and shift differentiation towards the myeloid lineage. (Mazumdar et al., 2015). This same study also found that cohesin mutations specifically regulate expression of ETS transcription factor (ERG), GATA binding protein 2 (GATA2), and RUNX1 in HSCs. Interestingly, a single published study suggests an opposite role for cohesin in stem cell differentiation in mice; shRNA of cohesin subunits in mouse embryonic stem cells (mESC) showed that SMC1A, SMC3, STAG2, and NIPBL were required to maintain mESC stemness (Kagey et al., 2010).

1.3 Cancer Hallmarks

Cancer is a disease of unregulated cell proliferation that leads to tumor growth and metastasis. Cells are thought to become cancerous through a stepwise accumulation of advantageous mutations that promote a set of key cancer hallmarks, as defined by Hanahan and Weinberg in 2000. These hallmarks include sustained proliferative signaling, evasion of growth suppressors, activation of invasion and metastasis, enabling of replicative immortality, induction of angiogenesis, and resistance to cell death (Hanahan and Weinberg, 2000). In 2011, after a decade of further cancer research, Hanahan and Weinberg added two hallmarks, immune evasion and deregulated cellular metabolism, and two enabling characteristics, tumor-promoted

inflammation, and genome instability and mutation (Hanahan and Weinberg, 2011). In short, cancer cells are thought to accumulate mutations that support unchecked cell growth and survival and also allow cells to evolve in order to leave their original tissue and flourish in new locations in the body, all while promoting the best tumor-environment from which to carry out this unchecked cancer growth. Genomic instability is an important instigator of these cancer hallmarks.

1.3.1 Aneuploidy and Cancer

Aneuploidy, a cancer hallmark, is present in ninety percent of solid tumors (Gordon et al., 2012; Holland and Cleveland, 2009), but the cause(s) of aneuploidy in cancer are still unclear. Mitotic defects including merotelic attachments, defective SAC, and impaired cohesion have all been linked to increased aneuploidy (Reviewed in Thompson et al., 2010; Gordon et al., 2012). But, with the exception of the cohesin complex, mitotic gene mutations are relatively rare in cancers, and cannot not fully explain the prevalence of aneuploidy in cancers. For example, mutations in the mitotic checkpoint serine/threonine kinase BUB1 lead to merotelic attachments and chromosome mis-segregation and can even promote tumorigenesis in mice when coupled with other cancer mutations (Baker et al., 2009; Ricke et al., 2012). However, BUB1 is mutated in less than 1% of all cancer cases (Cerami et al., 2012; Gao et al., 2013).

It is also somewhat unclear how cells respond to aneuploid events. Aneuploidy is highly detrimental (Santaguida and Amon, 2015a) in all organisms analyzed to date. Aneuploid budding and fission yeast show proliferation defects under standard growth conditions (Niwa et al., 2006; Torres et al., 2007). In multicellular organisms, chromosomal gain or loss is largely lethal (Hodgkin, 2005; Lindsley et al., 1972; Lorke, 1994). In humans, for example, all monosomies and most trisomies cause embryonic lethality (Reviewed in Hassold and Hunt, 2001). Only trisomy of the gene poorest chromosome, chromosome 21, is compatible with survival into adulthood. However, even this trisomy leads to high levels of embryonic lethality. Only 12.5% of trisomy 21 fetuses survive to birth (Reviewed in Roper and Reeves, 2006).

The adverse effects of an incorrect karyotype are also observed at the cellular level. Aneuploid mammalian and yeast cells exhibit metabolic alterations (Williams et al., 2008), proliferation defects (Santaguida et al., 2015; Stingele et al., 2012; Tang et al., 2011; Thompson and Compton, 2010; Torres et al., 2007; Williams et al., 2008), genome instability (Blank et al., 2015; Meena et al., 2015; Ohashi et al., 2015; Passerini et al., 2016; Sheltzer et al., 2011; Zhu et al., 2012), and proteotoxic stress (Oromendia et al., 2012; Santaguida et al., 2015; Santaguida and Amon, 2015b; Stingele et al., 2012; Tang and Amon, 2013), and aneuploid mammalian cells have been reported to activate p53 (Hinchcliffe et al., 2016; Li et al., 2010; López-García et al., 2017; Sansregret et al., 2017; Thompson and Compton, 2010). In addition to traits observed in a broad range of

aneuploidies, aneuploid cells exhibit gene-specific phenotypes in which changes in dosage of a particular gene cause a specific phenotype (e.g., Dodgson et al., 2016).

On the other hand, despite the adverse effects of an aneuploid karyotype on normal cell physiology, aneuploidy is also a hallmark of cancer, a disease characterized by excessive cell proliferation. Multiple, not mutually exclusive hypotheses have been put forth to explain the prevalence of abnormal karyotypes in cancer. Chromosome copy-number alterations have been proposed to drive disease by modulating the dosage of cancer driver genes (Davoli et al., 2013). Aneuploidy also endows cells with phenotypic variability (Beach et al., 2017; Chen et al., 2015; Rutledge et al., 2016), which could help facilitate metastasis or resistance to therapeutic interventions. Indeed, aneuploidy has been shown to be associated with metastatic behavior, resistance to chemotherapy and poor patient outcome (Bakhoum et al., 2011; Heilig et al., 2009; Lee et al., 2011; Walther et al., 2008). Finally, the process of chromosome mis-segregation and aneuploidy of many chromosomes have been shown to cause genomic instability (Blank et al., 2015; Crasta et al., 2012; Janssen et al., 2011; Ohashi et al., 2015; Passerini et al., 2016; Sheltzer et al., 2011; Zhu et al., 2012), which could fuel cancer genome evolution.

Given the potential link between aneuploidy and tumorigenesis, it is critical to understand how abnormal karyotypes affect cellular physiology. It has been proposed that cells recognize single aneuploidy events and respond by p53-

induced cellular arrest (Thompson and Compton, 2010). However, it has also been suggested that p53-induced arrest in these experiments is actually the result of a mitotic timer and not the mis-segregation itself, which happened to correlate with mitotic timing in these particular experiments (Uetake and Sluder, 2010). In summary, while aneuploidy is present in many cancers, the mechanisms and consequences of aneuploidy are still not well defined.

1.4 Cohesin Mutations in Cancer

Subunits of the cohesin complex are frequently mutated in many cancer types. Early work on this subject linked cohesin complex mutations to colon cancer through a screen for genes that protect genome stability (Barber et al., 2008) and through other unbiased approaches in ovarian cancer (Gorringe et al., 2009) and myeloid diseases (Rocquain et al., 2010). In support of these findings, as of June 2018, the online cancer study repository cBioPortal reports that cohesin is mutated in 12% of their database's cancer samples. A list of the top 15 cancers with frequent cohesin mutations reported by cBioPortal are included in Fig. 1.2A (Cerami et al., 2012; Gao et al., 2013).

Subsequent studies have specifically identified the cohesin subunit STAG2 as one of the most frequently mutated genes in a wide variety of cancers. These cancers include Ewing sarcoma (Solomon et al., 2011; Brohl et al., 2014), bladder cancer (Solomon et al., 2011; Guo et al., 2013), colorectal cancer (Barber et al., 2008; Solomon et al., 2011), and glioblastoma (Solomon et al., 2011). A reported 40% of these *STAG2* mutations are nonsense, frameshift, or

deletion mutations (Fig. 1.2B; Cerami et al., 2012; Gao et al., 2013). For the most part, these truncating mutations are distributed throughout the protein. The one exception is a minor hotspot of mutation in arginine-216 in the STAG domain (Fig. 1.2C; Cerami et al., 2012; Gao et al., 2013). Because *STAG2* is located on the X chromosome, a single truncating mutation abolishes STAG2 protein expression. Loss of STAG2 is the only viable loss of a cohesin subunit, because a paralog of STAG2, STAG1, is functionally redundant for survival in these cells (van der Lelij et al., 2017; Benedetti et al., 2017). This raises the importance of finding the differential effect(s) of STAG2 loss compared to STAG1 loss in cells.

1.5 Effect of STAG2 Loss in Cancers

Although it is well established that *STAG2* is frequently mutated in cancers, the consequences of STAG2 loss are not yet clearly defined. Does STAG2 loss lead to the generation of cancer? If so, how? Two of cohesin's cellular functions, sister chromatid cohesion and DNA repair, protect cells against genome instability. Defective sister chromatid cohesion could lead to chromosome mis-segregation and aneuploidy, which is the basis of chromosomal instability. Also, whole chromosome aneuploidies could alter the dosage of important regulatory genes. Secondly, defective DNA repair could generate genomic instability through an accumulation of DNA mutations or through replication stress and subsequent structural chromosome defects. Cohesin's remaining cellular function, transcriptional regulation, could in theory regulate any one of the cancer hallmarks. Loss of cohesin could, for example,

lead to the generation of angiogenesis, metastasis, or changes in metabolism, all depending on which transcriptional programs cohesin controls in different cell types.

As previously described, when I started this research project, recently published studies had suggested that STAG2 loss impairs sister chromatid cohesion and promoted CIN in colorectal cancer and glioblastoma cells (Solomon et al., 2011) and bladder cancer cells (Li et al., 2015). But it subsequently became clear that *STAG2* mutations do not always correlate with aneuploidy, as evidenced by studies of bladder tumors (Balbás-Martínez et al., 2013; Taylor et al., 2014; Kim et al., 2016). Additionally, *STAG2* has also been found to be frequently mutated in cancers, such as Ewing sarcoma and Acute Myeloid Leukemia (AML), which are not characterized by aneuploidy (Ding et al., 2013; Crompton et al., 2014). STAG2 has subsequently been linked to the cohesin complex functions of DNA repair and gene expression. STAG2 has been implicated in the promotion of accurate DNA repair through HR (Kong et al., 2014), and STAG2 loss has been linked to sensitivity to PARP inhibition (Bailey et al., 2014), which would also suggest a link between STAG2 and HR. However, a clear causal link between STAG2 loss and increased mutational burden has not been demonstrated in a cancer context to date. Additionally, some of the cancers with frequent *STAG2* mutations, like Ewing sarcoma, have especially low mutational burdens (Crompton et al., 2014), suggesting that at least in some cancers, STAG2 loss contributes to cancer in another way.

Instead, current evidence points to a role for STAG2 in lineage-specific transcriptional regulation. As mentioned previously, STAG2 loss has a differential effect on 3D genome organization compared to STAG1 in some cell types (Kojic et al., 2017). STAG2 has also been linked to the expression of super enhancers and the promotion of differentiation in hematopoietic lineages (Mullenders et al., 2015; Galeev et al., 2016). This connection is interesting, because *STAG2* is frequently mutated in AML, which is thought to develop as HSCs accumulate key mutations over time, while also undergoing expansion of undifferentiated myeloid cells (Lowenberg et al., 1999; Estey and Dohner, 2006). Cohesin mutations often occur early in AML cancer progression (Corces-Zimmerman et al., 2014), and early loss of cohesin could promote stemness, allowing progenitor cells to accumulate key mutations over time.

Finally, STAG2 has been linked to regulation of gene expression in Ewing sarcoma tumors and cell lines (Crompton et al., 2014). There, loss of STAG2 is associated with enrichment of metastasis genes. This particular cancer context is especially fascinating, because Ewing sarcoma is driven by a fusion protein, EWS-FLI, that generates cancer through aberrant gene expression (Riggi et al., 2014; Tomazou et al., 2015; Boulay et al., 2017). Additionally, *STAG2*-null mutations are enriched in recurrent and metastatic Ewing sarcoma tumors (Crompton et al., 2014) and are associated with shortened life expectancy, especially in conjunction with p53 mutations (Tirode et al). In summary, cohesin mutations could, in theory, lead to the generation of cancer through any of

cohesin’s cellular functions. Each role warrants further investigation, especially the role for cohesin mutations in the generation of cancer through lineage-specific aberrant gene expression in cancers like AML and Ewing Sarcoma.

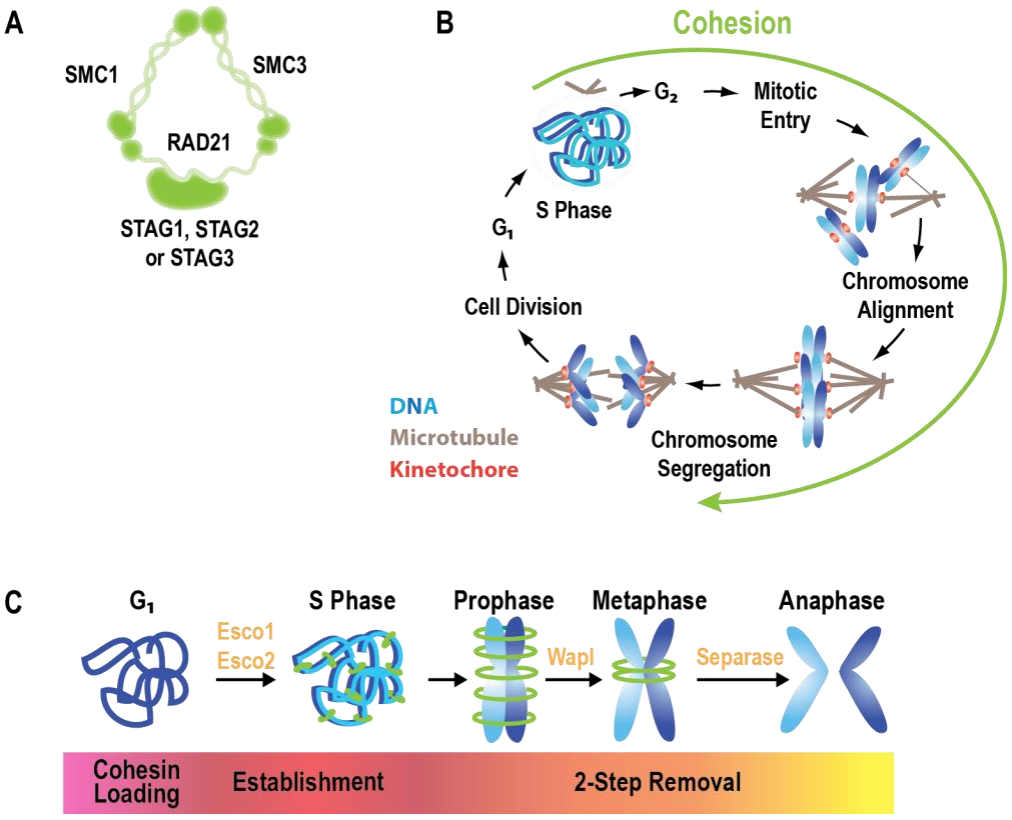

Figure 1.1 Cohesin Complex and Cohesion Regulation

(A) The structure of the cohesin complex. **(B)** Sister chromatid cohesion persists from S phase until just prior to anaphase. DNA is light and dark blue. Microtubules are tan. Kinetochore is red. Cohesion is indicated by the green arrow. **(C)** Cohesin is precisely regulated throughout the cell cycle. DNA is light and dark blue, and cohesin is green.

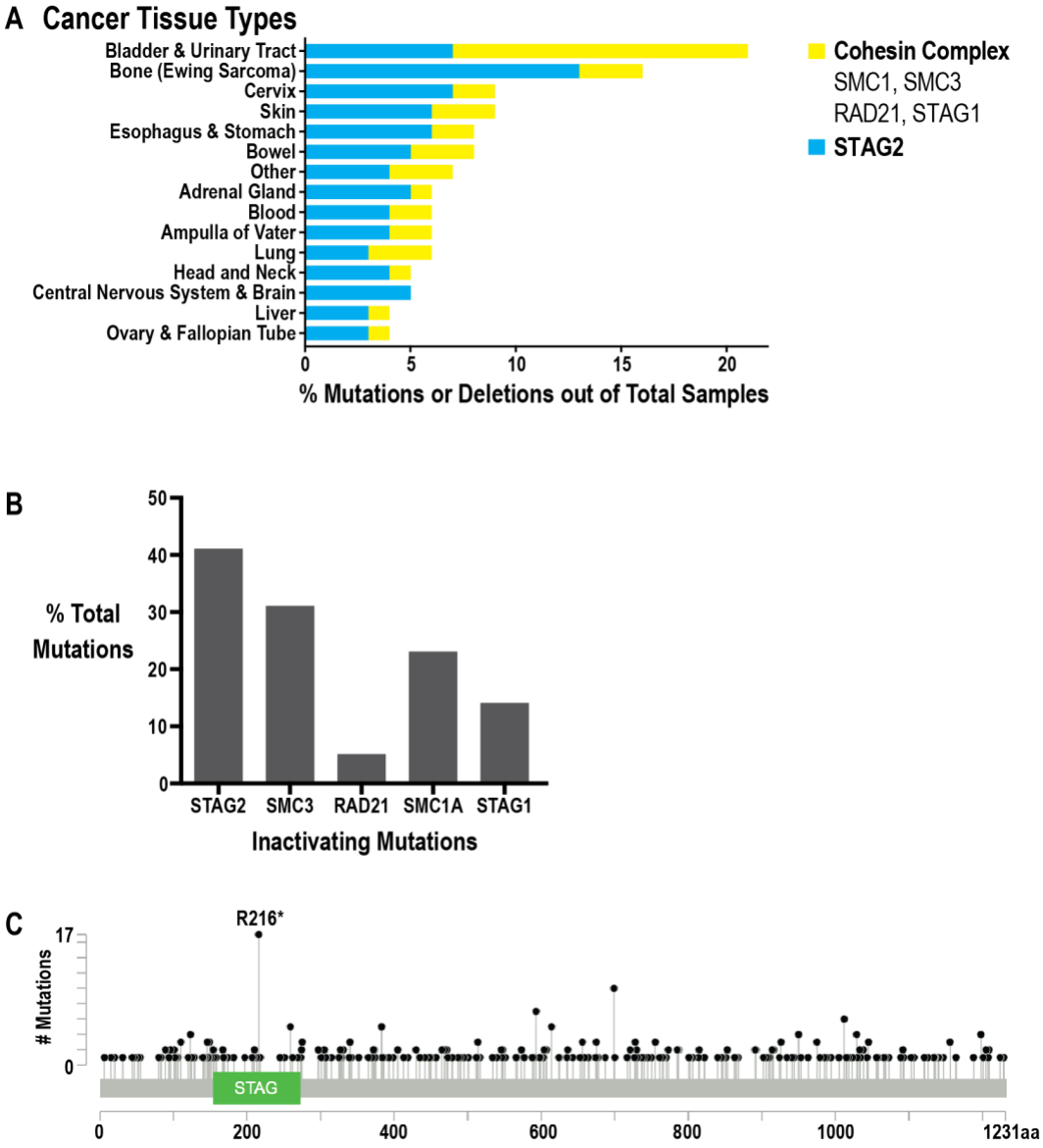

Figure 1.2 Frequent Cohesin Cancer Mutations

(A) Cohesin mutation frequencies are presented for the top 15 cancers with frequent cohesin mutations. All data in this figure was obtained from cBioPortal in June 2018. **(B)** Frequency of inactivating mutations (deletions, insertions, nonsense, frameshift) in cohesin subunits. **(C)** Location of inactivating mutations in *STAG2*. R216* indicates a mutation hotspot in the STAG domain.

CHAPTER 2: DEFINING THE CELLLULAR CONSEQUENCES OF LOSS OF COHESIN SUBUNIT STAG2 IN CANCER CELLS

2.1 Summary

The cohesin subunit Stromal AntiGen 2 (*STAG2)* is frequently mutated and STAG2 protein expression lost in many cancer types. Despite the frequency of these mutations across many cancers, a clear role for loss of STAG2 expression in cancer progression has not been defined. Here we show, through time lapse microscopy of cohesion loss in live cells, and through quantification of inter-kinetochore stretch and anaphase defects, that loss of STAG2 expression does not impair cohesin's role in sister chromatid cohesion. We also show, after assessment of DNA repair of double-strand breaks (DSBs) through homologous recombination (HR) and non-homologous end joining (NHEJ), that STAG2 is not required for DNA repair. Instead, we demonstrate that STAG2 is required for cohesin's role in regulating gene expression in Ewing sarcoma cells. Total mRNA sequencing of STAG2- and STAG1-depleted Ewing sarcoma A673 cells, which are STAG2 wild type, reveals a differential effect for STAG2 loss on gene expression compared to STAG1 loss in Ewing sarcoma cells. These results suggest a role for STAG2 loss in the regulation of gene expression in cancers that are driven by aberrant gene expression.

2.2 Introduction

Identification of frequent cancer mutations and their mechanism(s) of action in cancer are important steps towards targeted treatment of those cancers. Mutations in the cohesin complex are frequent in many cancer types, but their mechanism of action has not yet been clearly defined. Cohesin complex mutations were initially identified in colon cancer through a screen for genes that protect genome stability (Barber et al., 2008) and through other unbiased approaches in ovarian cancer (Gorringe et al., 2009) and myeloid diseases (Rocquain et al., 2010). Subsequent studies have identified the cohesin subunit *STAG2* as one of the most frequently mutated genes in a wide variety of cancers, including Ewing sarcoma (Solomon et al., 2011; Brohl et al., 2014), bladder cancer (Solomon et al., 2011; Guo 2013), colorectal cancer (Barber et al., 2008; Solomon et al., 2011), and glioblastoma (Solomon et al., 2011).

The majority of these *STAG2* mutations are nonsense, frameshift, or deletion (Cerami et al., 2012; Gao et al., 2013), and because *STAG2* is located on the X chromosome, most *STAG2*-mutant cancer cells are null for STAG2 protein expression. A paralog of STAG2, STAG1, is functionally redundant for survival in these cells (van der Lelij et al., 2017; Benedetti et al., 2017). So, although it is well established that *STAG2* is frequently mutated in cancers, STAG2 null cells are viable, and the consequences of STAG2 loss are not yet clearly defined.

Early work in this area has suggested that STAG2 loss impairs sister chromatid cohesion, which leads to accumulated aneuploidy and chromosomal instability (CIN) in colorectal cancer and glioblastoma cells (Solomon et al., 2011) and bladder cancer cells (Li et al., 2015). But *STAG2* mutations do not always correlate with aneuploidy, as evidenced by studies of bladder tumors (Kim et al., 2016; Balbás-Martínez et al., 2013; Taylor et al., 2014). Additionally, *STAG2* is frequently mutated in cancers, such as Ewing sarcoma, which are not characterized by aneuploidy (Crompton et al., 2014). Thus, the consequences of STAG2 loss are still an open question. STAG2 has subsequently been linked to the cohesin complex functions of DNA repair and gene expression. STAG2 has been implicated in the promotion of accurate DNA repair through HR (Kong et al., 2014). STAG2 has a differential effect on 3D genome organization compared to STAG1 in some cell types (Kojic et al., 2017). STAG2 has also been linked to the expression of super enhancers and promotion of differentiation in hematopoietic stem cell (HSC) lineages (Mullenders et al., 2015; Galeev et al., 2016) and to regulation of gene expression in Ewing sarcoma tumors and cell lines (Crompton et al., 2014).

To clarify the role of STAG2 loss in cancer, a comprehensive analysis of the effect of STAG2 loss on sister chromatid cohesion, DNA repair, and regulation of gene expression was required. Given the presence of the paralog STAG1, we focused on identifying differential effect(s) of STAG2 loss relative to STAG1. We found, through a quantitative assay for cohesion strength in live

cells, that STAG2 loss does not impair sister chromatid cohesion. We show, through analysis of inter-kinetochore stretch and anaphase defects, that STAG2 loss does not affect cohesin's mitotic functions and that STAG1 can compensate for these functions. We also demonstrate, through quantification of DNA repair kinetics, HR, and NHEJ, that STAG2 loss does not impair DNA repair or alter choice of DNA repair pathway. Furthermore, STAG2 loss does not sensitize cells to poly(ADP-ribose) polymerase (PARP) inhibition, as has been previously reported (Bailey et al., 2014), or to other compounds in a library of small molecule inhibitors. Instead, we demonstrate, by RNA sequencing (RNA-seq), that STAG2 loss has a differential effect on gene expression in Ewing sarcoma cells compared to STAG1. We identify a subset of genes that are down-regulated by STAG2 depletion and up-regulated by STAG1 depletion in Ewing sarcoma cells. We also identify a subset of genes that are down-regulated by STAG2 depletion or loss in more than one cell type. These results elucidate a potential mechanism for STAG2 loss in generating cancer through dysregulation of lineage-specific gene expression patterns.

2.3 Results

2.3.1 Loss of STAG2 Does Not Impair Cohesion *In Vivo*

Previous work from the Waldman lab and others has suggested a role for STAG2 in maintaining sister chromatid cohesion, and loss of this function through STAG2 mutation has been proposed to generate CIN, thus explaining a role for frequent *STAG2* mutations in cancer (Solomon et al., 2011). To further

investigate a role for STAG2 in sister chromatid cohesion, we developed a quantitative *in vivo* assay, which monitors cohesion fatigue timing following loss of STAG2; this assay is based on the observation that cohesion strength determines cohesion fatigue timing (Daum et al., 2011). To induce cohesion fatigue, we trigger metaphase arrest by treating wild type and STAG2 defective, RFP-histone H2B labeled cell lines with proTAME, a small molecule inhibitor of the Anaphase Promoting Complex/Clyclosome (APC/C; Zheng et al., 2010; Lara-Gonzalez and Taylor, 2012; Saptoka et al., 2018). Next, we follow cells in real-time, using high throughput live cell imaging to observe mitotic outcome and cohesion fatigue (Fig. 2.1A). Since proTAME treatment leads to almost 100% cohesion fatigue in all tested cell lines (Fig. S2.1A), we report cohesion fatigue timing only, which we define as the interval between nuclear envelope breakdown (NEBD) and the appearance of the first scattered chromatids (Fig. 2.1B).

To validate our assay, we first measured cohesion fatigue timing in proTAME-treated hTERT RPE-1 cells after siRNA depletion of mitotic paralogs STAG1 or STAG2 or both (Fig. 2.1C). Co-depletion of STAG1 and STAG2 served as a positive control for impaired cohesion in this assay; proTAME-treated, STAG1 and STAG2 co-depleted cells underwent almost two-fold faster cohesion fatigue (3.0±1.1 hours compared to 5.5±2.4 hours in control non-targeting siRNA cells; Fig. 2.1D). We also observed, within the timeframe of this assay, that co-depletion of STAG1 and STAG2 leads to frequent anaphase

defects (Fig. S2.1B) and spontaneous cohesion fatigue without metaphase arrest in 27% of cells (Fig. S2.1C). In the longer-term, co-depletion of STAG1 and STAG2 decreases clonogenic survival, presumably through accumulated mis-segregation events and subsequent cell death (Fig. S2.1D-E).

Next, we looked at the effect of STAG1 or STAG2 single-depletions on cohesion fatigue timing (Fig. 2.1D). STAG1 depletion in hTERT RPE-1 cells had no effect on timing relative to controls (5.6±2.6 hours vs. 5.5±2.4 hours). While STAG2 depletion in hTERT RPE-1 cells was expected to show decreased cohesion fatigue timing, we observed a mild but significant increase in cohesion fatigue timing (7.0±3.1 hours vs. 5.5±2.4 hours). These results suggest that our assay is sensitive enough to detect changes in cohesion fatigue and that transient siRNA depletion of STAG1 and STAG2 does not decrease cohesion fatigue timing.

To investigate the effect of STAG2 loss on cohesion fatigue timing, we measured cohesion fatigue timing in paired HCT116 colorectal cancer or H4 glioblastoma cell lines stably expressing functional or defective *STAG2*, which were previously generated in the Waldman lab (Solomon et al., 2011; Fig. 2.2A). Loss of STAG2 expression in HCT116 STAG2 knock-out cells had no effect on cohesion fatigue timing (3.9±2.0 hours vs 3.9±2.2 hours in wild type STAG2 parental control cells; Fig. 2.2B-C). Stably rescued expression of endogenous STAG2 in H4 STAG2 knock-in cells has almost no effect on cohesion fatigue

timing (1.9±0.5 hours in rescued STAG2 knock-in cells compared to 1.6±0.5 hours in STAG2 null parental control cells; Fig. 2.2D).

To corroborate our cohesion fatigue timing results, we also assessed the effect of defective STAG2 on inter-kinetochore stretch, which is another measure of cohesion strength, in a panel of STAG2 wild type and STAG2 defective cell lines. As predicted, co-depletion of STAG1 and STAG2 in hTERT RPE-1 cells greatly increases inter-kinetochore distance compared to control cells (1.72±0.69 μm compared to 1.16±0.20 μm in control cells; Fig. 2.2E-F); this inter-kinetochore stretch can be observed as visibly separated chromatids at kinetochores (Fig. 2.2E inset). In all other single perturbations of STAG1 and STAG2 we observed only mild effects on inter-kinetochore stretch. In RPE-1 cells, single-depletion of STAG1 or STAG2 increases inter-kinetochore stretch by 7% (1.23±0.34 μm and 1.26±0.35 μm respectively compared to 1.16±0.20 μm in control cells; Fig. 2.2F). In H4 cells, rescue of STAG2 expression reduces inter-kinetochore stretch by 11% (1.28±0.27 compared to 1.15±0.18 in control H4 STAG knock-in cells; Fig. S2.2A-B). And in two HCT116 clones, loss of STAG2 increases inter-kinetochore stretch by 2% (1.37±0.26 and 1.37±0.24 in two STAG2 null clones compared to 1.34±0.25 in control STAG2 wild-type parental cells; Fig. S2.2A-C). These results stand in contrast to published data showing a greater increase in inter-kinetochore stretch in STAG2 siRNA-depleted RPE-1 and HCT116 cells (Solomon et al., 2011; Kleyman et al., 2014).

2.3.2 Chromosome Segregation Fidelity is Maintained in STAG2 Null Cells

While our results do not support a consistent role for STAG2 in mitotic sister chromatid cohesion, loss and reduction of STAG2 have been linked to increased anaphase defects (Solomon et al., 2011; Kleyman et al., 2014, Kim et al., 2016), which can arise as a consequence of impaired cohesin function during mitotic chromosome alignment or during DNA replication and repair. These processes can then generate lagging chromosomes or acentric fragments and chromosome bridges respectively (Cimini et al., 2001; Bakhoum et al., 2009; Bakhoum et al., 2014, Burrell et al., 2014). To further test for evidence of impaired cohesion in STAG2 null cells, we fixed STAG2 wild type and STAG2 null HCT116 and H4 cell lines (Fig. 2.3A) and measured the frequency of these mitotic and pre-mitotic anaphase defects (Fig. 2.3B, Fig. S2.3A, Table S2.1). We observed increased mitotic anaphase defects in STAG2 null colorectal HCT116 cells compared to wild type parental cells but not in STAG2 null glioblastoma H4 cells compared to paired STAG2 knock-in cells. Loss of STAG2 in HCT116 cells results in approximately a two- to three-fold increase in mitotic anaphase defects (4.7±0.6 % and 7.7±2.5 % in two STAG2 null clones compared to 2.0±1.0 % in control cells; Fig. 2.3C). Loss of STAG2 in HCT116 cells does not result in a significant increase in pre-mitotic anaphase defects (14.3±3.2 % and 15.3±6.7 %; Fig. 2.3D). These results are consistent with recent observations where loss of STAG2 in HCT116 cells results in increased mitotic anaphase defects but has no

significant effect on pre-mitotic anaphase defects in these cell lines (Solomon et al., 2011; Kim et al., 2016).

We next looked at anaphase defects in STAG2 null and knock-in H4 cells (Fig. S2.3A). We did not observe a statistically significant change in either mitotic (6.3±1.5 % compared to 3.0±2 % in control STAG2 null cells; Fig. 2.3E) or pre-mitotic (13.0±11.1 % compared to 6.3±2.1 % in control STAG2 null cells; Fig. 2.3F) anaphase defects upon rescue of STAG2 expression in H4 cells. Our results in this cell line are not consistent with previous observations that find that STAG2 rescue decreases anaphase defects in the same cell H4 cell lines (Solomon et al., 2011). Our different observations may arise from the relatively low frequency of anaphase defects that result in variation between experiments. In summary, our results do not support a differential role for cohesin-STAG2 in cohesin's mitotic functions. Instead, defective cohesin-STAG2 may uniquely contribute to cancer-related phenotypes through a non-mitotic-based mechanism.

2.3.3 Homologous Recombination Ability is Maintained in STAG2 Depleted Cells

The cohesin complex is required for repair of DNA DSBs through homologous HR (Ström et al., 2004; Potts et al., 2006). Recent work specifically implicates cohesin-STAG2 in DSB repair through HR (Kong et al., 2014) and suggests that loss of STAG2 shifts DNA repair from more accurate HR to less accurate NHEJ. This work presents a differential role for loss of cohesin-STAG2

in genome instability in cancer through increased mutational burden. We therefore sought to investigate whether a non-mitotic role for STAG2 exists in DNA repair. We first tested whether loss of STAG2 alters the kinetics of DSB by quantifying DSB foci after ionizing radiation. For this purpose, H4 STAG2 null and knock-in cells were treated with two Gy ionizing radiation to induce DSBs and then DSB repair foci were quantified in fixed cells at one, four, eight, and 24 hours after ionizing radiation (Fig. S2.4A). DSB foci containing two co-localized markers, tumor protein p53 binding protein (53BP1) and phosphorylated histone H2AX (yH2AX), were quantified by automated analysis in ImageJ (Fig. S2.4B). As expected, DSB repair foci levels were low in control cells, peaked at one hour after ionizing radiation, and returned to control levels after 24 hours (Fig. S2.4C). Our quantification shows that DSB repair foci reached similar maximum levels in H4 STAG2 null and knock-in cells and were resolved with the same kinetics (Fig. S2.4D). We conclude that loss of STAG2 does not affect the formation and clearance of DSB repair foci, and that DSB repair response is likely intact in STAG2 null cells.

Quantification of DSB repair foci is a common tool for visualizing DSB repair, but it cannot distinguish between different DNA repair pathways. Because loss of STAG2 has been implicated specifically in HR (Kong et al., 2014), we next tested if loss of STAG2 expression shifts DSB repair from HR to NHEJ. For this purpose, we carried out a DSB repair reporter assay developed in the Powell and Jasin labs (Bindra et al., 2013). In this system in U-2 OS cells, small

molecule-induced expression of the endonuclease I-SceI introduces site-specific DSBs in two integrated reporter constructs, a GFP reporter of HR and a dsRed reporter of NHEJ (Fig. 2.4A). Successful DSB repair events lead to cellular expression of GFP or dsRed or both, and repair events are measured in single cells through flow cytometry analysis for GFP or dsRed (Fig. 2.4B). The reporter system is described in further detail in the methods section and in Bindra et al. 2013. We used this assay to measure HR and NHEJ in STAG1- and STAG2-depleted cells (Fig. 2.4C). HR and NHEJ frequencies were normalized to baseline repair levels in control siRNA-treated cells (Fig. 2.4E). Representative flow cytometry results are presented in Fig. 2.4D.

Two positive controls demonstrate the effectiveness of this assay; consistent with published results, depletion of DNA repair associated BRAC2, which is required for HR, reduced HR frequency (0.13±0.03 GFP normalized to control) and increased NHEJ frequency (1.16±0.21 dsRed normalized to control; Fig. 2.4D-E). Also, depletion of X-ray repair cross complementing 4 (XRCC4), which is required for canonical NHEJ, increased both HR (2.02±0.25) and NHEJ frequency (1.51±0.33).

To test the role of STAG2 in DNA repair pathway choice, HR and NHEJ events were quantified in cells with single- and co-depletions of STAG2 and STAG1 (Fig. 2.4E). We did not observe a change in HR and NHEJ frequency upon depletion of STAG2 (0.97±0.08 GFP and 0.86±0.07 dsRed relative to control; Fig. 2.4D-E) or STAG1 (1.08±0.09 GFP and 0.98±0.08 dsRed relative to

control). Co-depletion of STAG2 and STAG1 mildly increases HR (1.35±0.19 GFP relative to control) but not NHEJ (1.04±0.12 dsRed relative to control), which is a previously unreported phenotype (Bindra et al., 2013). The results of this assay do not support a role for STAG2 in HR.

2.3.4 STAG2 Null Cells are Not Consistently Sensitive to PARP Inhibition

Although our DSB foci quantification and DNA repair reporter assays do not suggest a role for STAG2 in DNA repair, we are aware of studies that link cohesin mutations (MeLellan et al., 2012) and loss of STAG2 (Bailey et al., 2014) to sensitivity to poly(ADP-ribose) polymerase (PARP) inhibition. To further probe this connection between loss of STAG2 and DNA damage sensitivity, we first measured cell survival in H4 STAG2 null and STAG2 knock-in cells after four-day treatment with the PARP1/2 inhibitor Olaparib (Fig. 2.5A). Cell survival was measured in fixed cells stained with Hoechst by automated nuclei count using CQ-1 analysis software. We observed a mild but significant five-fold sensitivity of STAG2 null H4 cells to Olaparib (IC50=0.09 μM compared to 0.47 μM in STAG2 knock-in cells; Fig. 2.5B).

As our observed Olaparib sensitivity is subtler than previously observed (Bailey et al., 2014), we also carried out PARP inhibition in a more sensitive clonogenic cell survival assay with a panel of STAG2 null cell lines. For this purpose, we treated STAG2 null and wild type H4, HCT116, and hTERT RPE-1 cells with dose curves of Olaparib or with a later generation, highly potent

PARP1/2 inhibitor, Talazoparib (Shen et al., 2013), and measured clonogenic cell survival by quantifying total crystal violet signal per well (Fig. 2.5C, Fig. S2.5A). As a positive control for PARP sensitivity, DLD-1 parental and BRCA2 null cells were also assayed as described above. DLD-1 BRCA2 null cells were 1000-fold more sensitive to Olaparib and 50-fold more sensitive to Talazoparib when compared to DLD-1 parental cells (Fig. 2.5D, Table S2.2). Using a sensitivity threshold of two-fold change (FC) in IC50, we observed that H4 STAG2 null cells are mildly sensitive to Olaparib (IC50 FC=2.5 compared to H4 STAG2 knock-in cells) but not to Talazoparib (IC50 FC=1.4; Fig. 2.5E, Table S2.2). Of the remaining tested cell lines, one of two STAG2 null HCT116 clones and one of two STAG2 null RPE-1 clones were sensitive to Olaparib (IC50 FC=3.3 and IC50 FC=2.6 respectively) but not to Talazoparib (IC50 FC=1.7 and IC50 FC=1.3 respectively; Fig. S2.5B-C, Table S2.2). No tested cell lines were sensitive to both Olaparib and Talazoparib. In summary, we find that only a subset of STAG2 null cell lines show more than two-fold sensitivity to Olaparib, and that no tested STAG2 null cell lines are sensitive to a second PARP inhibitor, Talazoparib. We conclude then that loss of STAG2 expression does not render cells sensitive to PARP inhibitors, and that treatment of STAG2 null cancers with PARP inhibitors may not prove to be a successful therapeutic approach in all cases.

2.4.5 Testing a Curated Library of Small Molecule Inhibitors Against STAG2 Null Cells

Several recent publications have highlighted the synthetic lethality between mitotic paralogs STAG1 and STAG2 and have called for further research into therapeutic treatments that would selectively target STAG2 null cancer cells (Benedetti et al., 2017; van der Lelij et al., 2017). As there are currently no available inhibitors of STAG1, such therapies would necessarily target as yet undiscovered functions specific to cohesin-STAG2 or to cohesin-independent STAG2. To test for undiscovered STAG2-specific functions or drug sensitivities, we treated STAG2 null and knock-in H4 cells with a library of small molecule inhibitors curated by the Shiau lab. This library consists of approximately 750 small molecule inhibitors and includes compound classes that inhibit processes previously implicated in cohesin cellular function; these include inhibitors of acetyltransferases (Dasgupta et al., 2016), DNA replication and microtubule dynamics (MeLellan et al., 2012), DNA repair (Bailey et al., 2014; Kong et al., 2014), and kinesin family member 2C (MCAK) and Aurora Kinase B (AURKB; Kleyman et al., 2014), as well as a comprehensive panel of 120 kinase inhibitors and other compounds. After four days treatment with the inhibitor library, cells survival was assessed by measuring total ATP signal per well.

As a first pass at analysis, we manually inspected survival curves and compared IC50 values between both cell lines for each library compound. H4 STAG2 null cells showed increased sensitivity and reduced IC50 when treated

with the histone deacetylase (HDAC) inhibitor, Belinostat (data not shown). Activity of HDAC8 is required for normal removal of cohesin from chromosome arms at prophase, and inhibition of HDAC8 has also been implicated in replication fork progression (Terret et al., 2009).

To validate this potential genetic interaction, cell survival was measured in STAG2 null and wild type H4, HCT116, and RPE-1 cells after treatment with two pan-HDAC inhibitors with different mechanisms of action, Belinostat or Panobinostat (Plumb et al., 2003; Giles et al., 2006). Cell survival was assessed after four days by measuring total ATP per well (Fig. 2.5F). Unexpectedly, we found that STAG2 knock-in H4 cells and not STAG2 null cells are five-fold more sensitive to Belinostat (Fig. 2.5G, Table S2.3). However, H4 STAG2 knock-in cells are not sensitive to the pan-HDAC inhibitor, Panobinostat. Additionally, no sensitivity to either Belinostat or Panobinostat was observed between STAG2 null and wild type HCT116 and RPE-1 cell lines (Fig. S2.5D-E, Table S2.3). Our failure to observe a consistent sensitivity to HDAC inhibitors between STAG2 null and wild type paired cell lines corroborates a recent published observation that HDAC8 depletion does not reduce cell viability in HCT116 Clustered Regularly Interspaced Short Palindromic Repeats (CRISPR) STAG2 knock-out cells compared to control cells (Benedetti et al., 2017; van der Lelij et al., 2017). Because the observed sensitivity to HDAC inhibitor Belinostat is unique to H4 STAG2 knock-in cells and to the compound Belinostat, we conclude that there is no general genetic interaction between STAG2 and HDAC.

As our screen did not reveal genetic interactions between STAG2 and any tested compounds, we do not report the results here. However, we are in the process of curating these results, and will make them publicly available in the hopes of focusing future work carried out to discover therapeutic treatments for STAG2-null cells. While this pilot screen did not reveal novel genetic interactors or therapeutic avenues for treating STAG2 null cancers, we can take away a valuable lesson that the search for therapeutic approaches to STAG2 null cancers is not immediately straightforward and requires further inquiry.

2.3.6 Gene Expression Regulation in STAG2 Depleted and STAG2 Null Cell Lines

Our research has not revealed a role for STAG2 in mitotic sister chromatid cohesion, chromosome segregation fidelity, DNA repair through homologous recombination, or replication fork stability. At this point, we turned to investigate the emerging role of the cohesin complex in regulating gene expression through chromatin organization. Recent work has proposed a lineage-specific role for cohesin-STAG2 in maintaining undifferentiated gene expression programs in hematopoietic lineages (Mullenders et al., 2015; Galeev et al., 2016). In another interesting cellular context, loss of cohesin-STAG2, a frequent mutation in Ewing sarcoma (Brohl et al., 2014), has been associated with a unique gene expression signature in Ewing sarcoma tumors and cell lines (Crompton et al., 2014). This particular cancer context is especially fascinating, because Ewing sarcoma is driven by a fusion protein, EWS-FLI, that generates cancer through aberrant

gene expression (Riggi et al., 2014; Tomazou et al., 2015; Boulay et al., 2017). Additionally, STAG2-null mutations are enriched in recurrent and metastatic Ewing sarcoma tumors (Crompton et al., 2014) and are associated with shortened life expectancy, especially in conjunction with p53 mutations (Tirode et al., 2014).

To test for a potential lineage-specific role for cohesin-STAG2 in Ewing sarcoma, we treated Ewing sarcoma A673 cells, which are STAG1 and STAG2 wild type, with siRNA against STAG1 or STAG2 and quantified gene expression by total mRNA sequencing in these cells (Fig. 2.6A-B). We observed different patterns of altered gene expression in STAG1- and STAG2-depleted A673 cells. STAG1 depletion resulted in down-regulation of 34 genes and up-regulation of 179 genes (Fig. 2.6C). STAG2 depletion resulted in down-regulation of 201 genes and up-regulation of 54 genes (Fig. 2.6D). Notably, a subset of 31 genes is downregulated in STAG2-depleted A673 cells and upregulated in STAG1-depleted A673 cells (Table S2.4). We then tested to see if CRISPR knock-out of STAG1 and STAG2 also results in a differential effect on gene expression in transformed RPE-1 cells. However, in RPE-1 cells, both STAG1 and STAG2 loss lead to a similar pattern of gene down-regulation (Fig. S2.6A-B) with significant overlap between these down-regulated gene sets. Although our results and published work support a lineage-specific role for STAG2 loss in regulating gene expression, we do observe a small subset of genes that are down-regulated by loss of STAG2 in multiple cell types. For this analysis, we measured gene

expression by RNA-seq in a third cell type, STAG2 null and STAG2 wild type H4 glioma cells (Fig. S2.6C) and identified recurring genes that are down-regulated by STAG2 loss in two or more cell types (Table S2.5).

2.4 Discussion

We have thoroughly characterized the effect of STAG2 loss on cohesin's cellular functions of sister chromatid cohesion, chromosome segregation, and DNA repair and have shown that STAG2 is not required for these functions in the presence of its paralog STAG1. We have also probed the sensitivity of STAG2 null cells to small molecule inhibitors and provided evidence that PARP and HDAC inhibition do not selectively kill STAG2 null cancer cells. Instead, we have shown that STAG2 loss has a differential effect on gene expression in the unique genetic background of Ewing sarcoma cells. Our initial results suggest several lines of additional inquiry. First, would depletion of STAG2 and STAG1 result in similar patterns of gene expression in other STAG2 wild type Ewing sarcoma cell lines? Next, does depletion of STAG2 and STAG1 result in unique cohesin localization patterns as detected by Chromatin ImmunoPrecipitation sequencing (ChIP-seq)? And does chromatin location of cohesin-STAG2 and cohesin-STAG1 correlate with differentially regulated genes? Does differential expression of any of these genes introduce a drugable sensitivity in STAG2 null cells? Finally, are there other cancer types that experience differential gene expression upon loss of STAG2? Addressing these questions will be the main focus of future research on this topic.

2.5 Materials and Methods

2.5.1 Cell Culture

RPE-1 hTERT (ATCC), HCT116 and H4 (gift from Todd Waldman), and A673 (ATCC) cell lines were cultured in DMEM (Invitrogen) supplemented with 10% FBS (Invitrogen), and 100 U/ml penicillin/streptomycin (Invitrogen). DLD-1 cells (Horizon Discovery) were cultured in RPMI 1640 (Invitrogen) supplemented with 10% FBS and 100 U/ml penicillin/streptomycin. All cells were grown at 37°C with 5% CO_2 in a humidified environment. To generate RPE-1 hTERT, HCT116, and H4 cell lines expressing H2B-RFP, cells were transduced with pBABE-Puro, a vector encoding human histone H2B C-terminally fused to mRFP1 3 (gift from Don Cleveland). A population of cells expressing the transgene at moderate levels was selected by fluorescence activated cell sorting (FACS). U-2 OS EJ-DR cells (gift from Simon Powell), which contain chromosomally integrated EJ-RFP and DR-GFP cassettes to measure NHEJ and HR respectively, and which have been described previously (Bindra et al., 2013), were cultured in high-glucose DMEM supplemented (Invitrogen) with 10% charcoal-stripped FBS (Invitrogen) and no penicillin/streptomycin. An initial population of GFP- and dsRed-negative U-2 OS EJ-DR cells was selected by FACS and subsequently used in all experiments. U-2 OS parental unlabeled cells and U-2 OS cells stably expressing GFP or dsRed (gift from Simon Powell) were cultured in DMEM supplemented with 10% FBS, and 100 U/ml penicillin/streptomycin, and used as controls for gating GFP+ and dsRed+ U-2 OS EJ-DR cells. All flow cytometry was performed

with the support of the Flow Cytometry Core at the San Diego Center for AIDS Research (P30 A1036214), the VA San Diego Health Care System, and the San Diego Veterans Medical Research Foundation.

2.5.2 Cohesion Fatigue Assay

hTERT RPE-1 H2B::RFP cells were transfected with 100nM total pooled ON-TARGETplus siRNAs (Dharmacon) against human STAG1, STAG2, or both, or with non-targeting pool siRNA using the recommended Lipofectamine RNAimax protocol (Thermo Fisher). After two days, cells were plated on 96-well µCLEAR plates (Greiner) and synchronized by 16 hr treatment with 5 mM thymidine (Sigma) treatment followed by 8 hrs washout. Cells were then treated with DMSO (Sigma) or 15 µM proTAME (BostonBiochem) and immediately filmed for 24 hrs using a Yokogawa CV7000 microscope with a 20x objective. Images were acquired every 6 minutes for the duration of filming. Cohesion fatigue timing was measured using Metamorph software. Paired HCT116 and H4 cell lines with wild type and STAG2 null were synchronized by 24 hr treatment with 2 mM thymidine treatment followed by 5 hrs washout. Cells were imaged and analyzed as described above.

2.5.3 Western Blots

Immunoblots were performed using the following antibodies: goat anti-STAG1 (Abcam), goat anti-STAG2 (Abcam), rabbit anti-XRCC4 (Sigma), mouse anti-tubulin (Sigma), and rabbit anti-BRCA2 (Bethyl Labs). Cell pellets for BRCA2 immunoblots were resuspended in 2x Laemelli Sample Buffer, run on Tris-

Acetate PAGE gels (Invitrogen), transferred to PVDF membrane (Life Technologies) in 10% methanol, and blocked in 0.1% TBS-TWEEN. Signal was detected using ECL detection regent (Thermo). For all remaining immunoblot preparations, cell pellets were resuspended in RIPA buffer, sonicated for five min on ice, centrifuged at full speed for 10 min at 4° C, and supernatant was collected. Protein was quantified using a Bradford assay (Bio-Rad), and pre-cast SDS Page Gels (Bio-Rad) were run using Tris/Glycine/SDS buffer and transferred using Trans-Blot Turbo Mini PVDF Transfer Packs (Bio-Rad) and a Trans-Blot Turbo Transfer System (Bio-Rad). Immunoblots were blocked in 0.1% PBS-TWEEN and 5% milk, and antibodies were used at 1:2000 (STAG1, STAG2), 1:5000 (XRCC4), or 1:10000 (Tubulin). Secondary goat anti-HRP (Novex) and mouse anti-HRP (GE Healthcare) antibodies were used at 1:1000 and visualized using the WesternBright Sirius Chemiluminescent Detection Kit (Advansta). Immunoblots were visualized using Bio-Rad ChemiDoc Imager and Bio-Rad Imaging software.

2.5.4 Clonogenic Assays

Cells were plated in six-well tissue culture plates. After 24 hrs, plates were fixed with 10% acetic acid/10% methanol in PBS, washed with PBS, stained for 5 min with 1% crystal violet in methanol, washed 3X with water and dried, and then remaining crystal violet was extracted with 10% acetic acid in water. Plates were agitated for 20 min, and then 200ul of extracted crystal violet solution was transferred to a 96-well plate, and absorbance was read @ 570nm using a

Microplate Reader (Tecan). All fixation, staining, and extraction steps were carried out at room temperature. For clonogenic assays of STAG1 and STAG2 depleted hTERT RPE-1 cells, cells were first treated with siRNA for 3 days as previously described and then plated on six-well plates for clonogenic assays. For clonogenic assays of PARP inhibited cells, PARP inhibition is described in section 2.5.8.

2.5.5 Immunostaining

Unsynchronized paired HCT116 and H4 cell lines with wild type and STAG2 were plated overnight on eight-well polymer coverslips, fixed in 1% formaldehyde in PBS for 5 min, washed with 0.1% PBS Triton-X 100, and incubated with anti-sheep Aurora B (gift from Stephen Taylor), anti-mouse Ndc80, anti-human ACA, and Hoechst, followed by incubation with Cy2, Cy3, or Cy5 labeled secondary antibodies (Jackson Immunoresearch). hTERT RPE-1 cells were first transfected with siRNA as previously described and then plated overnight on eight-well polymer coverslips as described above. To measure inter-kinetochore stretch, fixed cells with clear metaphase or prometaphase plates were imaged using a DeltaVision (DV) microscope with a 100X objective and 1.5x supplemental objective. Within each cell, Ndc80 pairs with clear paired ACA foci present in the same z-slice were measured by drawing a single line from the midpoint of each Ndc80 foci. 10+ pairs were measured per cell. To quantify anaphase defects, fixed cells anaphase cells were imaged using a DV microscope with a 60X objective.

2.5.6 Irradiation

Cells were plated on 18mm coated coverslips, and after 24 hrs cells were irradiated with 2 Gy ionizing radiation or not irradiated as a negative control. At 1, 4, 8, and 24 hrs after irradiation, cells were fixed in 4% formaldehyde in PBS for 10 minutes, washed with 0.1% PBS Triton-X 100, and incubated with and incubated with rabbit anti-53BP1 (Cell Signaling), anti-γH2AX (Cell Signaling), and Hoechst, followed by incubation with secondary antibodies. Fixed cells were imaged using a DV microscope with a 60X objective. DSB foci were quantified using ImageJ. First, images were cropped to contain individual nuclei. Then a Maximum Entropy Threshold was applied to the 53BP1 and γH2AX channels. These channels were converted to binary, and a composite image of co-localized foci was generated for each nucleus. Finally, co-localized foci were counted using the Analyze Particles plugin.

2.5.7 NHEJ and HR Assay

U-2 OS EJDRs cells were transfected with 100nM pooled ON-TARGETplus siRNAs (Dharmacon) against human BRCA2, XRCC4, STAG1, STAG2, or with non-targeting pool siRNA using the recommended Lipofectamine RNAimax protocol. After three days, a population of cells were collected to verify siRNA depletion, and remaining cells were treated with Shield1 (final concentration is 100 nM) and triamcinolone (TA; final concentration is 1μM) for 24 hrs to stabilize nuclear I-SceI expression and induce double-strand breaks. After four or five more days cells were collected for analysis by flow cytometry. U-

2 OS parental cells served as a -GFP/-dsRed control, and U-2 OS cells with constitutive GFP or dsRed expression served as single-channel controls to gate GFP+ and dsRed+ cells. Approximately 50,000 events were collected for triplicate samples for each control and siRNA perturbation.

2.5.8 Drug Treatments

An initial PARP inhibition experiment was carried out in H4 STAG2 wild type and STAG2 null cells, which were plated on 96-well plates overnight and then treated with a dose curve of Olaparib diluted in DMSO. Final concentration of Olaparib in each well was 5µM, 2.5µM, 1.25µM, 0.625µM, or 0µM. After four days, cells were fixed for 10 min in warmed (37°C) 3% paraformaldehyde and 0.2% Triton-X in PBS by x method and stained with Hoechst to visualize nuclei. Fixed cells were imaged using the Yokogawa CQ-1 microscope with a 10X objective, and nuclei were counted using CQ-1's automated analysis software.

For clonogenic PARP inhibition assays, cells were plated on six-well tissue culture plates, and after 24 hrs, cells were treated with dose curves of Olaparib or Talazoparib. Final concentrations of Olaparib were 80µM, 20µM, 5µM, 1.25µM, 0.08µM, and 0µM for all HCT116 and H4 cell lines and for DLD-1 BRCA2 wild type cells and 100nM, 20µM, 4nM, 0.8nM, 0.16nM, and 0nM for DLD-1 BRCA2 null cells. Final concentrations of Talazoparib were 20µM, 1µM, 1µM, 0.1µM, 0.001µM, 0.0001µM, and 0µM for all HCT116 and H4 cell lines and for DLD-1 BRCA2 wild type cells and 1000nM, 100nM, 1nM, 0.1nM, 0.01nM, and 0nM for DLD-1 BRCA2 null cells. Cells were collected after 7 days (hTERT RPE-

1), 9 days (HCT116 and H4 cells), or 11 days (DLD-1), and extracted crystal violet signal was measured as described previously.

For cell survival assays with HDAC inhibitor treatment, cells were plated overnight on white 384-well plates, and then treated with dose curves of Belinostat or Panobinostat. Compounds were diluted in DMSO across a 10-point, three-fold titration, with an 11^{th} DMSO-only dose point. Final concentrations of Belinostat were 3.00E+01 to 5.08E-04 µM, and final concentrations of Panobinostat were 1.11E+00 to 1.88E-05 µM. After four days, cell survival was quantified by ATPlite Luminescence assay (PerkinElmer) according to the recommended protocol, and luminescence signal was measured using a Microplate Reader (Tecan).

2.5.9 CPAL Screen

The CPAL is a library of small molecule inhibitors curated the Shiau lab consisting of 3 x 384-well plates. Each well contains a unique compound, and each plate contains internal DMSO control wells. The library, titrated across 5 dose-points (10µM, 3µM, 1µM, 0.3µM, 0.1µM), was added by robot to 384-well plates, and the cell lines of interest were dispensed by robot into those same plates. After four days, cell survival was quantified by ATPlite Luminescence assay (PerkinElmer) using a Microplate Reader (Tecan). Dose curves for individual compounds are normalized to internal plate DMSO controls.

2.5.10 RNA-seq

For mRNA-Seq, total RNA was extracted using a Qiagen RNeasy Mini Kit. Total RNA was assessed for quality using an Agilent Tapestation; the RNA Integrity Number (RIN) for samples ranged from 9.7-10. RNA libraries were generated using Illumina's TruSeq Stranded mRNA Sample Prep Kit using 500 ng of total RNA following manufacturer instructions. RNA libraries were multiplexed and sequenced with 50 basepair (bp) single end reads (SR50) to a depth of approximately 25 million reads per sample on an Illumina HiSeq2500 using V4 chemistry for H4 cell lines or to a depth of approximately 40 million reads with Illumina HiSeq4000 by SBS chemistry for hTERT RPE-1 and A673 cell lines. RNA-Seq reads were mapped to the human reference genome (hg19) using STAR with the parameters as suggested by its user manual: --genomeLoad NoSharedMemory \ --runMode alignReads \ --quantMode TranscriptomeSAM \ --outFilterType BySJout \ --outFilterMultimapNmax 20 \ --alignSJoverhangMin 8 \ --alignSJDBoverhangMin 1 \ --outFilterMismatchNmax 999 \ --outFilterMismatchNoverLmax 0.04 \ --alignIntronMin 20 \ --alignIntronMax 1000000 \ --alignMatesGapMax 1000000

After alignment, gene expression was quantified using function 'rsem-calculate-expression' in the RSEM package (RSEM-1.2.25) with the following parameters: --bam --no-bam-output -p 10 --forward-prob 0 \ --estimate-rspd --calc-ci --seed 12345 \

Each experiment contains three replicates which allows us to perform differential expression analysis. Briefly, for each gene, we used the negative binomial test implemented by edgeR to quantify the significance level (p-value) of differential expression between the control and experiment samples. The p-value was then corrected to FDR using Benjamini & Hochberg approach. Genes of FDR less than 0.05 were selected as significantly differentially expressed.

2.6 Acknowledgements

We thank T Waldman and SN Powell for cell lines, J Anzola, D Jenkins, and R Davis for technical assistance, F Meitinger for CRISPR experimental design and reagents, and R Green and R Kabeche for comments on this manuscript. We thank Andy Shiau (Head, Ludwig Small Molecule Discovery Group) for providing inhibitors and for access to high-content imaging and tissue culture equipment. Flow cytometry was performed with the support of the Flow Cytometry Core at the San Diego Center for AIDS Research (P30 A1036214), the VA San Diego Health Care System, and the San Diego Veterans Medical Research Foundation. RNA-seq was conducted at the IGM Genomics Center, University of California, San Diego, La Jolla, CA.

Chapter 2, in part, is currently being prepared for submission for publication. Richardson A, Fang R, Lara-Gonzalez P, Ren B, Oegema K, Desai A. The dissertation author was the primary investigator and author of this material.

Figure 2.1. Cohesion fatigue timing is a functional assay for cohesion strength.

(A) The experimental scheme to measure cohesion fatigue timing. hTERT RPE-1 cells labeled with RFP-tagged histone H2B were treated with pooled siRNA to deplete STAG1, STAG2, or both, or were treated with non-targeting siRNA as a negative control. Cells were then synchronized by single thymidine block, treated with DMSO or with proTAME to arrest cells in metaphase, and finally filmed to follow cells through mitotic entry and mitotic exit or cohesion fatigue. **(B)** Examples of normal mitotic exit in DMSO-treated hTERT RPE1 histone H2B::RFP cells and of cohesion fatigue in proTAME-treated cells. Fatigued chromosomes are indicated by yellow arrows. In these experiments we define cohesion fatigue as beginning when the first visible chromosome falls off the metaphase plate and remains off the metaphase plate. A gamma filter is applied to better visualize fatigued chromosomes. (**C)** Western blot of STAG1 and STAG2 protein levels after 72 hrs of siRNA depletion. Tubulin protein levels are used as a loading control. **(D)** Cohesion fatigue timing in cells treated with non-targeting siRNA, or with co-depleted STAG1 and STAG2, or with singly depleted STAG1 or STAG2. Results are from three combined experiments.

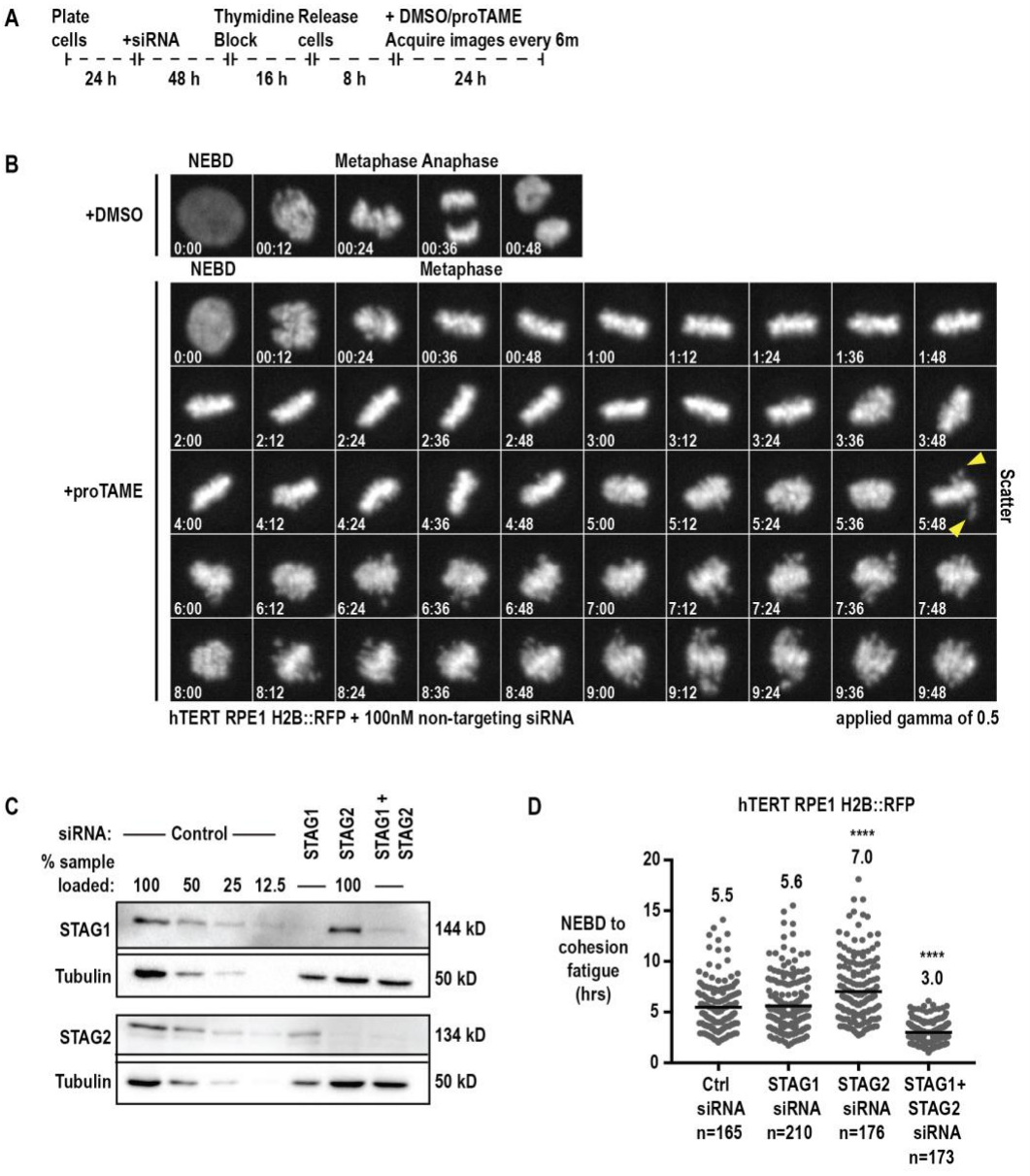
A
Plate cells
+siRNA
Thymidine Block
Release cells
+ DMSO/proTAME
Acquire images every 6m
24 h
48 h
16 h
8 h
24 h
B
NEBD
Metaphase
Anaphase
+DMSO
+proTAME
Scatter
hTERT RPE1 H2B::RFP + 100nM non-targeting siRNA
applied gamma of 0.5
C
siRNA:
Control
STAG1
STAG2
STAG1 + STAG2
% sample loaded:
100
50
25
12.5
100
STAG1
Tubulin
STAG2
Tubulin
144 kD
50 kD
134 kD
50 kD
D
hTERT RPE1 H2B::RFP
NEBD to cohesion fatigue (hrs)
5.5
5.6
7.0
3.0
****
****
Ctrl siRNA n=165
STAG1 siRNA n=210
STAG2 siRNA n=176
STAG1+ STAG2 siRNA n=173

Figure 2.2. Loss of STAG2 does not accelerate cohesion fatigue timing or increase inter-kinetochore stretch.

(A) The experimental scheme to measure cohesion fatigue timing in HCT116 and H4 cells expressing wild type or null mutations of *STAG2*. **(B)** Example images of mitotic timing in DMSO-treated, STAG2 wild type (+) and null (Δ) HCT116 cells and of cohesion fatigue timing after proTAME treatment in the same cell lines. Fatigued chromosomes are indicated by yellow arrows. A gamma filter is applied to better visualize fatigued chromosomes. **(C)** Cohesion fatigue timing in HCT116 cells expressing wild type (+) or null (Δ) *STAG2*. Results are combined from three experiments. **(D)** Cohesion fatigue timing in H4 cells expressing null (Δ) or knock-in (+) *STAG2*. Results are from one experiment. **(E)** Representative images of kinetochore (Ndc80) and centromere (ACA) staining in metaphase hTERT RPE-1 cells treated with non-targeting (Ctrl), STAG1, STAG2, or both siRNA. An example of increased inter-kinetochore stretch in STAG1 and STAG2 co-depleted cells is indicated by a yellow arrow and enlarged in the inset on the right. **(F)** Quantification of the distance between paired Hdc80 foci in control and STAG1- and STAG2-depleted hTERT RPE-1 cells. Distance was measured between Ndc80 foci if the foci were in the same plane and were part of a clear pair of ACA foci. Only metaphase staged cells with nine or more clear foci pairs are included in the analysis. Results are from two combined experiments.

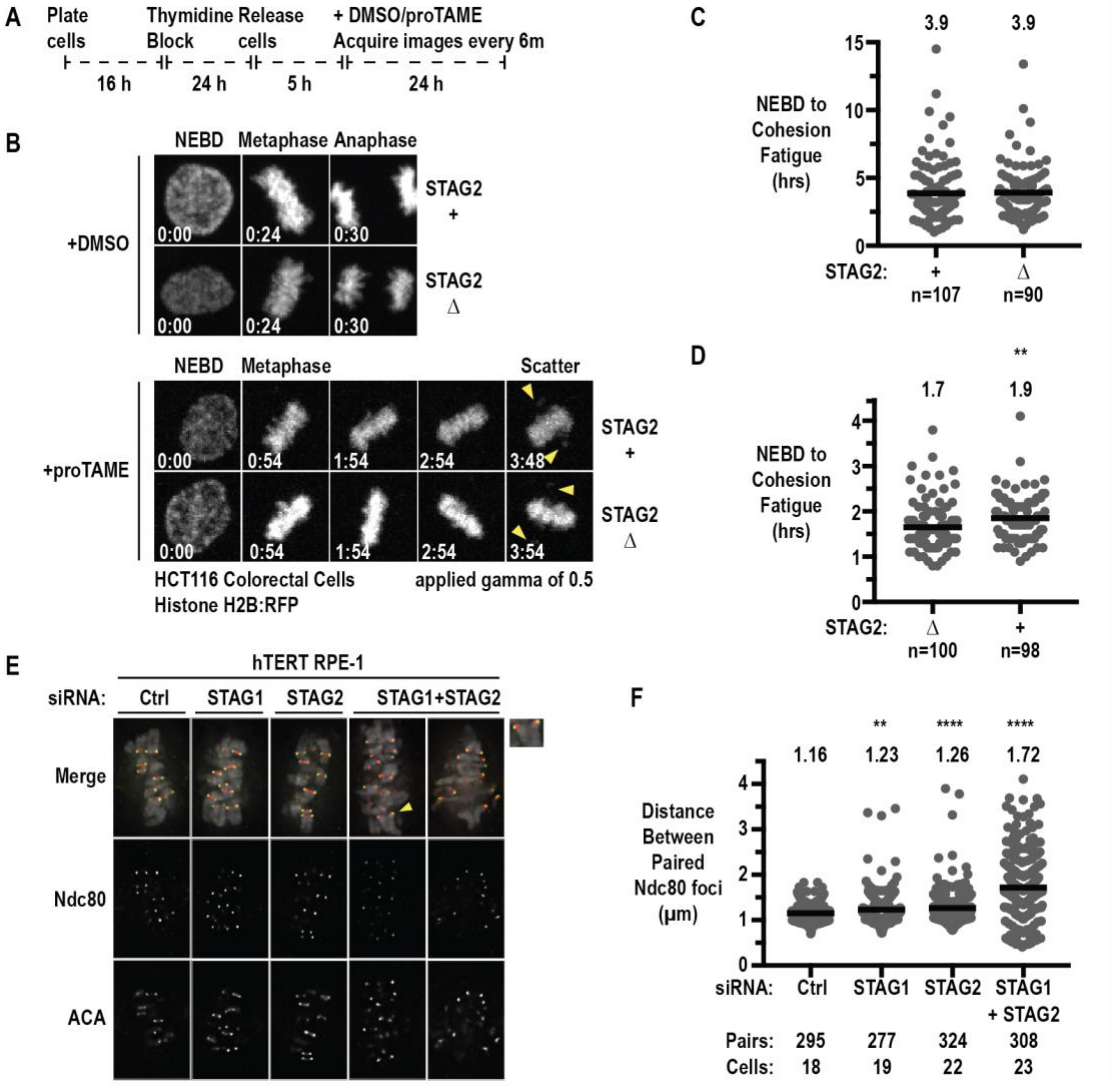
A
Plate cells
Thymidine Block
Release cells
+ DMSO/proTAME
Acquire images every 6m
16 h
24 h
5 h
24 h
B
NEBD
Metaphase
Anaphase
+DMSO
STAG2 +
STAG2 Δ
0:00
0:24
0:30
NEBD
Metaphase
Scatter
+proTAME
0:00
0:54
1:54
2:54
3:48
3:54
HCT116 Colorectal Cells
Histone H2B:RFP
applied gamma of 0.5
C
NEBD to Cohesion Fatigue (hrs)
3.9
3.9
STAG2:
+
Δ
n=107
n=90
D
**
1.7
1.9
NEBD to Cohesion Fatigue (hrs)
STAG2:
Δ
+
n=100
n=98
E
hTERT RPE-1
siRNA:
Ctrl
STAG1
STAG2
STAG1+STAG2
Merge
Ndc80
ACA
F
**
****
****
1.16
1.23
1.26
1.72
Distance Between Paired Ndc80 foci (μm)
siRNA:
Ctrl
STAG1
STAG2
STAG1 + STAG2
Pairs:
295
277
324
308
Cells:
18
19
22
23

Figure 2.3. Loss of STAG2 increases anaphase defects in HCT116 cells but not in H4 cells.

(A) Anaphase defects were quantified in fixed cells immunostained to visualize DNA (Hoechst) and centromeres (ACA). (**B)** Example images of anaphase defects in HCT116 cells. Anaphase defect categories include two types of pre-mitotic defects: chromosome bridges (DNA stretches across the midzone) and acentric fragments (DNA in the midzone with no visible centromere staining), and one type of mitotic defect: lagging chromosomes (non-contiguous DNA in the midzone with centromere staining). **(C)** Quantification of mitotic defects in HCT116 cells expressing wild type (+) or null (Δ) *STAG2*. Error bars are S.D., and an asterix indicates significance in a t-test. **(D)** Quantification of pre-mitotic defects in HCT116 cells expressing wild type (+) or null (Δ) *STAG2*. Error bars are S.D. **(E, F)** Quantification of mitotic and pre-mitotic defects in H4 cells expressing null (Δ) or knock-in (+) STAG. Error bars are S.D.

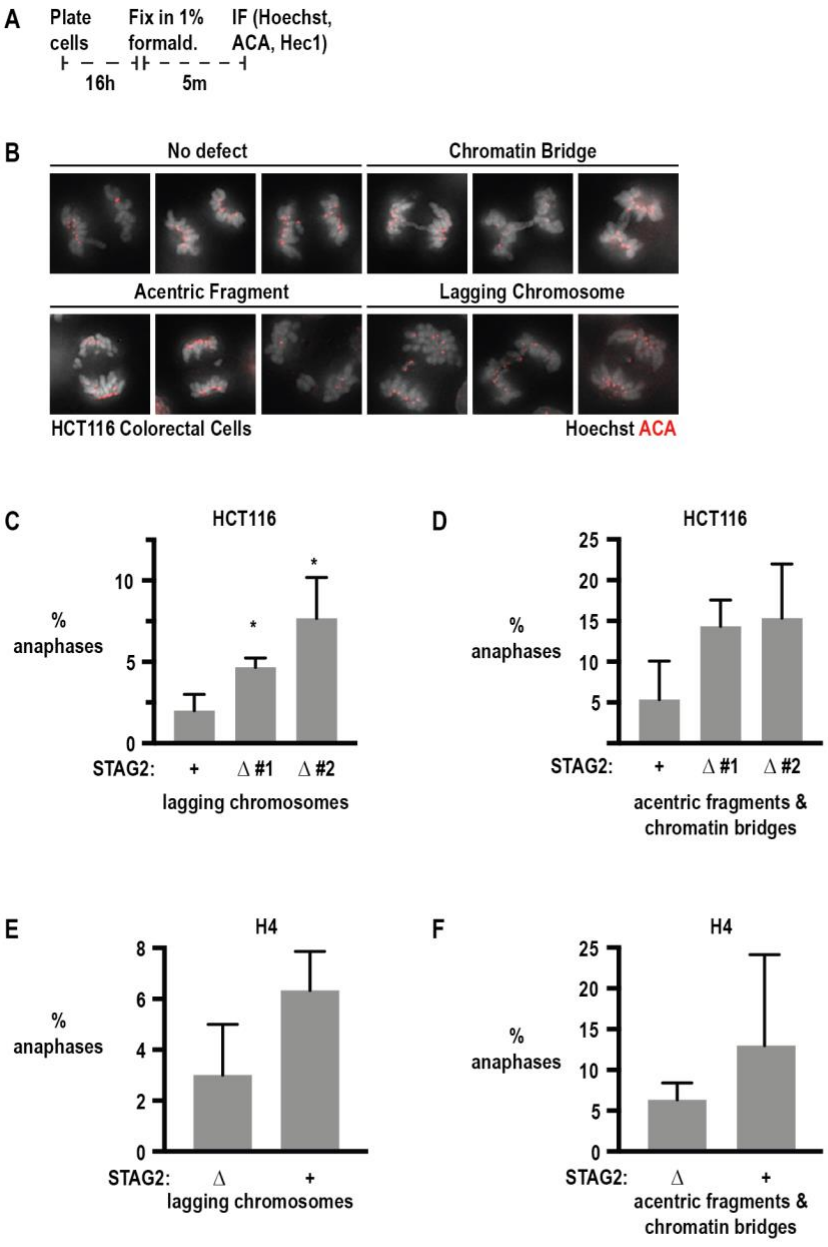
A
Plate cells
Fix in 1% formald.
IF (Hoechst, ACA, Hec1)
16h
5m
B
No defect
Chromatin Bridge
Acentric Fragment
Lagging Chromosome
HCT116 Colorectal Cells
Hoechst ACA
C
HCT116
% anaphases
STAG2: + Δ #1 Δ #2
lagging chromosomes
D
HCT116
% anaphases
STAG2: + Δ #1 Δ #2
acentric fragments & chromatin bridges
E
H4
% anaphases
STAG2: Δ +
lagging chromosomes
F
H4
% anaphases
STAG2: Δ +
acentric fragments & chromatin bridges

Figure 2.4. STAG2 depletion does not affect repair of double-strand breaks by NHEJ or HR.

(A) NHEJ and HR of site-specific DSB were measured using a reporter system developed in U-2 OS cells by Bindra et al. 2013. These cells have two integrated reporter constructs, both with I-SceI cut sites. The first construct contains dsRed under Tet repression. Repair of the inducible DSB through NHEJ may lead to a frame shift, thus disrupting TetR expression and de-repressing expression of dsRed. The second construct contains mutant GFP and a truncated GFP repair template. Repair of an inducible DSB through HR using this template restores GFP expression. **(B)** The experimental scheme to induce site-specific DSBs in U-2 OS EJDRs cells depleted of STAG1, STAG2, or both. An integrated I-SceI construct is normally degraded and transported to the cytoplasm, but nuclear expression is restored in inducible fashion upon addition of two ligands. See Bindra et al. 2013 and the methods section for more information. Repair is measured by flow analysis. **(C)** Western blot of protein depletion at the time of DSB induction. Tubulin is used as a loading control, except for BRCA2 blots, which do not have a loading control. **(D)** Example flow analysis plots. Upper left: untreated U-2 OS EJDRs cells express dsRed and GFP at low basal levels. Middle left: addition of ligands induces DSBs, repair, and thus increases dsRed and GFP expression. Lower left: depletion of BRCA2 results in reduced GFP expression (HR) and increased dsRed expression (NHEJ). Upper right: depletion of STAG2 has little effect on GFP and dsRed expression levels compared to the treated control (middle left). **(E)** Quantification of NHEJ and HR. Results are normalized to % dsRed and GFP expressing cells in the non-targeting siRNA + ligands control. Results are averaged from four experiments, and error bars are S.D.

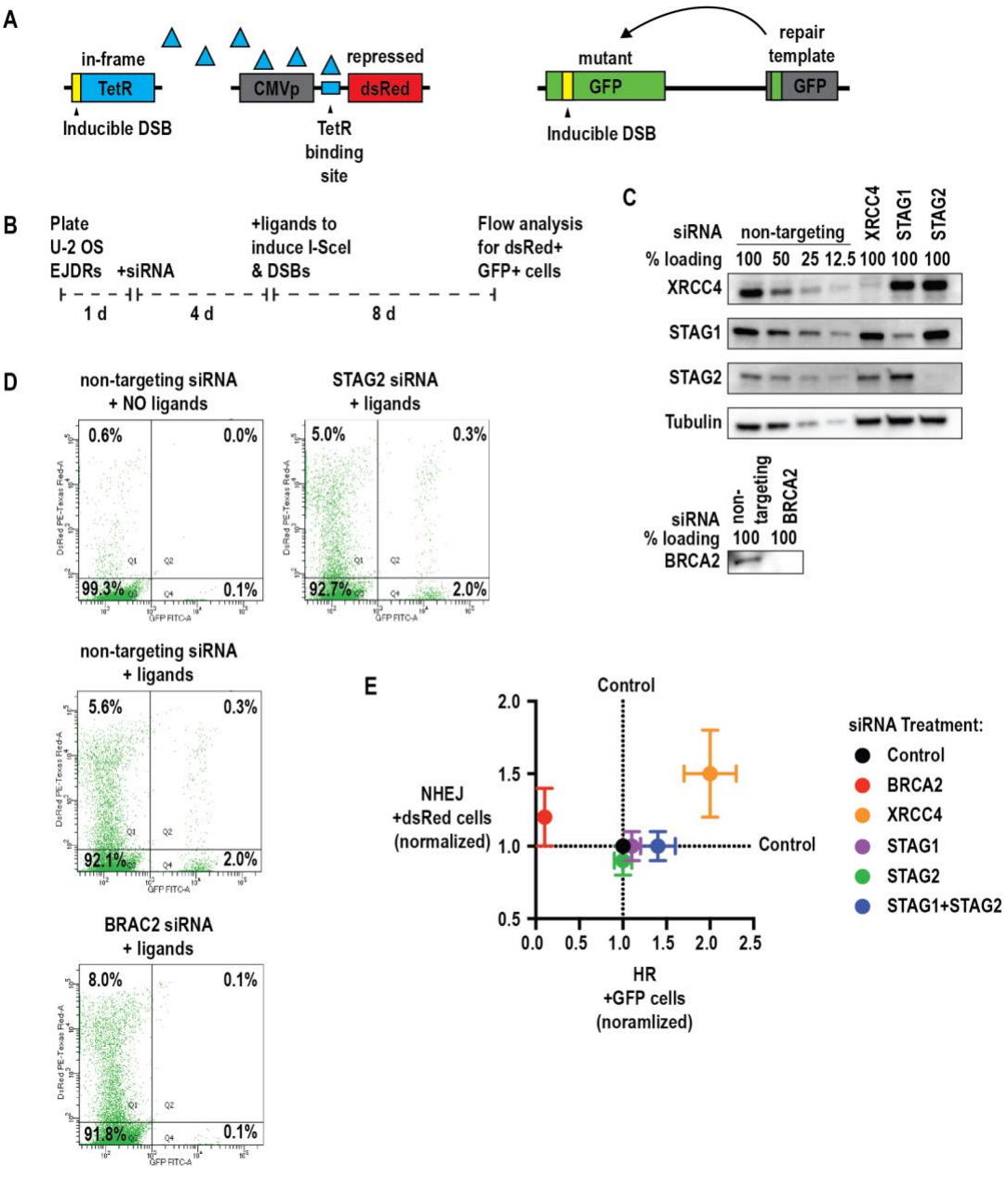
A
in-frame
TetR
Inducible DSB
CMVp
repressed
dsRed
TetR
binding
site
mutant
GFP
repair
template
GFP
Inducible DSB
B
Plate
U-2 OS
EJDRs
+siRNA
+ligands to
induce I-SceI
& DSBs
Flow analysis
for dsRed+
GFP+ cells
1 d
4 d
8 d
C
siRNA
non-targeting
XRCC4
STAG1
STAG2
% loading
100 50 25 12.5 100 100 100
XRCC4
STAG1
STAG2
Tubulin
siRNA
non-targeting
BRCA2
% loading
100 100
BRCA2
D
non-targeting siRNA
+ NO ligands
0.6%
0.0%
99.3%
0.1%
STAG2 siRNA
+ ligands
5.0%
0.3%
92.7%
2.0%
non-targeting siRNA
+ ligands
5.6%
0.3%
92.1%
2.0%
BRAC2 siRNA
+ ligands
8.0%
0.1%
91.8%
0.1%
DsRed PE-Texas Red-A
GFP FITC-A
E
Control
NHEJ
+dsRed cells
(normalized)
Control
HR
+GFP cells
(noramlized)
siRNA Treatment:
Control
BRCA2
XRCC4
STAG1
STAG2
STAG1+STAG2

Figure 2.5. Loss of STAG2 does not sensitize cells to PARP or HDAC inhibition.

(A) Experimental scheme for drug treatment and subsequent quantification of cell survival as measured by nuclei count. **(B)** Quantification of cell survival in H4 cells expressing null (Δ) or knock-in (+) *STAG2*. Results are one experiment with six total replicates per drug dose. **(C)** Experimental scheme for drug treatment and subsequent quantification of cell survival by clonogenic assays. Clonogenic survival was assessed by measuring total crystal violet signal after seven (hTERT RPE-1), nine (H4, HCT116), or 11 (DLD-1) days. **(D)** Quantification of clonogenic cell survival after PARP inhibition (Olaparib or Talazoparib dose curves) in DLD-1 cells expressing wild type (+/+) or null (-/-) BRAC2. Results are from two experiments with four total replicates per drug dose. **(E)** Quantification of clonogenic cell survival after the same PARP inhibition in H4 cells expressing null (Δ) or knock-in (+) *STAG2*. **(F)** Experimental scheme for HDAC inhibition and subsequent quantification of cell survival as measured by total ATP signal. (G) Quantification of cell survival after HDAC inhibition (Belinostat or Panobinostat dose curves) in H4 cells expressing null (Δ) or knock-in (+) *STAG2*. Results are from two experiments with eight total replicates per drug dose.

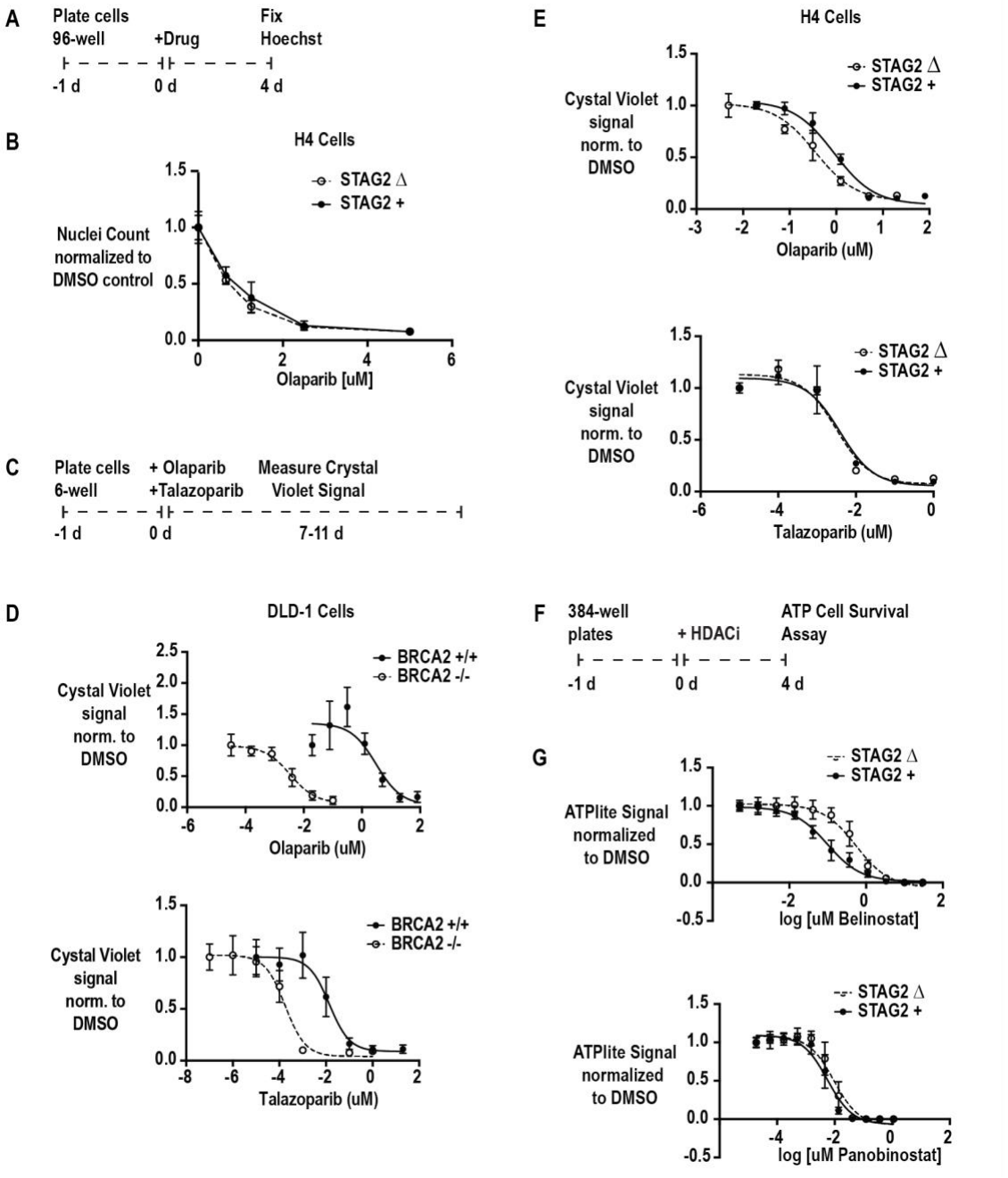
A
Plate cells
96-well
+Drug
Fix
Hoechst
-1 d
0 d
4 d
B
H4 Cells
STAG2 Δ
STAG2 +
Nuclei Count
normalized to
DMSO control
Olaparib [uM]
C
Plate cells
6-well
+ Olaparib
+Talazoparib
Measure Crystal
Violet Signal
-1 d
0 d
7-11 d
D
DLD-1 Cells
BRCA2 +/+
BRCA2 -/-
Cystal Violet
signal
norm. to
DMSO
Olaparib (uM)
Talazoparib (uM)
E
H4 Cells
STAG2 Δ
STAG2 +
Cystal Violet
signal
norm. to
DMSO
Olaparib (uM)
Talazoparib (uM)
F
384-well
plates
+ HDACi
ATP Cell Survival
Assay
-1 d
0 d
4 d
G
STAG2 Δ
STAG2 +
ATPlite Signal
normalized
to DMSO
log [uM Belinostat]
log [uM Panobinostat]

Figure 2.6. STAG2 depletion has a differential effect relative to STAG1 on gene expression in A673 Ewing Sarcoma cells.

(A) Experimental scheme for measuring gene expression in an Ewing sarcoma genetic background. STAG2 wild type A673 cells are depleted of STAG1 or STAG2 by siRNA and then differential gene expression is measured by RNA-seq relative to control A673 cells. **(B)** Western blot of STAG1 and STAG2 protein depletion in A673 cells. Tubulin is used as a loading control. **(C)** Differential gene expression of STAG1-depleted A673 cells relative to control cells (logFC) and gene expression levels (logCPM) are plotted. A logCPM threshold of 2.5 and FDR threshold of < 0.05 are applied to define differentially expressed genes. Up- and down-regulated genes have logFC values that are greater than 0.6 or less than -0.6 respectively. A subset of 31 genes are upregulated by STAG1 depletion and downregulated by STAG2 depletion. These are indicated by a black-outlined circle. Down-regulated STAG1 is indicated by a red-outlined open circle. **(D)** Differential gene expression of STAG2-depleted A673 cells relative to control cells as described previously. Also note the subset of recurrent genes down-regulated by STAG2 depletion that are up-regulated by STAG1 depletion and indicated by black-outlined circles and that STAG2 down-regulated is indicated by a red-outlined open circle.

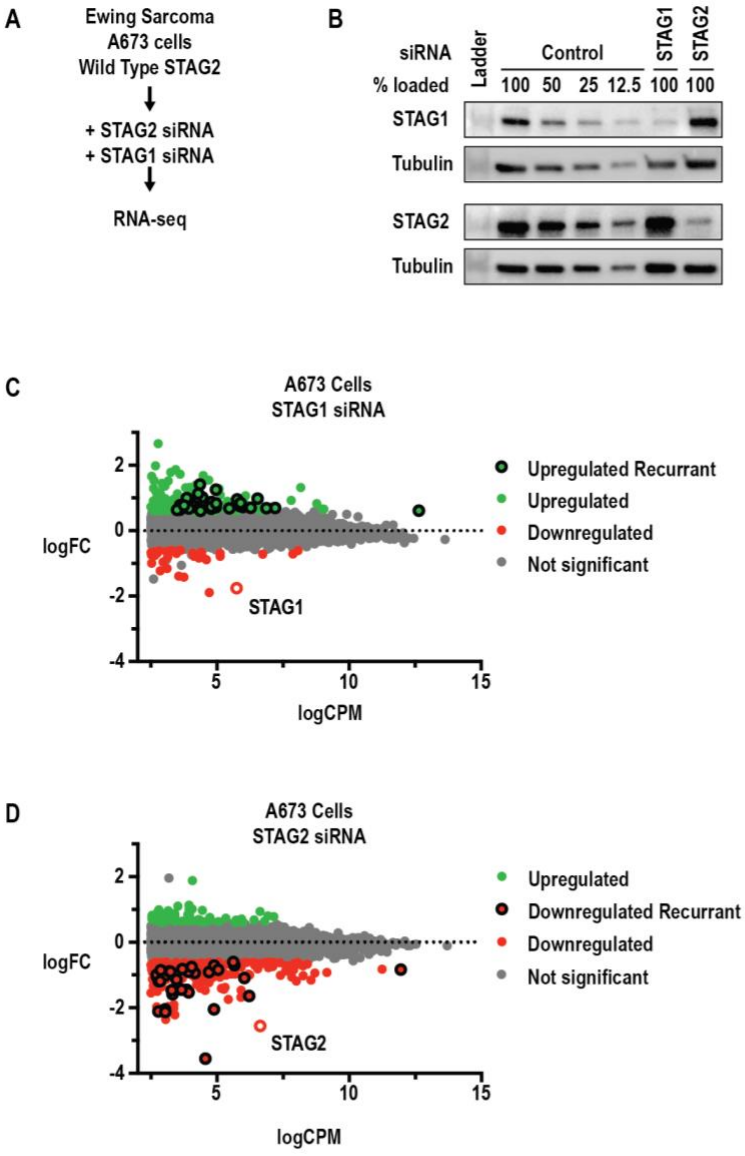
A
Ewing Sarcoma
A673 cells
Wild Type STAG2
+ STAG2 siRNA
+ STAG1 siRNA
RNA-seq
B
siRNA
Ladder
Control
STAG1
STAG2
% loaded
100 50 25 12.5 100 100
STAG1
Tubulin
STAG2
Tubulin
C
A673 Cells
STAG1 siRNA
logFC
logCPM
STAG1
Upregulated Recurrant
Upregulated
Downregulated
Not significant
D
A673 Cells
STAG2 siRNA
logFC
logCPM
STAG2
Upregulated
Downregulated Recurrant
Downregulated
Not significant

Figure S2.1. STAG1 and STAG2 are redundant for cohesin's mitotic functions.

(A) Treatment with proTAME induces cohesion fatigue during a window of proTAME activity. Other mitotic outcomes include anaphase, or a "transition" phenotype which starts with fatigue-like loss of individual chromosomes off the metaphase plate and is quickly followed by anaphase-like separation of two chromosome masses. For our analysis of cohesion fatigue timing, we only counted cells that entered mitosis during the first eight hours of filming when more than 50% of cells exited mitosis with cohesion fatigue. An example plot of mitotic exit is shown for one experiment. **(B)** Anaphase defects (lagging chromosomes, bridges, and micronuclei) in DMSO-treated hTERT RPE-1 histone H2B::RFP cells treated with non-targeting, STAG1, STAG2, or both siRNA. Results are from one experiment. **(C)** Mitotic outcome in DMSO-treated hTERT RPE-1 histone H2B::RFP cells. 100% of cells treated with non-targeting, STAG1, or STAG2 siRNA exit mitosis via anaphase. Only 66.4% of cells treated with STAG1 and STAG2 siRNA exit via anaphase. The other 36.6% of DMSO-treated cells undergo cohesion fatigue. **(D)** Experimental scheme for clonogenic assays. Total crystal violet signal is measured after staining and extraction. See methods section. **(E)** Quantification of total extracted crystal violet signal in hTERT RPE-1 cells is an average of two experiments plated in triplicate.

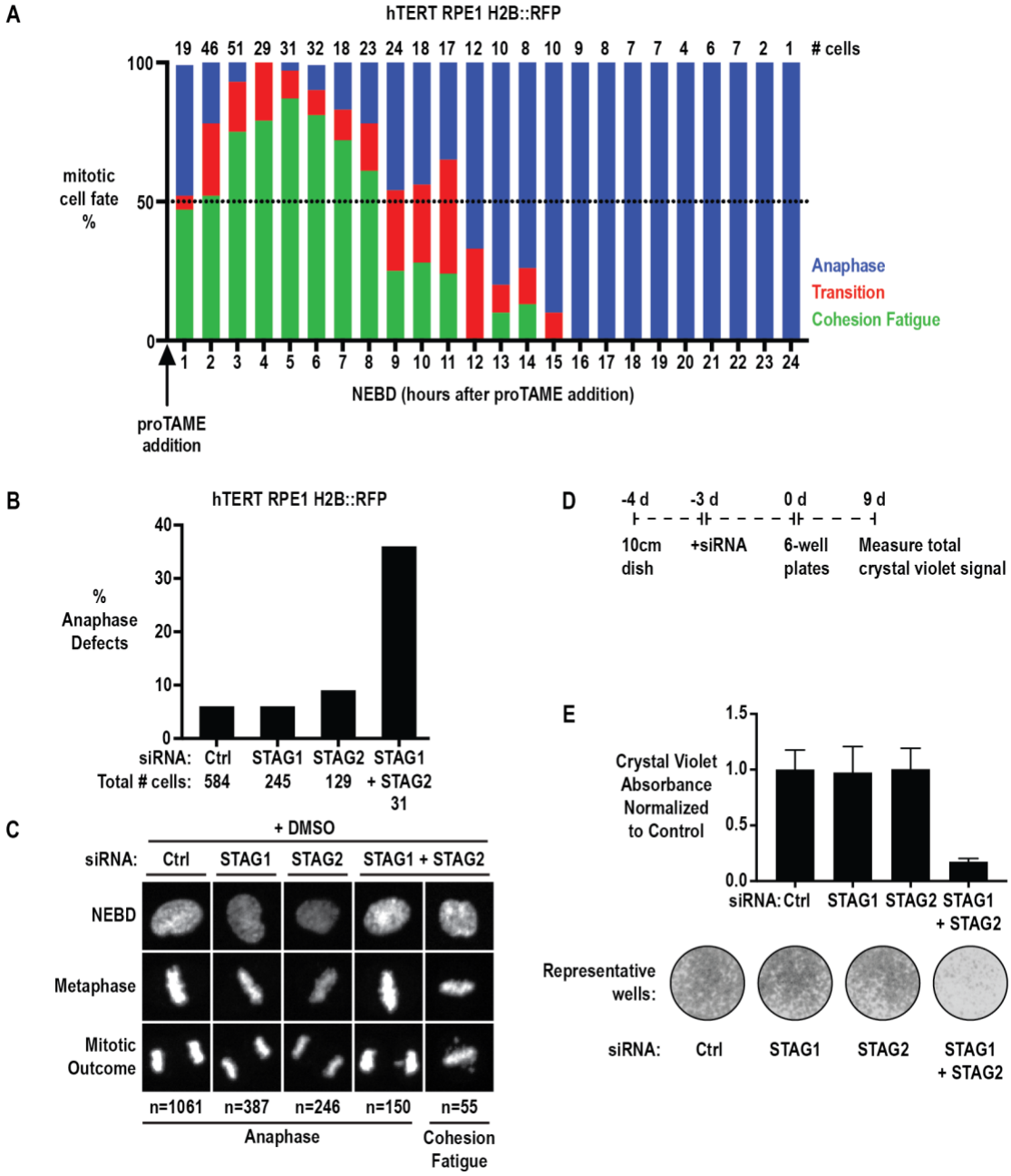
A
hTERT RPE1 H2B::RFP
19 46 51 29 31 32 18 23 24 18 17 12 10 8 10 9 8 7 7 4 6 7 2 1 # cells
100
mitotic cell fate %
50
0
Anaphase
Transition
Cohesion Fatigue
1 2 3 4 5 6 7 8 9 10 11 12 13 14 15 16 17 18 19 20 21 22 23 24
NEBD (hours after proTAME addition)
proTAME addition
B
hTERT RPE1 H2B::RFP
40
% Anaphase Defects
30
20
10
0
siRNA: Ctrl STAG1 STAG2 STAG1 + STAG2
Total # cells: 584 245 129 31
C
+ DMSO
siRNA: Ctrl STAG1 STAG2 STAG1 + STAG2
NEBD
Metaphase
Mitotic Outcome
n=1061 n=387 n=246 n=150 n=55
Anaphase
Cohesion Fatigue
D
-4 d -3 d 0 d 9 d
10cm dish
+siRNA
6-well plates
Measure total crystal violet signal
E
Crystal Violet Absorbance Normalized to Control
1.5
1.0
0.5
0.0
siRNA: Ctrl STAG1 STAG2 STAG1 + STAG2
Representative wells:
siRNA: Ctrl STAG1 STAG2 STAG1 + STAG2

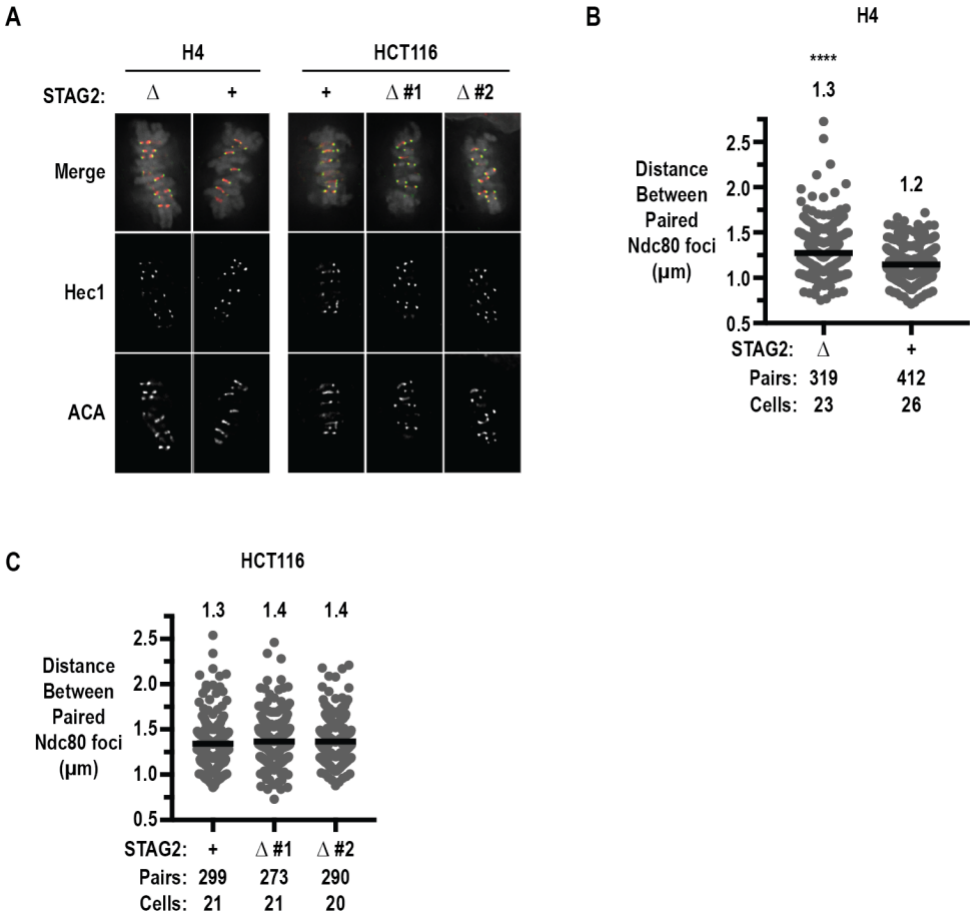

Figure S2.2. Inter-kinetochore stretch is maintained in STAG2 null H4 and HCT116 cells.

(A) Representative images of kinetochore (Ndc80) and centromere (ACA) staining in metaphase H4 and HCT116 cells expressing wild type (+) or null (Δ) *STAG2*. For this experiment, two STAG2 null HCT116 clones were analyzed. Clone 1 is described in Solomon et al., 2011, and clone 2 is mutant S1075X, which is described in Kim et al., 2016. **(B)** Quantification of the distance between paired Hdc80 foci in H4 cell lines as described previously. **(C)** Quantification of the distance between paired Hdc80 foci in HCT116 cell lines as described previously.

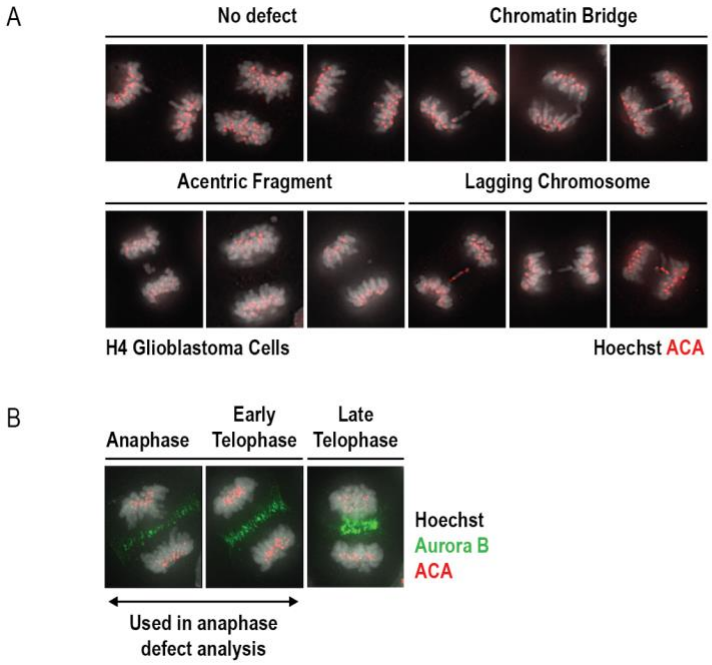

Figure S2.3. Anaphase defect analysis.

(A) Example images of anaphase defects categories in H4 cells as described previously. **(B)** In addition to immunostaining to visualize DNA (Hoechst) and centromeres (ACA), cells were immunostained to visualize the spindle midzone (Aurora B) in order to stage cells at anaphase and early telophase for quantification of anaphase defects.

Figure S2.4. Loss of STAG2 in H4 cells does not impair DSB repair after irradiation.

(A) Experimental scheme for quantifying DSB repair foci after irradiation. **(B)** Example images of DSB repair foci immunostained with 53BP1 and γH2AX (top row) or represented by binary composite images in ImageJ (bottom row). Small foci are indicated in the top left panel by yellow arrows. Co-localized foci counts are indicated in white (top row) or black (bottom row) as obtained by manual or automated analysis respectively. See Methods for more information on the automated analysis. **(C)** Representative images of DSB repair foci in non-irradiated cells and at several timepoints after irradiation. **(D)** Quantification of DSB repair foci by automated analysis. Results are from one experiment and 50+ cells per condition. Error bars are S.D.

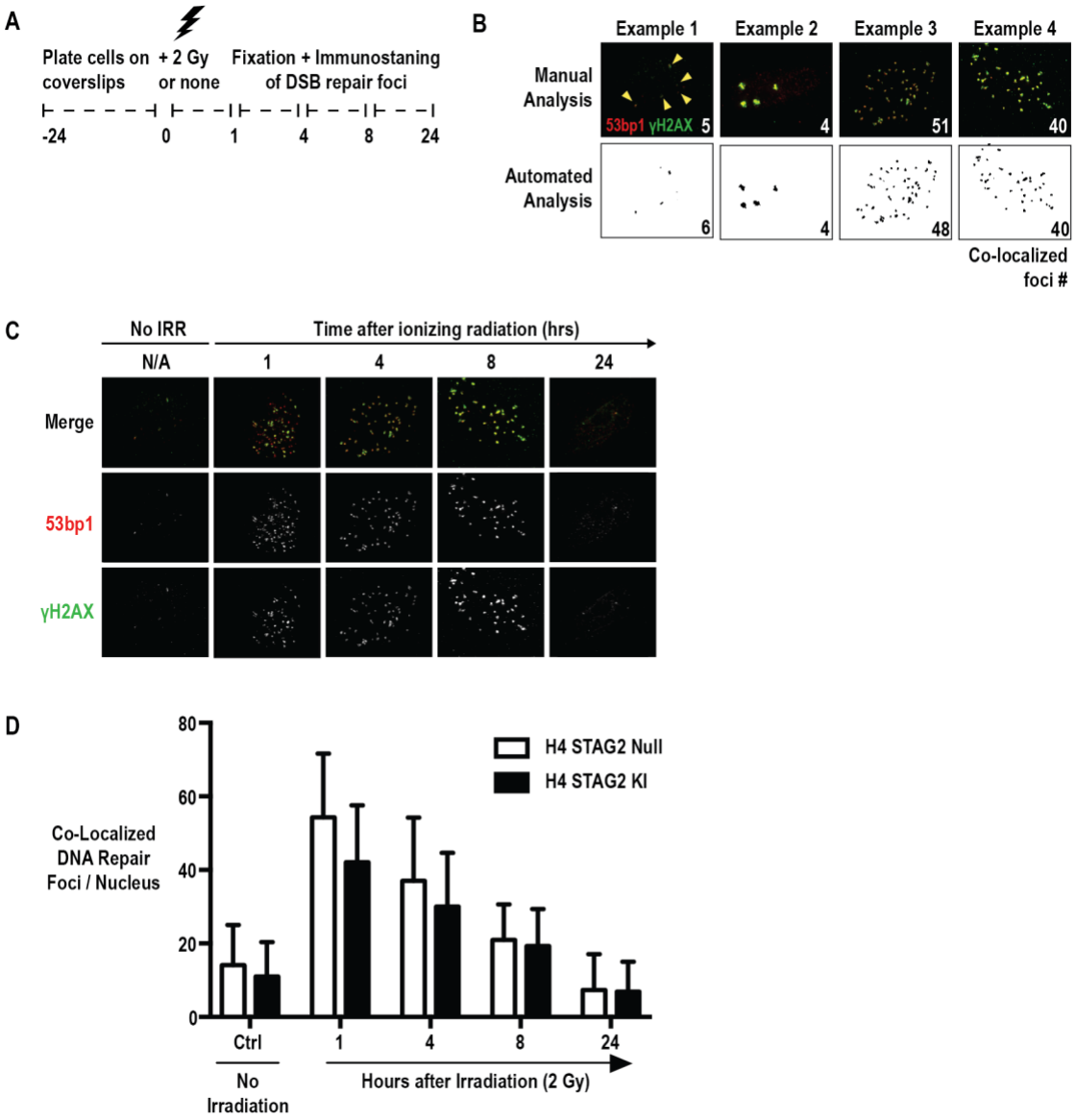
A
Plate cells on coverslips
+ 2 Gy or none
Fixation + Immunostaining of DSB repair foci
-24
0
1
4
8
24
B
Example 1
Example 2
Example 3
Example 4
Manual Analysis
53bp1 γH2AX
5
4
51
40
Automated Analysis
6
4
48
40
Co-localized foci #
C
No IRR
Time after ionizing radiation (hrs)
N/A
1
4
8
24
Merge
53bp1
γH2AX
D
Co-Localized DNA Repair Foci / Nucleus
80
60
40
20
0
H4 STAG2 Null
H4 STAG2 KI
Ctrl
1
4
8
24
No Irradiation
Hours after Irradiation (2 Gy)

Figure S2.5. STAG2 loss does not sensitize HCT116 and hTERT RPE-1 cells to PARP or HDAC inhibition.

(A) Representative images of clonogenic assay wells. **(B-C)** Quantification of clonogenic cell survival after PARP inhibition (Olaparib or Talazoparib dose curves) in HCT116 cells expressing wild type (+) or null (Δ) *STAG2* as previously described or in hTERT RPE-1 cells expressing wild type (+) *STAG1* and *STAG2*, or null (Δ) *STAG1* or *STAG2*. Results are from two experiments with four total replicates per drug dose. **(D-E)** Quantification of cell survival after HDAC inhibition (Belinostat or Panobinostat dose curves) in HCT116 cells expressing wild type (+) or null (Δ) *STAG2* as previously described or in hTERT RPE-1 cells expressing wild type (+) *STAG1* and *STAG2*, or null (Δ) *STAG1* or *STAG2*. Results are from two experiments each with eight total replicates per drug dose per cell line.

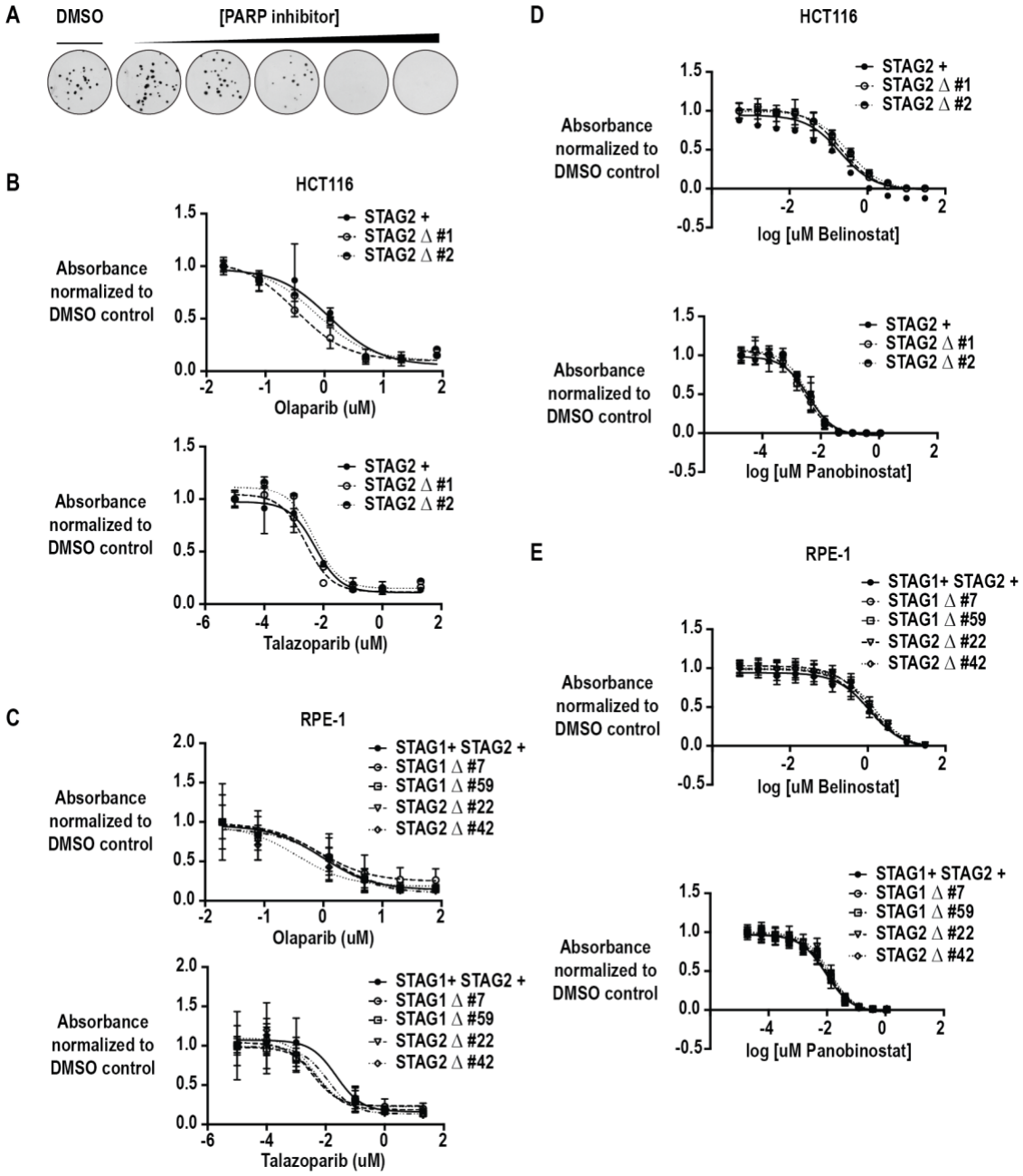
A
DMSO
[PARP inhibitor]
B
HCT116
Absorbance normalized to DMSO control
STAG2 +
STAG2 Δ #1
STAG2 Δ #2
Olaparib (uM)
Talazoparib (uM)
C
RPE-1
STAG1+ STAG2 +
STAG1 Δ #7
STAG1 Δ #59
STAG2 Δ #22
STAG2 Δ #42
D
HCT116
log [uM Belinostat]
log [uM Panobinostat]
E
RPE-1

Figure S2.6. Loss of STAG2 and STAG1 similarly effect gene expression in hTERT RPE-1 cells.

(A) Differential gene expression in a STAG1 null hTERT RPE-1 cell line relative to STAG1 wild type parental cells. A second STAG1 null clone, not pictured, has a similar pattern of gene expression compared to control cells. **(B)** Differential gene expression in a STAG1 null hTERT RPE-1 cell line relative to STAG2 wild type parental cells. A second STAG2 null clone, not pictured, has a similar pattern of gene expression compared to control cells. **(C)** Differential gene expression in STAG2 knock-in cells compared to STAG2 null parental cells.

A

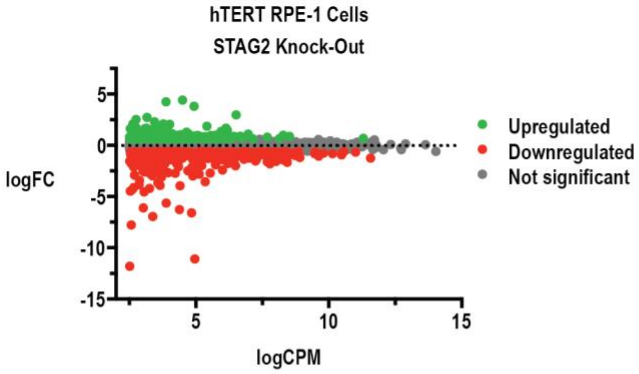
hTERT RPE-1 Cells
STAG2 Knock-Out
logFC
5
0
-5
-10
-15
5
10
15
logCPM
Upregulated
Downregulated
Not significant

B

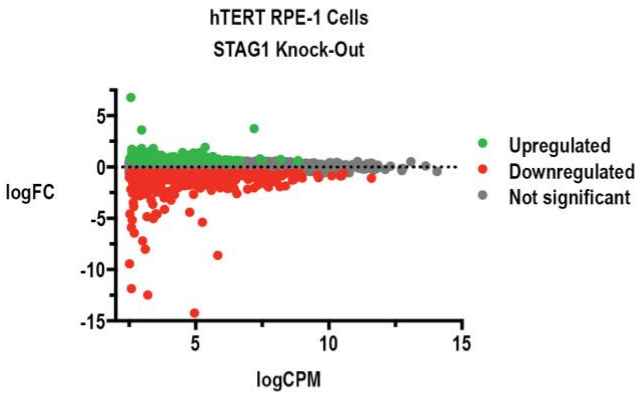
hTERT RPE-1 Cells
STAG1 Knock-Out
logFC
5
0
-5
-10
-15
5
10
15
logCPM
Upregulated
Downregulated
Not significant

C

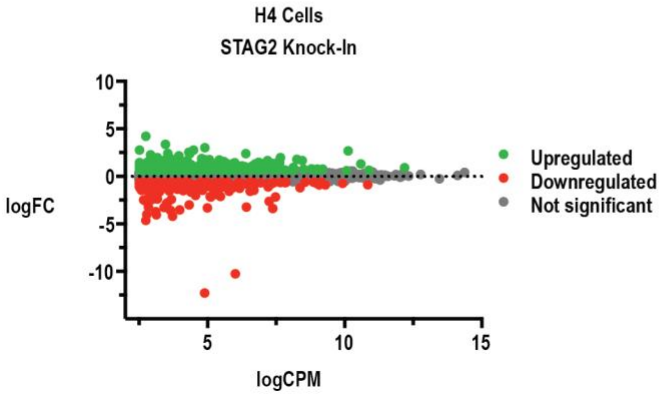
H4 Cells
STAG2 Knock-In
logFC
10
5
0
-5
-10
5
10
15
logCPM
Upregulated
Downregulated
Not significant

Table S2.1. Quantification of anaphase defects upon loss of STAG2 in H4 and HCT116 cells.

Cell Line	*STAG2* Allele	No Defect		Lagging Chromosome(s)		Acentric Fragment(s) Chromosome Bridge(s)	
		#	%	#	%	#	%
H4	Null (Δ)	351	90	12	3	29	7
	Knock-in (+)	331	84	28	7	36	9
HCT116	Wild-type (+)	252	93	6	2	14	5
	Knock-out (Δ #1) Solomon et al. 2011	205	81	12	5	37	15
	Knock-out (Δ #2) Kim et al. 2016, S1075X	240	78	23	7	44	14

Table S2.2. IC50 values for PARP inhibitor-treated cell lines.

Cell Line	Allele	+ Olaparib		
		IC50[1]	IC50[2]	IC50 Fold Change[3]
DLD-1	BRCA2 Wild Type (+/+)	2.55E+00	3.76E+00	-
	BRCA Null (-/-)	5.23E-03	2.27E-03	1073.42
H4	Null (Δ)	6.27E-01	2.18E-01	2.53
	Knock-in (+)	1.24E+00	6.70E-01	-
HCT116	Wild-type (+)	1.23E+00	1.30 E+00	-
	Knock-out (Δ #1) Solomon et al. 2011	4.62E-01	3.32E-01	3.28
	Knock-out (Δ #2) Kim et al. 2016, S1075X	7.47E-01	8.47E-01	1.59
hTERT RPE-1	*STAG1* & *STAG2* Wild Type	1.82E-01	5.04E-01	-
	STAG1 Knock-out (Δ #7)	1.51E-01	5.62E-01	1.05
	STAG1 Knock-out (Δ #59)	7.18E-01	3.79E-01	0.79
	STAG2 Knock-out (Δ #22)	5.45E-01	5.14E-01	0.66
	STAG2 Knock-out (Δ #42)	2.29E-01	1.16E-01	2.57

Cell Line	Allele	+ Talazoparib		
		IC50[1]	IC50[2]	IC50 Fold Change[3]
DLD-1	BRCA2 Wild Type (+/+)	6.31E-03	1.19E-02	-
	BRCA Null (-/-)	1.15E-04	2.61E-04	50.32
H4	Null (Δ)	3.97E-03	2.17E-03	1.36
	Knock-in (+)	4.54E-03	3.42E-03	-
HCT116	Wild-type (+)	4.17E-03	5.38E-03	-
	Knock-out (Δ #1) Solomon et al. 2011	4.78E-03	2.09E-03	1.72
	Knock-out (Δ #2) Kim et al. 2016, S1075X	1.07E-02	4.71E-03	0.77
hTERT RPE-1	*STAG1* & *STAG2* Wild Type	3.98E-03	6.49E-03	-
	STAG1 Knock-out (Δ #7)	3.93E-03	2.91E-03	1.62
	STAG1 Knock-out (Δ #59)	8.91E-03	2.75E-03	1.40
	STAG2 Knock-out (Δ #22)	7.59E-03	3.74E-03	1.13
	STAG2 Knock-out (Δ #42)	6.62E-03	3.15E-03	1.33

[1]Experiment 1
[2]Experiment 2
[3]Average IC50 Fold Change

Table S2.3. IC50 values for HDAC inhibitor-treated cell lines.

Cell Line	Allele	+ Belinostat			
		IC50[1]	IC50[2]	Average IC50	IC50 Fold Change[3]
H4	Null (Δ)	7.99E-01	3.83E-01	5.91E-01	-
	Knock-in (+)	1.64E-01	6.45E-02	1.14E-01	5.19
HCT116	Wild-type (+)	2.47E-01	1.68E-01	2.07E-01	-
	Knock-out (Δ #1) Solomon et al. 2011	2.03E-01	2.27E-01	2.15E-01	0.96
	Knock-out (Δ #2) Kim et al. 2016, S1075X	3.40E-01	2.72E-01	3.06E-01	0.68
hTERT RPE-1	*STAG1* & *STAG2* Wild Type	1.15E+00	1.17E+00	1.16E+00	-
	STAG1 Knock-out (Δ #7)	1.17E+00	1.07E+00	1.12E+00	1.04
	STAG1 Knock-out (Δ #59)	1.33E+00	6.89E-01	1.01E+00	1.15
	STAG2 Knock-out (Δ #22)	2.11E+00	1.16E+00	1.63E+00	0.71
	STAG2 Knock-out (Δ #42)	1.72E+00	1.11E+00	1.42E+00	0.82

Cell Line	Allele	+ Panobinostat			
		IC50[1]	IC50[2]	Average IC50	IC50 Fold Change[3]
H4	Null (Δ)	6.23E-03	1.36E-02	9.92E-03	-
	Knock-in (+)	4.47E-03	7.19E-03	5.83E-03	1.70
HCT116	Wild-type (+)	2.37E-03	5.84E-03	4.10E-03	-
	Knock-out (Δ #1) Solomon et al. 2011	2.41E-03	2.96E-03	2.69E-03	1.53
	Knock-out (Δ #2) Kim et al. 2016, S1075X	2.70E-03	5.09E-03	3.89E-03	1.05
hTERT RPE-1	*STAG1* & *STAG2* Wild Type	6.38E-03	1.37E-02	1.00E-02	-
	STAG1 Knock-out (Δ #7)	8.64E-03	1.19E-02	1.03E-02	0.98
	STAG1 Knock-out (Δ #59)	7.59E-03	1.46E-02	1.11E-02	0.90
	STAG2 Knock-out (Δ #22)	1.05E-02	1.63E-02	1.34E-02	0.75
	STAG2 Knock-out (Δ #42)	8.83E-03	1.65E-02	1.26E-02	0.79

[1]Experiment 1
[2]Experiment 2
[3]Average IC50 Fold Change

Table S2.4. List of genes that are up-regulated by STAG1 depletion and down-regulated by STAG2 depletion in A673 Ewing Sarcoma cells.

	STAG2 siRNA		STAG1 siRNA	
Recurrent Gene	**logFC**	**FDR**	**logFC**	**FDR**
DGKK	-3.56	1.96E-11	0.75	4.58E-05
EHD2	-2.13	9.50E-09	0.74	4.87E-05
MMP9	-2.11	3.20E-09	1.41	2.11E-07
ADORA2A	-2.05	2.00E-09	0.86	6.05E-06
NID2	-2.05	9.50E-11	0.72	4.37E-06
SERTM1	-1.64	9.50E-11	0.69	4.37E-06
CEACAM6	-1.59	1.79E-08	0.88	1.87E-06
FRZB	-1.53	3.91E-08	0.83	2.86E-04
FBLN7	-1.47	2.86E-08	1.02	2.63E-06
LGALS3	-1.46	1.36E-08	0.67	3.49E-05
FBLN5	-1.45	5.52E-07	1.25	6.45E-07
ITGB2	-1.19	2.68E-06	1.00	1.07E-04
SYNM	-1.19	3.92E-05	0.77	1.41E-03
NEDD9	-1.14	5.92E-07	0.67	1.30E-04
ATP8B1	-1.09	8.08E-09	0.69	6.91E-06
OLFML2A	-1.06	2.53E-06	0.78	3.19E-05
PIPOX	-1.01	1.40E-06	0.86	6.05E-06
KIAA1644	-0.99	5.73E-06	0.64	3.26E-04
SYNDIG1	-0.94	4.01E-07	0.72	2.23E-05
CRIP1	-0.91	9.25E-07	0.68	3.01E-05
FOS	-0.90	1.57E-03	1.13	1.36E-02
ITGA7	-0.90	1.29E-06	0.87	2.63E-06
LOXL2	-0.89	1.33E-05	0.67	7.71E-04
OLFML2B	-0.85	1.49E-05	0.64	2.45E-04
SERPINF1	-0.84	3.06E-05	0.84	9.12E-05
FN1	-0.83	4.71E-07	0.61	8.24E-05
LONRF2	-0.82	3.55E-05	0.61	2.01E-03
KREMEN1	-0.75	3.96E-06	0.73	1.07E-04
PCOLCE	-0.71	1.28E-06	0.96	1.15E-07
PDGFRB	-0.70	2.60E-07	0.98	9.86E-08
TSPAN8	-0.60	9.01E-06	0.70	6.50E-06

Table S2.5. List of genes that are down-regulated by STAG2 loss or depletion in more than one cell type.

Genes	# Cell Types	Cell Types
CLSTN2	3	A673, H4, HTERT RPE-1
COL1A1	3	A673, H4, HTERT RPE-1
NID2	3	A673, H4, HTERT RPE-1
PAG1	3	A673, H4, HTERT RPE-1
PDGFRB	3	A673, H4, HTERT RPE-1
RAB3B	3	A673, H4, HTERT RPE-1
SERPINE1	3	A673, H4, HTERT RPE-1
ABCA7	2	A673, HTERT RPE-1
ADCY9	2	A673, HTERT RPE-1
ALDH6A1	2	A673, HTERT RPE-1
APOL6	2	A673, HTERT RPE-1
ASL	2	A673, HTERT RPE-1
BEX1	2	A673, HTERT RPE-1
CASP1	2	A673, HTERT RPE-1
EHD2	2	A673, HTERT RPE-1
EMP1	2	A673, HTERT RPE-1
FAM49A	2	A673, HTERT RPE-1
FN1	2	A673, HTERT RPE-1
FOS	2	A673, HTERT RPE-1
G0S2	2	A673, HTERT RPE-1
ITGA7	2	A673, HTERT RPE-1
KIAA1161	2	A673, HTERT RPE-1
KIAA1644	2	A673, HTERT RPE-1
KLHDC8B	2	A673, HTERT RPE-1
KRT8	2	A673, HTERT RPE-1
LGALS3	2	A673, HTERT RPE-1
LPAR1	2	A673, HTERT RPE-1
NCKAP5	2	A673, HTERT RPE-1
NEDD9	2	A673, HTERT RPE-1
OLFML2A	2	A673, HTERT RPE-1
PCDHGC3	2	A673, HTERT RPE-1
PDE4DIP	2	A673, HTERT RPE-1
PTK2B	2	A673, HTERT RPE-1
S1PR3	2	A673, HTERT RPE-1

Table S2.5. List of genes that are down-regulated by STAG2 loss or depletion in more than one cell type, continued

SERPINE2	2	A673, HTERT RPE-1
SLC26A2	2	A673, HTERT RPE-1
SMPD1	2	A673, HTERT RPE-1
STAG2	2	A673, HTERT RPE-1
SYNM	2	A673, HTERT RPE-1
TGIF2-C20orf24	2	A673, HTERT RPE-1
EPHB3	2	A673, H4
GPR160	2	A673, H4
LONRF2	2	A673, H4
LOXL2	2	A673, H4
P2RY1	2	A673, H4
SCG2	2	A673, H4
SLC1A1	2	A673, H4
STEAP1	2	A673, H4
TNFAIP6	2	A673, H4
ABCA1	2	H4, HTERT RPE-1
ADAMTS12	2	H4, HTERT RPE-1
ADAMTS15	2	H4, HTERT RPE-1
ARHGDIB	2	H4, HTERT RPE-1
CACNG8	2	H4, HTERT RPE-1
CHST2	2	H4, HTERT RPE-1
CRISPLD2	2	H4, HTERT RPE-1
CTGF	2	H4, HTERT RPE-1
DIO2	2	H4, HTERT RPE-1
DKK1	2	H4, HTERT RPE-1
DUSP6	2	H4, HTERT RPE-1
FST	2	H4, HTERT RPE-1
GADD45B	2	H4, HTERT RPE-1
GFPT2	2	H4, HTERT RPE-1
GPRC5A	2	H4, HTERT RPE-1
HBEGF	2	H4, HTERT RPE-1
HHIP	2	H4, HTERT RPE-1
IER3	2	H4, HTERT RPE-1
IFFO2	2	H4, HTERT RPE-1
ITGA11	2	H4, HTERT RPE-1

Table S2.5. List of genes that are down-regulated by STAG2 loss or depletion in more than one cell type, continued

KRT7	2	H4, HTERT RPE-1
KRT81	2	H4, HTERT RPE-1
LACTB	2	H4, HTERT RPE-1
LBH	2	H4, HTERT RPE-1
LOC728392	2	H4, HTERT RPE-1
LTBP2	2	H4, HTERT RPE-1
MDGA1	2	H4, HTERT RPE-1
MICAL2	2	H4, HTERT RPE-1
NAT8L	2	H4, HTERT RPE-1
NTN4	2	H4, HTERT RPE-1
NUAK2	2	H4, HTERT RPE-1
NUP210	2	H4, HTERT RPE-1
PDGFRA	2	H4, HTERT RPE-1
PELI2	2	H4, HTERT RPE-1
PXDC1	2	H4, HTERT RPE-1
SHROOM2	2	H4, HTERT RPE-1
SHROOM3	2	H4, HTERT RPE-1
SLC7A5	2	H4, HTERT RPE-1
SRGN	2	H4, HTERT RPE-1
THBS1	2	H4, HTERT RPE-1
TNFRSF21	2	H4, HTERT RPE-1
ZNF469	2	H4, HTERT RPE-1

CHAPTER 3: P53 ACTIVATION IS NOT AN OBLIGATORY CONSEQUENCE OF CHROMOSOME MIS-SEGREGATION

3.1 Summary

Aneuploidy, a state of karyotype imbalance, is a hallmark of cancer. Changes in chromosome copy number have been proposed to drive disease by modulating the dosage of cancer driver genes and by promoting cancer genome evolution. Given the potential of cells with abnormal karyotypes to become cancerous, do pathways that limit the prevalence of such cells exist? Are cells able to recognize a single mis-segregation event as has been previously proposed, or do they rely on other mechanisms to arrest potentially unfit cells? We investigated the immediate consequences of mis-segregation (aneuploidy) and mitotic delay by live cell imaging and discovered two possible outcomes after mis-segregation events. The majority of mis-segregation events do not lead to immediate cell-cycle arrest; instead, we found that delayed mitotic timing was responsible for most observed cell-cycle arrest. A much smaller portion of mis-segregation events do lead to immediate p53-dependent arrest, but this arrest is likely a result of subsequent acquired DNA damage and is not a direct consequence of aneuploidy.

3.2 Introduction

In all organisms analyzed to date, aneuploidy, an unbalanced karyotype in which one or more chromosomes are present in excess or reduced copy number,

is highly detrimental (Santaguida and Amon, 2015a). Aneuploid budding and fission yeast show proliferation defects under standard growth conditions (Niwa et al., 2006; Torres et al., 2007). In multicellular organisms, chromosomal gain or loss is largely lethal (Hodgkin, 2005; Lindsley et al., 1972; Lorke, 1994). In humans, for example, all monosomies and most trisomies cause embryonic lethality (Reviewed in Hassold and Hunt, 2001). Only trisomy of the gene poorest chromosome, chromosome 21, is compatible with survival into adulthood. However, even this trisomy leads to high levels of embryonic lethality. Only 12.5% of trisomy 21 fetuses survive to birth (Reviewed in Roper and Reeves, 2006).

The adverse effects of an incorrect karyotype are also observed at the cellular level. Aneuploid mammalian and yeast cells exhibit metabolic alterations (Williams et al., 2008), proliferation defects (Santaguida et al., 2015; Stingele et al., 2012; Tang et al., 2011; Thompson and Compton, 2010; Torres et al., 2007; Williams et al., 2008), genome instability (Blank et al., 2015; Meena et al., 2015; Ohashi et al., 2015; Passerini et al., 2016; Sheltzer et al., 2011; Zhu et al., 2012), and proteotoxic stress (Oromendia et al., 2012; Santaguida et al., 2015; Santaguida and Amon, 2015b; Stingele et al., 2012; Tang and Amon, 2013), and aneuploid mammalian cells have been reported to activate p53 (Hinchcliffe et al., 2016; Li et al., 2010; López-García et al., 2017; Sansregret et al., 2017; Thompson and Compton, 2010). In addition to traits observed in a broad range of aneuploidies, aneuploid cells exhibit gene-specific phenotypes in which changes

in dosage of a particular gene cause a specific phenotype (e.g., Dodgson et al., 2016).

Paradoxically, despite the adverse effects of an aneuploid karyotype on normal cell physiology, the condition is also a hallmark of cancer, a disease characterized by excessive cell proliferation. Ninety percent of solid tumors harbor whole chromosome gains and/or losses (Gordon et al., 2012; Holland and Cleveland, 2009). Multiple, not mutually exclusive hypotheses have been put forth to explain the prevalence of abnormal karyotypes in cancer. Chromosome copy-number alterations have been proposed to drive disease by modulating the dosage of cancer driver genes (Davoli et al., 2013). Aneuploidy also endows cells with phenotypic variability (Beach et al., 2017; Chen et al., 2015; Rutledge et al., 2016), which could help facilitate metastasis or resistance to therapeutic interventions. Indeed, aneuploidy has been shown to be associated with metastatic behavior, resistance to chemotherapy and poor patient outcome (Bakhoum et al., 2011; Heilig et al., 2009; Lee et al., 2011; Walther et al., 2008). Finally, the process of chromosome mis-segregation and aneuploidy of many chromosomes have been shown to cause genomic instability (Blank et al., 2015; Crasta et al., 2012; Janssen et al., 2011; Ohashi et al., 2015; Passerini et al., 2016; Sheltzer et al., 2011; Zhu et al., 2012), which could fuel cancer genome evolution.

Given the potential link between aneuploidy and tumorigenesis, it is critical to understand how abnormal karyotypes affect cellular physiology. Here, we

examine the immediate consequences of chromosome mis-segregation. We demonstrate, by live cell imaging of mis-segregating mother cells and their daughters, that most mis-segregation events do not trigger immediate arrest in the next cell cycle. Instead, we show, as previously published (Uetake and Sluder, 2010), that a mitotic timer triggers immediate G_1 arrest in the next cell cycle after mother cells take longer than ~100 min to accomplish mitosis.

3.3.1 Chromosome mis-segregation and subsequent G_1 arrest increase with increased mitotic timing

Previous studies reported that chromosome mis-segregation causes p53 activation and a p53-dependent cell-cycle arrest (Li et al., 2010; Thompson and Compton, 2010). The aneuploid state per se or events accompanying chromosome mis-segregation could be responsible for this p53 activation. To distinguish between these possibilities, we examined the immediate consequences of chromosome mis-segregation using live cell imaging.

Several methods have been developed to induce chromosome mis-segregation. For example, compounds that interfere with microtubule dynamics or microtubule-kinetochore attachment cause a Spindle Assembly Checkpoint (SAC)-dependent delay in mitosis and induce chromosome mis-segregation. Inducing chromosome mis-segregation in this manner was shown to be associated with p53 activation in the subsequent G_1 phase (Thompson and Compton, 2010).

However, mitotic arrest exceeding ~100 min induces a p53 dependent G_1 arrest irrespective of whether or not chromosomes are mis-segregated (Uetake and Sluder, 2010). We too observed his phenomenon. We analyzed cells that experienced an extended mitosis induced by the kinesin Eg5 inhibitor monastrol by live cell imaging (Mayer et al., 1999). This analysis showed that the frequency of chromosome mis-segregation and subsequent G_1 arrest increased with time spent in mitosis (Fig. S3.1), highlighting that without live imaging it is difficult to compare fates of cells with and without mis-segregation due to the missing information about arrest duration.

3.3.2 Mitotic timing and not aneuploidy causes G_1 arrest in daughter cells

To avoid G_1 arrest caused by a prolonged mitosis, we generated aneuploid cells by interfering with SAC function rather than by activating the checkpoint. SAC inactivation does not delay cells in mitosis but instead accelerates progression through this cell-cycle stage even when chromosomes are not attached to the spindle correctly (Fig. S3.2A), and results in aneuploid progeny.

We examined hTERT immortalized RPE-1 cells stably expressing proliferating cell nuclear antigen (PCNA)-GFP (to determine S-phase initiation) and RFP-H2B (to monitor chromosome segregation) grown in the presence of NMS-P715 or reversine. Both compounds inhibit the SAC kinase Mps1 (Colombo et al., 2010; Santaguida et al., 2010). Treatment with NMS-P715 or reversine led

to severe chromosome segregation defects. Each chromosome mis-segregated in 6%–8% of mitoses (Fig. S3.2D-F and Santaguida et al., 2015) and virtually all cells harbored lagging chromosomes during anaphase and micronuclei in the following G_1 (Fig. 3.1A, Fig. S3.2-C). Despite severe chromosome mis-segregation, however, mitotic arrest did not occur but cells in fact progressed through mitosis faster than vehicle-control treated cells (Fig. S3.2A). Notably, chromosome mis-segregation did not lead to arrest in the following G_1 in the vast majority of aneuploid daughter cells (~80%; Fig. 3.1B). This finding indicates that aneuploidy per se does not cause cell cycle arrest in G_1. Although 80% of cells that mis-segregated chromosomes continued to divide, 9% of cells arrested in G_1.

3.4 Discussion

It was previously reported that chromosome mis-segregation induced by interference with spindle function causes p53 activation (Thompson and Compton, 2010). This observation led to the interesting proposal that the cells somehow ‘‘know’’ how many chromosomes they have and that a chromosome number that deviates from the euploid karyotype triggers a p53 response. However, chromosome mis-segregation brought about by interfering with spindle function results in a mitotic delay, which when it exceeds 100 min causes p53 activation in the subsequent G_1 phase irrespective of whether or not chromosome mis-segregation occurred (Uetake and Sluder, 2010), and requires the DNA damage binding protein 53BP1 and the deubiquitinating enzyme USP28

(Lambrus and Holland, 2017). To examine the effects of chromosome mis-segregation on cell-cycle progression without this complication, we used methods to interfere with chromosome segregation that accelerated rather than delayed mitosis. Live cell imaging of cells induced to mis-segregate chromosomes in this manner showed that the vast majority of cells that mis-segregate chromosomes do not delay or arrest in G_1 following chromosome mis-segregation. p53 activation and a p53-dependent cell-cycle arrest do not occur in cells harboring constitutive aneuploidies either (Sheltzer et al., 2017; Tang et al., 2011), further supporting the idea that aneuploidy per se does not trigger a p53-dependent G_1 arrest. Additional work from this paper that is not included in this dissertation chapter suggests that the small portion of cells that do arrest immediately after mis-segregation do so indirectly as a result of aneuploidy-induced DNA damage or possibly physiological stress, both of which can activate p53-dependent arrest. Taken together these results clarify that cells do not count chromosomes, but instead rely on a mitotic timer and indirect p53 activation to arrest potentially damaged cells.

3.5 Materials & Methods

3.5.1 Experimental Model and Subject Details

RPE-1 hTERT cell lines and MEFs were cultured in DMEM (Invitrogen) supplemented with 10% FBS, 2 mM L-glutamine and 100 U/ml penicillin/streptomycin. Cells were grown at 37°C with 5% CO_2 in a humidified environment. To generate an RPE-1 hTERT cell line co-expressing GFP-PCNA

and H2B-RFP, cells were transduced with pBABE-Puro, a vector encoding human histone H2B C-terminally fused to mRFP1.3 (gift from Don Cleveland), and with an MGC collection human PCNA cDNA engineered to harbor an N-terminal eGFP fusion and cloned into pBABE-Hygro. A population of cells expressing both transgenes at moderate levels was selected by fluorescence activated cell sorting (FACS). This cell population was then cultured in DMEM/F12 (Invitrogen) supplemented with 10% FBS and 100U/ml penicillin/streptomycin and grown at 37°C with 5% CO_2 in a humidified environment.

3.5.2 Drug Treatments

Reversine was obtained from Cayman Chemical or Sigma-Aldrich and used at a working concentration of 0 5 μM or 2 μM; Monastrol (working concentration 100 μM) was obtained from Tocris; NMS-P715 (working concentration 1 μM) was obtained from EMD/Millipore.

3.5.3 Cell Imaging Methods Video Microscopy

Live cell imaging was performed either using a Yokagawa CQ1 spinning disk confocal (40x objective, reversine-treated cells) or Yokogawa CV1000 (20x objective, monastrol-treated cells). All microscopes were equipped with an incubation chamber maintained at 37°C in an atmosphere of 5% CO_2. For experiments described in Fig. S3.1, unsynchronized RPE-1 hTERT GFP-PCNA H2B-RFP cells were plated on Greiner SCREENSTAR 96-well plates (#655866), incubated overnight, and then treated with DMSO or 100 μM monastrol and

immediately filmed for 6 hrs using a Yokagawa CV1000 microscope with a 20x objective. After 6 hours plates were removed, cells were washed twice with complete medium, and returned to the microscope for an additional 50 hrs of filming. Because cells were unsynchronized, mother cells entered mitosis throughout monastrol treatment and thereby experienced variable mitotic delays. After drug washout, the mother cells exited mitosis and the cell cycle progression of their daughter cells was tracked. Images were acquired every 10 min for the first 8 hrs to capture mother cell mitotic timing and mis-segregation events, and then every 20 min to capture daughter cell cycle progression.

To quantify daughter cell S phase timing after chromosome mis-segregation in the mother cell, unsynchronized RPE1 hTERT GFP-PCNA H2B-RFP cells were plated on Greiner SCREENSTAR 96-well plates (#655866), incubated overnight, and then treated with DMSO, 0 5 µM, or 2 µM reversine. Cells were immediately filmed on a Yokagawa CQ1 with a 40x objective. Images were acquired every 5 minutes for 5 hrs and then every 20 min for a total of 48 hrs. Reversine was not washed out for the duration of the experiment. Because cells were unsynchronized, we determined the time from PCNA focus appearance to disappearance for two types of cells. The first type (G_1) were cells that progressed through mitosis before drug treatment and hence were exposed to reversine only during G_1 and S phase. The second type (G_2) were the daughters of mother cells that progressed through mitosis in the presence of reversine and had mis-segregated their chromosomes. To track daughter cell

cycle fate after mother cells had mis-segregated chromosomes, RPE-1 hTERT GFP-PCNA H2B-RFP cells were plated on 96-well cycloolefin plates overnight, treated with DMSO or 1 μM NMS-P715 and immediately filmed on a Yokagawa CV1000 microscope using a 20x objective. Images were acquired every 10 min for 8 hrs to capture mother cell mitosis and then every 15 min for 2 days to track daughter cell fate.

3.6 Acknowledgements

Conceptualization, S.S. and A.A.; Investigation, S.S., A.R., D.R.I., O.M., L.Z., K.A.K., and Y.L.W.; Writing, S.S. and A.A.; Funding Acquisition and Supervision, N.R., A.D., and A.A. All authors discussed the results and commented on the manuscript. A.R. acknowledges support from UC San Diego's Cancer Cell Biology training grant (NIH-NCI-T32-CA067754).

We thank members of the A.A. laboratory for discussions and reading of the manuscript. Work in the A.A. laboratory is supported by grants from the NIH (CA206157 and GM118066) and the Kathy and Curt Marble Cancer Research Fund. A.A. is an investigator of the Howard Hughes Medical Institute, the Paul F. Glenn Center for Biology of Aging Research at MIT, and the Ludwig Center at MIT. S.S. was supported by the American Italian Cancer Foundation (AICF), by a Fellowship in Cancer Research from Marie Curie Actions and the Italian Association for Cancer Research (AIRC), and by a KI Quinquennial Cancer Research Fellowship. K.A.K. is supported by National Institute of General Medical Sciences training grant T32GM007753. Work in the N.R. laboratory was

supported by grant GM98815 from NIGMS. Work by the A.D. group is supported by grant GM074215 from NIGMS and by the Ludwig Institute for Cancer Research. A.R. acknowledges support from UC San Diego's Cancer Cell Biology training grant (NIH-NCI-T32-CA067754). We thank Andy Shiau (Head, Ludwig Small Molecule Discovery Group) for providing inhibitors and for access to high-content imaging and tissue culture equipment.

Chapter 3, in part, was published under the following citation: Santaguida S, Richardson A, Iyer DR, M'Saad O, Zasadil L, Knouse KA, Wong YL, Rhind N, Desai A, Amon A. Chromosome Mis-segregation Generates Cell-Cycle-Arrested Cells with Complex Karyotypes that Are Eliminated by the Immune System. *Dev Cell*. 2017;41(6):638-651. The dissertation author was one of the primary investigators and the second author of this material.

Figure S3.1: Prolonged mitotic arrest causes G_1 arrest irrespective of whether or not chromosome mis-segregation occurred during the prolonged mitosis

(A) Experimental set up to examine the consequences of monastrol treatment on cell cycle progression. **(B)** Representative images of RPE1 cells co-expressing PCNA::GFP and RFP::H2B were acquired with a Yokagawa CV1000 confocal microscope using a 20x objective. Images shown are of DMSO- and monastrol-treated mother cell anaphases and the following G_1, S, and G_2 for one daughter cell. In this experiment unsynchronized cells were treated with DMSO or 100 μM monastrol and immediately filmed every 10 min for 6 hrs to capture mitotic entry. The plate was then removed, monastrol washed out, and the plate replaced. Cells were then immediately filmed every 10 min for 2 hrs to capture mitotic exit and then filmed every 20 min for 42 hrs to capture daughter cell cell cycle progression. In this way cell cycle progression in trios of mother and daughter cells was followed to correlate mother cell mitotic timing and mis-segregation with daughter cell cell cycle progression. **(C)** Daughter cell fate in monastrol-treated RPE1 cells co-expressing PCNA::GFP and RFP::H2B. Each bar represents a measurement from individual daughter cells. Height of the bar represents mother cell mitotic timing from NEBD to anaphase, and color indicates arrest (blue) or division (grey). Red asterisks indicate chromosome mis-segregation in the mother cell as measured by lagging chromosomes and/or micronucleus formation. Daughter cells arrest when mother cells spent more than ~116 min in mitosis, as indicated by the horizontal dashed black line. Data are combined from 3 replicate experiments. Note, mis-segregation is rare in monastrol-treated cells with short mitoses (<100 min). Thus, to obtain sufficient mis-segregation events in this group of mother cells, a significant number of cells with short mitoses was imaged but the analysis enriched for cells with a visible mis-segregation event. Thus, the frequency of mis-segregation in cells with short mitosis is artificially inflated in this graph. **(D)** Daughter cell fate is presented in four categories to determine its correlation with mother cell mitotic timing or mother cell chromosome mis-segregation. The categories include daughter cells with no mother cell mis-segregation and short mitosis (< 116 min as determined in Fig. S3.1C), mother cell mis-segregation and short mitosis, no mother cell mis-segregation and long mitosis (> 116 min), and mother cell mis-segregation and long mitosis. Cell fate is presented as % G_1 arrest per category, as indicated by no G_1 arrest (grey) and G_1 arrest (blue.) Data were combined from 3 replicate experiments.

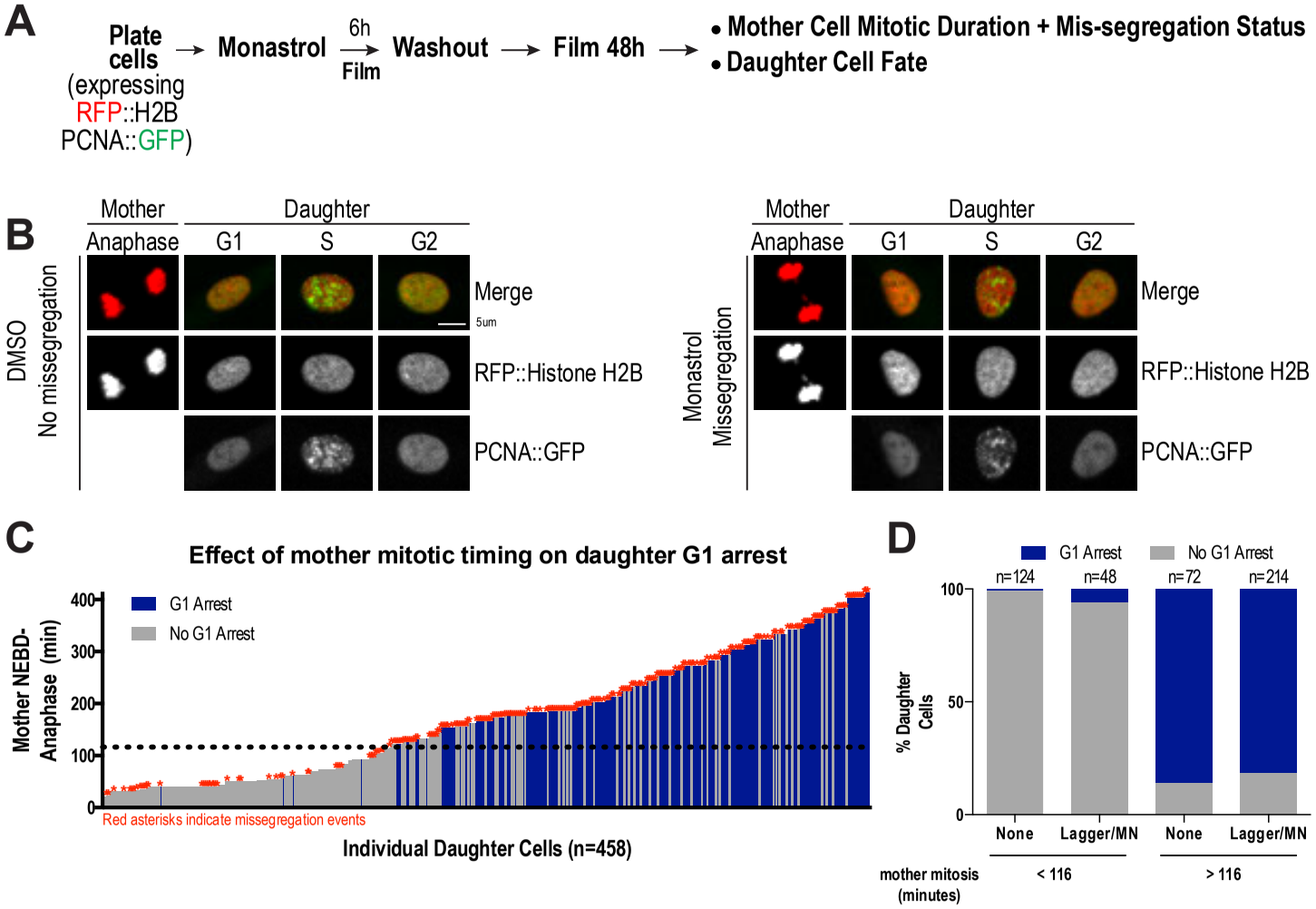
A
Plate cells (expressing RFP::H2B PCNA::GFP)
Monastrol
6h
Film
Washout
Film 48h
• Mother Cell Mitotic Duration + Mis-segregation Status
• Daughter Cell Fate
B
Mother
Daughter
Anaphase
G1
S
G2
DMSO
No missegregation
Merge
5um
RFP::Histone H2B
PCNA::GFP
Monastrol
Missegregation
C
Effect of mother mitotic timing on daughter G1 arrest
G1 Arrest
No G1 Arrest
Mother NEBD-Anaphase (min)
Red asterisks indicate missegregation events
Individual Daughter Cells (n=458)
D
G1 Arrest
No G1 Arrest
n=124
n=48
n=72
n=214
% Daughter Cells
None
Lagger/MN
None
Lagger/MN
mother mitosis (minutes)
< 116
> 116

Figure S3.2: Inhibition of Mps1 causes chromosome mis-segregation

(A) Mitotic duration in DMSO and NMS-P715 (1μM) treated hTERT RPE-1 cells co-expressing PCNA::GFP and RFP::H2B. Cells were immediately filmed after drug addition with a Yokagawa CV7000 spinning disk confocal microscope using a 20x objective. Images were acquired every 10 min for 8 hrs to capture mother cell mitoses and then every 15 min for 2 days to capture daughter cell fate. Mitotic duration (nuclear envelope break-down [NEBD] to anaphase onset; mean +/- S.D.) of 100 mother cells is plotted per condition and indicates accelerated mitosis in the presence of NMS-P715. **(B)** Representative anaphase images of DMSO-treated and NMS-P715-treated hTERTRPE-1 cells co-expressing PCNA::GFP and RFP::H2B.**(C)** Representative images of hTERT RPE-1 cells co-expressing PCNA::GFP and RFP::H2B were acquired on a Yokagawa CQ1 confocal microscope using a 40x objective. Unsynchronized cells were treated with DMSO, 0.5 μM, or 2 μM reversine and then immediately filmed for 48h. Cells were filmed every 5 min for 6 hrs to capture mitotic mis-segregation events and then every 20 min for 42 hrs to capture daughter cell S phase duration (estimated as the time between PCNA focus appearance and disappearance). Representative images are shown for DMSO- and reversine-treated mother cell anaphases and G_1, S, and G_2 of one of their daughter cells.

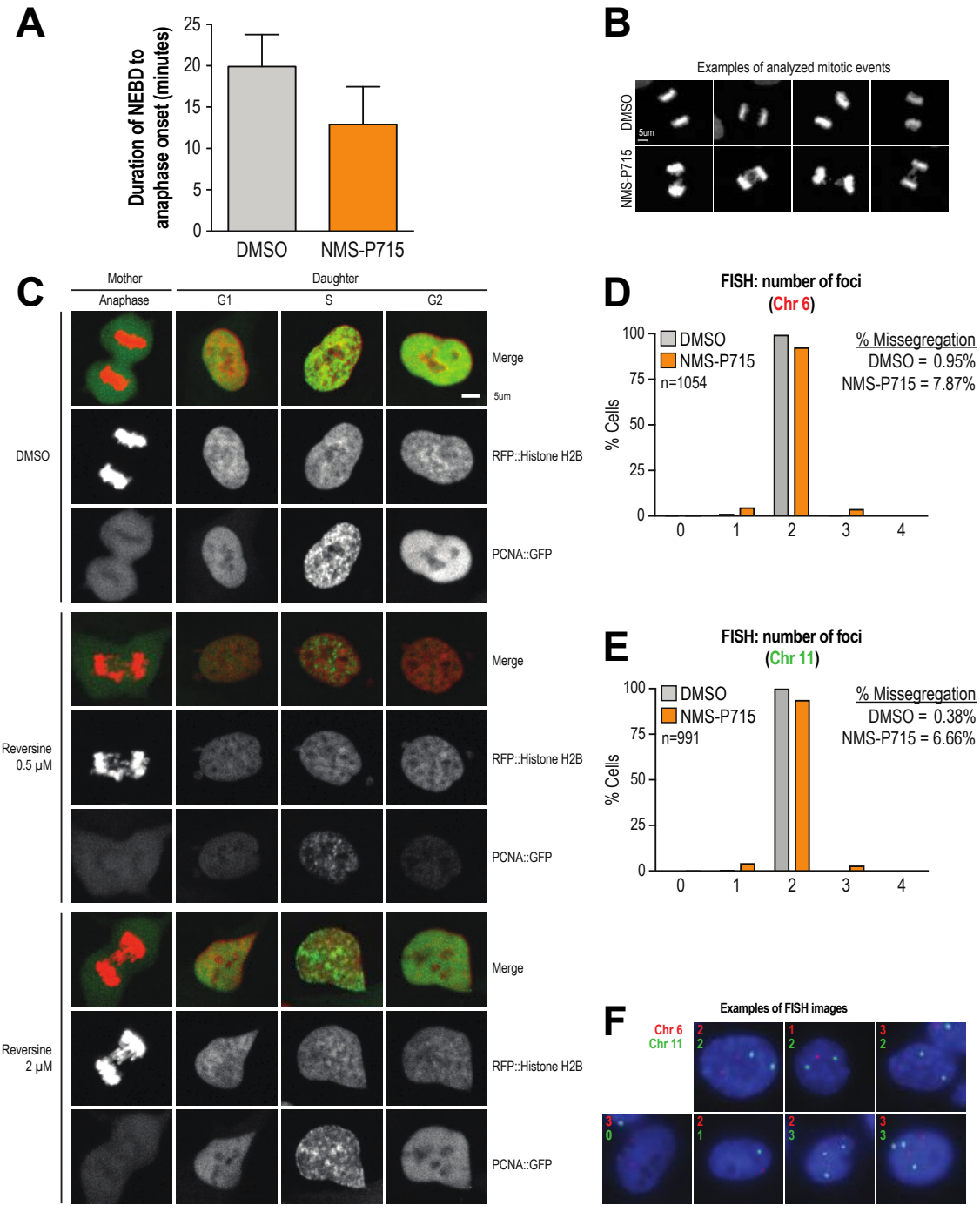
A
Duration of NEBD to anaphase onset (minutes)
25
20
15
10
5
0
DMSO
NMS-P715
B
Examples of analyzed mitotic events
DMSO
NMS-P715
5um
C
Mother
Daughter
Anaphase
G1
S
G2
DMSO
Reversine 0.5 µM
Reversine 2 µM
Merge
RFP::Histone H2B
PCNA::GFP
5um
D
FISH: number of foci
(Chr 6)
DMSO
NMS-P715
n=1054
% Missegregation
DMSO = 0.95%
NMS-P715 = 7.87%
% Cells
100
75
50
25
0
0
1
2
3
4
E
FISH: number of foci
(Chr 11)
DMSO
NMS-P715
n=991
% Missegregation
DMSO = 0.38%
NMS-P715 = 6.66%
% Cells
F
Examples of FISH images
Chr 6
Chr 11

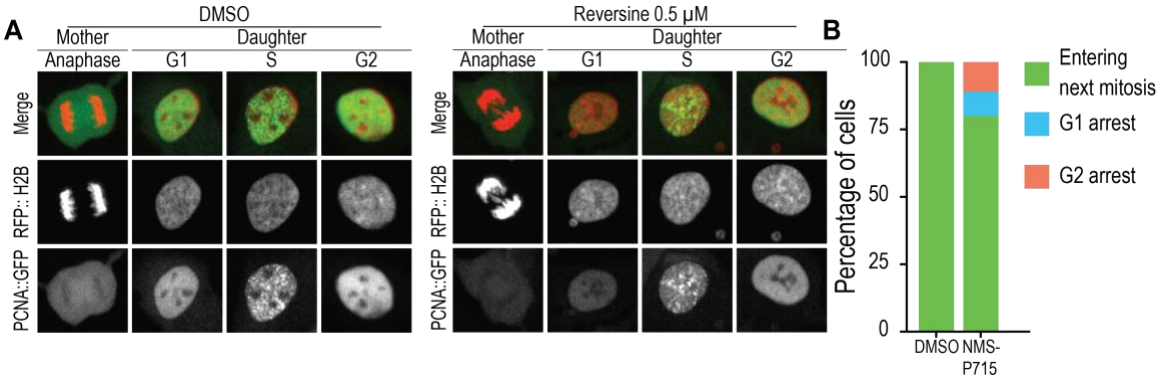

Figure 3.1. p53 Activation Is Not an Obligatory Consequence of Chromosome Mis-segregation

(A) Representative images of hTERT RPE1 cells co-expressing PCNA:GFP and RFP:H2B. Unsynchronized cells were treated with DMSO or 0.5 mM reversine and then immediately filmed for 48 hr. Cells were filmed every 5 min for 6 hr to capture mitotic mis-segregation events and then every 20 min for 42 hr to capture daughter cell S-phase timing. Scale bar, 5 mm. **(B)** Daughter cell fate in NMS-P715-treated hTERT RPE1 cells co-expressing PCNA:GFP and RFP:H2B. Unsynchronized cells were treated with DMSO or 1 mM NMS-P715 and immediately filmed as described in (A). Bars represent percentage of daughter cells with the indicated cell fate.

CHAPTER 4: CONCLUSIONS AND FUTURE DIRECTIONS

4.1 Consequences of the loss of cohesin subunit STAG2

Inactivating mutations in the cohesin subunit Stromal AntiGen 2 (STAG2) are frequent in many cancers, but the consequences of these mutations were not clearly defined. At the start of this project, STAG2 loss was shown to impair sister chromatid cohesion (Barber et al., 2008; Solomon et al., 2011), but it was not clear if this defect led to increased aneuploidy and chromosomal instability as initially proposed (Balbás-Martínez et al., 2013; Taylor et al., 2014; Kim et al., 2016). Other proposed roles for STAG2 loss in cohesin's cellular functions of DNA repair and transcriptional regulation had also not be completely explored. Thus, a thorough characterization of the consequences of STAG2 loss was the focus of my dissertation research.

4.1.1 STAG2 loss does not impair sister chromatid cohesion in live cells

Previously published work clearly demonstrated, through increased chromosome spread defects, increased inter-kinetochore stretch, and increased anaphase defects (Solomon et al., 2011; Kleyman et al., 2014) that STAG2 loss results in mildly impaired sister chromatid cohesion and a subsequent mild increase in error-prone chromosome segregation. These results suggested a mechanism whereby STAG2 loss generates cancer through persistent, low-level chromosomal instability (CIN). In an effort to measure and further understand

these effects, we developed a quantitative assay to measure sister chromatid cohesion strength in live cells. This assay was based on work from a previous graduate student in our lab (Stevens et al., 2011) and another lab (Daum et al., 2011), which showed that the timing of cohesion fatigue, a phenomenon of uncoordinated cohesion loss after metaphase arrest, is a readout for cohesion strength.

By filming the timing of loss of cohesion in STAG-perturbed, metaphase arrested cells, we showed that co-depletion of STAG1 and STAG2 accelerates cohesion fatigue timing, but single depletions of STAG1 and STAG2 or loss of STAG2 does not accelerate cohesion fatigue timing. Our results support a redundant role for STAG1 and STAG2 in sister chromatid cohesion, and do not support a role for STAG2 loss in impaired cohesion.

We were surprised by these results and carried out additional experiments to further understand the role of STAG2 loss in cohesion. First, we measured inter-kinetochore stretch after STAG perturbation, and again found that STAG1 and STAG2 are redundant for cohesion as measured by inter-kinetochore stretch. Next, we assessed anaphase defect frequency after STAG2 loss, and observed mixed results. We saw a mild increase in anaphase defects after STAG2 loss in HCT116 cells as previously reported (Solomon et al., 2011; Kleyman et al., 2014), but not in H4 cells. Our results in H4 cells varied significantly between three separate experiments, and our failure to observe

consistently increased anaphase defects in STAG2 null H4 cells may be due to the rare nature of such anaphase defects.

It is interesting to note, however, that follow-up research from the Waldman lab only detected increased anaphase defects in a subset of STAG2 null HCT116 cell lines, suggesting that the link between STAG2 loss and anaphase defects is not obligatory. We are also aware of recently published work that observes a reduction in cohesion strength after STAG2 depletion in a hybrid cohesion fatigue-chromosome spread assay (Sapkota et al., 2018). Our different observations may be explained by the additional mechanical separation forces exerted on cells during chromosome spread assays that are not present in live cells. Ultimately, we conclude that STAG2 loss does not have a differential effect on cohesin's mitotic functions relative to STAG1 loss, and we instead suggest that STAG2 loss may have an effect on cohesin's other cellular functions.

4.1.2 STAG2 loss does not impair DSB repair

STAG2 loss has been linked to double-strand break (DSB) DNA repair through observations of increased sensitivity to poly(ADP-ribose) polymerase (PARP) inhibition (Bailey et al., 2014) and a shift from homologous recombination (HR) to non-homologous end joining (NHEJ; Kong et al., 2014). These results suggest a mechanism by which STAG2 loss contributes to cancer generation through a persistent, mild increase in DNA mutations. We show, by quantification of DNA repair foci over time after irradiation, that loss of STAG2 does not alter DNA repair foci kinetics. We also show that depletion of STAG1 or STAG2 does

not alter the frequency of site-specific DSB repair via HR or NHEJ. Finally, we show that PARP inhibition by Olaparib treatment mildly suppresses proliferation in H4 cells, as previously published, but that this result does not extend to Talazoparib treatment of H4 cells, and that a panel of other STAG2 null cell types are not sensitive to PARP inhibition. Taken in total, we have been unable to demonstrate a clear link between STAG2 loss and defective DNA repair. Additionally, our results do not support the use of DNA repair pathways as a clear therapeutic approach across the spectrum of STAG2 null cancers.

4.1.3 STAG2 loss has a differential effect on gene expression in Ewing sarcoma cells compared to STAG1 loss

While cohesin has a clear role in regulating gene expression through higher-order chromatin organization, links between STAG2 loss and gene expression are still emerging. Early microarray experiments revealed mild, cell type-specific effects on gene expression after STAG2 loss (Solomon et al., 2011). The resulting differentially expressed genes did not suggest a clear role for STAG2 loss in the generation of cancer and did not support a consistent role for STAG2 loss across different cancer tissue types.

However, more recent research on the subject has reported clear links between STAG2 loss and changes in gene expression that could contribute to the generation of cancer. First, STAG2 loss leads to persistence of the undifferentiated state in hematopoietic stem cell (HSC) lineages and shifts delayed differentiation in a similar manner to that observed in leukemia

(Mullenders et al., 2015; Galeev et al., 2016). Secondly, STAG2 loss in Ewing sarcoma correlates with changes in gene expression, such as increased expression of metastatic genes (Crompton et al., 2014), which could drive cancer progression. This case is especially interesting, because Ewing sarcoma is driven by aberrant gene expression under a fusion transcription factor.

We chose to characterize STAG2's effect on gene expression by RNA sequencing (RNA-seq) in a panel of cell lines, which included hTERT RPE-1 immortalized cells, H4 glioblastoma cells, and STAG2 wild type A673 Ewing sarcoma cells. STAG1 and STAG2 were knocked out by Clustered Regularly Interspaced Short Palindromic Repeats (CRISPR) in hTERT RPE-1 and depleted by siRNA in A673 cells. Several important observations emerged. First, depletion or loss of STAG2 primarily resulted in down-regulation in all three cell types. A subset of 91 genes were recurrently downregulated by STAG2 perturbation in two or more cell types. Several genes that regulate the extracellular matrix are present in this gene list.

Secondly, we observed two different trends when comparing STAG1 and STAG2 perturbation within cell types. In hTERT RPE-1 cells, loss of STAG1 or STAG2 has similar effects on gene expression. Both perturbations primarily resulted in gene down-regulation, and significant overlap exists among the down-regulated genes.

However, in A673 Ewing sarcoma cells, depletion of STAG1 and STAG2 had opposite effects on gene expression. STAG1 depletion primarily up-

regulated genes, and STAG2 primarily down-regulated genes. A subset of the genes up-regulated by STAG1 depletion were down-regulated by STAG2 depletion. This is an exciting result, because it is our first observation of a differential effect for STAG2 perturbation compared to STAG1 perturbation. As such, it is our first clear evidence for a STAG2-specific role in a cancer context.

As these are preliminary results, we have several important lines of inquiry to pursue in the near future. First, if STAG1 and STAG2 differentially regulate gene expression in A673 cells, they may do so by localizing to and regulating different regions of interphase chromatin. We are currently carrying out Chromatin ImmunoPrecipitation sequencing (ChIP-seq) experiments to determine the location of chromatin-bound cohesin-STAG1 and cohesin-STAG2 in unperturbed, STAG1-depleted, and STAG2-depleted A673 cells. If cohesin-STAG1 and cohesin-STAG2 do localize differently, it will be interesting to characterize their chromatin-binding patterns. Do cohesin-STAG1 and cohesin-STAG2 preferentially interact with cohesin loops or topologically associated domains (TADs)? Do they localize with CCCTC-binding factor (CTCF) and mediator? Do they preferentially bind to promoters, enhancers, or insulators? (Zuin et al., 2014; Kojic et al., 2017).

Of course, we must also explore further the effects of STAG2 loss on gene expression. First, we must establish whether or not the recurrent differentially expressed genes are real “hits” that depend on STAG2 expression. If so, rescue of STAG2 expression should restore revert transcription levels of differentially

expressed genes to control levels. Then, we can determine if STAG2 loss down-regulates these same genes in other Ewing sarcoma cell lines or in other cell types. Additionally, we can look into whether or not STAG2 loss also has a differential effect on gene expression compared to STAG1 loss in hematopoietic lineages. To this author's knowledge, a comparison of STAG2 and STAG1 loss on gene expression has not been carried out in hematopoietic stem cells (HSCs).

Finally, we can pursue the functional consequences of gene down-regulation by STAG2 loss in Ewing sarcoma cells. Recurrent changes in extracellular matrix genes suggest a potential role for STAG2 in modifying the surrounding tumor environment and possibly in promoting metastasis. What are the effects of STAG2 loss on tumor growth and metastasis if these cells are transplanted in mouse tumor models? Further research into these questions will hopefully illuminate any potential role that STAG2 loss has on promoting cancer in Ewing sarcoma or other cancers types by regulation of gene expression.

4.2 Consequences of aneuploidy

My interest in STAG2 loss as a potential mechanism for the generation of aneuploidy in cancer led to my participation in a collaboration to understand the general immediate cellular consequences of aneuploidy. As part of my contribution to this research, I assessed the relationship between two key events, mis-segregation and delayed mitotic timing, and the activation of a subsequent p53-dependent cell cycle arrest. These experiments arose out of two published observations. First, mis-segregation induced by monastrol led to a p53-

dependent cell cycle arrest (Thompson and Compton 2010). This result suggested that cells can detect mis-segregation and that they react by arresting cells in the next cell cycle. However, another group induced mitotic arrest by monastrol or nocodazole treatment and observed that mitotic duration of greater than ninety minutes leads to subsequent cell cycle arrest (Uetake and Sluder 2010).

To test these two models, we observed chromosome mis-segregation, mitotic timing, and daughter cell cycle progression by live cell imaging of histone-labeled and S- and G1-marked cells. We found that monastrol treatment leads to mis-segregation, which also correlates with increased mitotic delay. Accordingly, in these experiments, cells experiencing both mis-segregation and mitotic delay tended to arrest in the next cell cycle. However, in reversine-treated cells, which mis-segregate chromosomes but proceed through mitosis in less than 90 minutes, daughter cells do not undergo cell cycle arrest. Therefore, mis-segregation itself is not the cause of daughter cell-cycle arrest. Instead, our results support the proposed mitotic timer model of p53-dependent cell cycle arrest. These findings are interesting, because they suggest that cells do not necessarily respond to mis-segregation with immediate arrest. Instead, in data not included in this dissertation, we found that a small portion of initial mis-segregation events trigger an evolution of more complex karyotypes, which cells can then recognize and eliminate through senescence and immune response (Santaguida et al., 2017).

REFERENCES

Arumugam P, Gruber S, Tanaka K, Haering CH, Mechtler K, Nasmyth K. ATP Hydrolysis Is Required for Cohesin's Association with Chromosomes. *Curr Biol*. 2003;13(22):1941-1953. doi:10.1016/j.cub.2003.10.036

Ashworth A. A synthetic lethal therapeutic approach: Poly(ADP) ribose polymerase inhibitors for the treatment of cancers deficient in DNA double-strand break repair. *J Clin Oncol*. 2008;26(22):3785-3790. doi:10.1200/JCO.2008.16.0812

Bailey ML, O'Neil NJ, van Pel DM, Solomon DA, Waldman T, Hieter P. Glioblastoma Cells Containing Mutations in the Cohesin Component STAG2 Are Sensitive to PARP Inhibition. *Mol Cancer Ther*. 2014;13(3):724-732. doi:10.1158/1535-7163.MCT-13-0749

Baker DJ, Jin F, Jeganathan KB, van Deursen JM. Whole Chromosome Instability Caused by Bub1 Insufficiency Drives Tumorigenesis through Tumor Suppressor Gene Loss of Heterozygosity. *Cancer Cell*. 2009;16(6):475-486. doi:10.1016/j.ccr.2009.10.023

Bakhoum SF, Danilova O V., Kaur P, Levy NB, Compton DA. Chromosomal Instability Substantiates Poor Prognosis in Patients with Diffuse Large B-cell Lymphoma. *Clin Cancer Res*. 2011;17(24):7704-7711. doi:10.1158/1078-0432.CCR-11-2049

Bakhoum SF, Silkworth WT, Nardi IK, Nicholson JM, Compton DA, Cimini D. The mitotic origin of chromosomal instability. *Curr Biol*. 2014;24(4):R148-R149. doi:10.1016/j.cub.2014.01.019

Bakhoum SF, Thompson SL, Manning AL, Compton DA. Genome stability is ensured by temporal control of kinetochore-microtubule dynamics. *Nat Cell Biol*. 2009;11(1):27-35. doi:10.1038/ncb1809

Balbás-Martínez C, Sagrera A, Carrillo-De-Santa-Pau E, Earl J, Márquez M, Vazquez M, Lapi E, Castro-Giner F, Beltran S, Bayés M, Carrato A, Cigudosa JC, Domínguez O, Gut M, Herranz J, Juanpere N, Kogevinas M, Langa X, López-Knowles E, et al. Recurrent inactivation of STAG2 in bladder cancer is not associated with aneuploidy. *Nat Genet*. 2013;45(12):1464-1469. doi:10.1038/ng.2799

Barber TD, McManus K, Yuen KWY, Reis M, Parmigiani G, Shen D, Barrett I, Nouhi Y, Spencer F, Markowitz S, Velculescu VE, Kinzler KW, Vogelstein B, Lengauer C, Hieter P. Chromatid cohesion defects may underlie chromosome instability in human colorectal cancers. *Proc Natl Acad Sci*. 2008;105(9):3443-3448. doi:10.1073/pnas.0712384105

Beach RR, Ricci-Tam C, Brennan CM, Moomau CA, Hsu P hsin, Hua B, Silberman RE, Springer M, Amon A. Aneuploidy Causes Non-Genetic Individuality. *Cell*. 2017;169(2):229-242.e21. doi:10.1016/j.cell.2017.03.021

Bekker-Jensen S, Lukas C, Kitagawa R, Melander F, Kastan MB, Bartek J, Lukas J. Spatial organization of the mammalian genome surveillance machinery in response to DNA strand breaks. *J Cell Biol*. 2006;173(2):195-206. doi:10.1083/jcb.200510130

Ben-Shahar TR, Heeger S, Lehane C, East P, Flynn H, Skehel M, Uhlmann F. Eco1-Dependent Cohesin Acetylation During Establishment of Sister Chromatid Cohesion. *Science (80-)*. 1008;321:563-566. doi:10.1101/cshperspect.a011130

Benedetti L, Cereda M, Monteverde L, Desai N, Ciccarelli FD. Synthetic lethal interaction between the tumour suppressor STAG2 and its paralog STAG1. *Oncotarget*. 2017;8(23):37619-37632. doi:10.18632/oncotarget.16838

Bindra RS, Goglia AG, Jasin M, Powell SN. Development of an assay to measure mutagenic non-homologous end-joining repair activity in mammalian cells. *Nucleic Acids Res*. 2013;41(11):1-17. doi:10.1093/nar/gkt255

Birkenbihl RP, Subramani S. Cloning and characterization of rad21 an essential gene of Schizosaccharomyces pombe involved in DNA double-strand-break repair. *Nucleic Acids Res*. 1992;20(24):6605-6611.

Blank HM, Sheltzer JM, Meehl CM, Amon A. Mitotic entry in the presence of DNA damage is a widespread property of aneuploidy in yeast. *Mol Biol Cell*. 2015;26(8):1440-1451. doi:10.1091/mbc.E14-10-1442

Boulay G, Sandoval GJ, Riggi N, Iyer S, Buisson R, Naigles B, Awad ME, Rengarajan S, Volorio A, McBride MJ, Broye LC, Zou L, Stamenkovic I, Kadoch C, Rivera MN. Cancer-Specific Retargeting of BAF Complexes by a Prion-like Domain. *Cell*. 2017;171(1):163-178.e19. doi:10.1016/j.cell.2017.07.036

Brohl AS, Solomon DA, Chang W, Wang J, Song Y, Sindiri S, Patidar R, Hurd L, Chen L, Shern JF, Liao H, Wen X, Gerard J, Kim JS, Lopez Guerrero JA, Machado I, Wai DH, Picci P, Triche T, et al. The Genomic Landscape of the

Ewing Sarcoma Family of Tumors Reveals Recurrent STAG2 Mutation. *PLoS Genet*. 2014;10(7):1-13. doi:10.1371/journal.pgen.1004475

Bryant HE, Schultz N, Thomas HD, Parker KM, Flower D, Lopez E, Kyle S, Meuth M, Curtin NJ, Helleday T. Specific killing of BRCA2-deficient tumours with inhibitors of poly (ADP-ribose) polymerase. *Nat Lett*. 2007;447(May):913-918. doi:10.1038/nature05789

Burrell RA, McClelland SE, Bartek J, Swanton C. Response to Bakhoum et al. *Curr Biol*. 2014;24(4):R150. doi:10.1016/j.cub.2014.01.021

Caldecott KW. Single-strand break repair and genetic disease. *Nat Rev Genet*. 2008;9(8):619-631. doi:10.1038/nrg2380

Canudas S, Smith S. Differential regulation of telomere and centromere cohesion by the Scc3 homologues SA1 and SA2, respectively, in human cells. *J Cell Biol*. 2009;187(2):165-173. doi:10.1083/jcb.200903096

Cerami E, Gao J, Dogrusoz U, Gross BE, Sumer SO, Aksoy BA, Jacobsen A, Byrne CJ, Heuer ML, Larsson E, Antipin Y, Reva B, Goldberg AP, Sander C, Schultz N. The cBio Cancer Genomics Portal: An open platform for exploring multidimensional cancer genomics data. *Cancer Discov*. 2012;2(5):401-404. doi:10.1158/2159-8290.CD-12-0095

Chen G, Mulla WA, Kucharavy A, Tsai HJ, Rubinstein B, Conkright J, McCroskey S, Bradford WD, Weems L, Haug JS, Seidel CW, Berman J, Li R. Targeting the adaptability of heterogeneous aneuploids. *Cell*. 2015;160(4):771-784. doi:10.1016/j.cell.2015.01.026

Ciccia A, Elledge SJ. The DNA Damage Response: Making It Safe to Play with Knives. *Mol Cell*. 2010;40(2):179-204. doi:10.1016/j.molcel.2010.09.019

Cimini D, Howell B, Maddox P, Khodjakov A, Degrassi F, Salmon ED. Merotelic kinetochore orientation is a major mechanism of aneuploidy in mitotic mammalian tissue cells. *J Cell Biol*. 2001;152(3):517-527. doi:10.1083/jcb.153.3.517

Ciosk R, Shirayama M, Shevchenko A, Tanaka T, Toth A, Shevchenko A, Nasmyth K. Cohesin's binding to chromosomes depends on a separate complex consisting of Scc2 and Scc4 proteins. *Mol Cell*. 2000;5(2):243-254. doi:10.1016/S1097-2765(00)80420-7

Colombo R, Caldarelli M, Mennecozzi M, Giorgini ML, Sola F, Cappella P, Perrera C, Re Depaolini S, Rusconi L, Cucchi U, Avanzi N, Bertrand JA, Bossi

RT, Pesenti E, Galvani A, Isacchi A, Colotta F, Donati D, Moll J. Targeting the mitotic checkpoint for cancer therapy with NMS-P715, an inhibitor of MPS1 kinase. *Cancer Res*. 2010;70(24):10255-10264. doi:10.1158/0008-5472.CAN-10-2101

Corces-Zimmerman MR, Hong W-J, Weissman IL, Medeiros BC, Majeti R. Preleukemic mutations in human acute myeloid leukemia affect epigenetic regulators and persist in remission. *Proc Natl Acad Sci*. 2014;111(7):2548-2553. doi:10.1073/pnas.1324297111

Corces MR, Corces VG. The three-dimensional cancer genome. *Curr Opin Genet Dev*. 2016;36:1-7. doi:10.1016/j.gde.2016.01.002

Crasta K, Ganem NJ, Dagher R, Lantermann AB, Ivanova E V., Pan Y, Nezi L, Protopopov A, Chowdhury D, Pellman D. DNA breaks and chromosome pulverization from errors in mitosis. *Nature*. 2012;482(7383):53-58. doi:10.1038/nature10802

Crompton BD, Stewart C, Taylor-Weiner A, Alexe G, Kurek KC, Calicchio ML, Kiezun A, Carter SL, Shukla SA, Mehta SS, Thorner AR, de Torres C, Lavarino C, Suñol M, McKenna A, Sivachenko A, Cibulskis K, Lawrence MS, Stojanov P, et al. The genomic landscape of pediatric Ewing sarcoma. *Cancer Discov*. 2014;4(11):1326-1341. doi:10.1158/2159-8290.CD-13-1037

Dasgupta T, Antony J, Braithwaite AW, Horsfield JA. HDAC8 Inhibition Blocks SMC3 Deacetylation and Delays Cell Cycle Progression without Affecting Cohesin-dependent Transcription in MCF7 Cancer Cells. *J Biol Chem*. 2016;291(24):12761-12770. doi:10.1074/jbc.M115.704627

Daum JR, Potapova TA, Sivakumar S, Daniel JJ, Flynn JN, Rankin S, Gorbsky GJ. Cohesion fatigue induces chromatid separation in cells delayed at metaphase. *Curr Biol*. 2011;21(12):1018-1024. doi:10.1016/j.cub.2011.05.032

Davoli T, Uno H, Wooten EC, Elledge SJ. Tumor aneuploidy correlates with markers of immune evasion and with reduced response to immunotherapy. *Science (80-)*. 2017;355(6322):1-14. doi:10.1126/science.aaf8399

Deardorff MA, Bando M, Nakato R, Watrin E, Itoh T, Minamino M, Saitoh K, Komata M, Katou Y, Clark D, Cole KE, De Baere E, Decroos C, Di Donato N, Ernst S, Francey LJ, Gyftodimou Y, Hirashima K, Hullings M, et al. HDAC8 mutations in Cornelia de Lange syndrome affect the cohesin acetylation cycle. *Nature*. 2012;489(7415):313-317. doi:10.1038/nature11316

Dixon JR, Selvaraj S, Yue F, Kim A, Li Y, Shen Y, Hu M, Liu JS, Ren B. Topological domains in mammalian genomes identified by analysis of chromatin interactions. *Nature*. 2012;485(7398):376-380. doi:10.1038/nature11082

Dodgson SE, Kim S, Costanzo M, Baryshnikova A, Morse DL, Kaiser CA, Boone C, Amon A. Chromosome-specific and global effects of aneuploidy in Saccharomyces cerevisiae. *Genetics*. 2016;202(4):1395-1409. doi:10.1534/genetics.115.185660

Dorsett D, Krantz ID. On the Molecular Etiology of Cornelia de Lange Syndrome. *Ann N Y Acad Sci*. 2009;1151:22-37. doi:10.1002/ar.20849.3D

Elihu Estey HD. Acute Myeloid Leukaemia. *Lancet*. 2006;368:1894–907. doi:10.1056/NEJMra1406184

Eng T, Guacci V, Koshland D. Interallelic complementation provides functional evidence for cohesin-cohesin interactions on DNA. *Mol Biol Cell*. 2015;26(23):4224-4235. doi:10.1091/mbc.E15-06-0331

Galeev R, Baudet A, Kumar P, Rundberg Nilsson A, Nilsson B, Soneji S, Törngren T, Borg Å, Kvist A, Larsson J. Genome-wide RNAi Screen Identifies Cohesin Genes as Modifiers of Renewal and Differentiation in Human HSCs. *Cell Rep*. 2016;14(12):2988-3000. doi:10.1016/j.celrep.2016.02.082

Gandhi R, Gillespie PJ, Hirano T. Human Wapl Is a Cohesin-Binding Protein that Promotes Sister-Chromatid Resolution in Mitotic Prophase. *Curr Biol*. 2006;16(24):2406-2417. doi:10.1016/j.cub.2006.10.061

Gao J, Aksoy B arman, Dogrusoz U, Dresdner G, Gross B, Sumer SO, Sun Y, Jacobsen A, Sinha R, Larsson E, Cerami E, Sander C, Schultz N. Integrative Analysis of Complex Cancer Genomics and Clinical Profiles Using the cBioPortal. *Sci Signal*. 2013;6(269):1-19. doi:10.1109/TDEI.2009.5211872

Giles F, Fischer T, Cortes J, Garcia-Manero G, Beck J, Ravandi F, Masson E, Rae P, Laird G, Sharma S, Kantarjian H, Dugan M, Albitar M, Bhalla K. A phase I study of intravenous LBH589, a novel cinnamic hydroxamic acid analogue histone deacetylase inhibitor, in patients with refractory hematologic malignancies. *Clin Cancer Res*. 2006;12(15):4628-4635. doi:10.1158/1078-0432.CCR-06-0511

Gligoris TG, Scheinost JC, Bürmann F, Petela N, Chan KL, Uluocak P, Beckouët F, Gruber S, Nasmyth K, Löwe J. Closing the cohesin ring: Structure and function of its Smc3-kleisin interface. *Science (80-)*. 2014;346(6212):963-967. doi:10.1126/science.1256917

Gordon DJ, Resio B, Pellman D. Causes and consequences of aneuploidy in cancer. *Nat Rev Genet*. 2012;13(3):189-203. doi:10.1038/nrg3123

Gorringe KL, Ramakrishna M, Williams LH, Sridhar A, Boyle SE, Bearfoot JL, Li J, Anglesio MS, Campbell IG. Are There Any More Ovarian Tumor Suppressor Genes? A New Perspective Using Ultra High-Resolution Copy Number and Loss of Heterozygosity Analysis. *Genes Chromosomes Cancer*. 2000;48:931-942. doi:10.1002/gcc

Grove CS, Vassiliou GS. Acute myeloid leukaemia: a paradigm for the clonal evolution of cancer? *Dis Model Mech*. 2014;7(8):941-951. doi:10.1242/dmm.015974

Gruber S, Arumugam P, Katou Y, Kuglitsch D, Helmhart W, Shirahige K, Nasmyth K. Evidence that Loading of Cohesin Onto Chromosomes Involves Opening of Its SMC Hinge. *Cell*. 2006;127(3):523-537. doi:10.1016/j.cell.2006.08.048

Guo G, Sun X, Chen C, Wu S, Huang P, Li Z, Dean M, Huang Y, Jia W, Zhou Q, Tang A, Yang Z, Li X, Song P, Zhao X, Ye R, Zhang S, Lin Z, Qi M, et al. Whole-genome and whole-exome sequencing of bladder cancer identifies frequent alterations in genes involved in sister chromatid cohesion and segregation. *Nat Genet*. 2013;45(12):1459-1463. doi:10.1038/ng.2798

Hanahan D, Weinberg R. The Hallmarks of Cancer Review University of California at San Francisco. *Cell*. 2000;100:57-70.

Hanahan D, Weinberg RA. Hallmarks of cancer: The next generation. *Cell*. 2011;144(5):646-674. doi:10.1016/j.cell.2011.02.013

Hassold T, Hunt P. To err (meiotically) is human: The genesis of human aneuploidy. *Nat Rev Genet*. 2001;2(4):280-291. doi:10.1038/35066065

Hauf S, Roitinger E, Koch B, Dittrich CM, Mechtler K, Peters JM. Dissociation of cohesin from chromosome arms and loss of arm cohesion during early mitosis depends on phosphorylation of SA2. *PLoS Biol*. 2005;3(3):0419-0432. doi:10.1371/journal.pbio.0030069

Heilig CE, Löffler H, Mahlknecht U, Janssen JWG, Ho AD, Jauch A, Krämer A. Chromosomal instability correlates with poor outcome in patients with myelodysplastic syndromes irrespectively of the cytogenetic risk group. *J Cell Mol Med*. 2010;14(4):895-902. doi:10.1111/j.1582-4934.2009.00905.x

Hinchcliffe EH, Day CA, Karanjeet KB, Fadness S, Langfald A, Vaughan KT, Dong Z. Chromosome missegregation during anaphase triggers p53 cell cycle arrest through histone H3.3 Ser31 phosphorylation. *Nat Cell Biol*. 2016;18(6):668-675. doi:10.1038/ncb3348

Hnisz D, Abraham BJ, Lee TI, Lau A, Saint-André V, Sigova AA, Hoke HA, Young RA. Super-enhancers in the control of cell identity and disease. *Cell*. 2013;155(4):934-947. doi:10.1016/j.cell.2013.09.053

Hodgkin J. Karyotype, ploidy, and gene dosage. *WormBook*. 2005:1-9. doi:10.1895/wormbook.1.3.1

Holland AJ, Cleveland DW. Boveri revisited: Chromosomal instability, aneuploidy and tumorigenesis. *Nat Rev Mol Cell Biol*. 2009;10(7):478-487. doi:10.1038/nrm2718

Horsfield JA, Anagnostou SH, Hu JK-H, Cho KHY, Geisler R, Lieschke G, Crosier KE, Crosier PS. Cohesin-dependent regulation of Runx genes. *Development*. 2007;134(14):2639-2649. doi:10.1242/dev.002485

Huang CE, Milutinovich M, Koshland D. Rings, bracelet or snaps: fashionable alternatives for Smc complexes. *Philos Trans R Soc B Biol Sci*. 2005;360(1455):537-542. doi:10.1098/rstb.2004.1609

Huis In't Veld PJ, Herzog F, Ladurner R, Davidson IF, Piric S, Kreidl E, Bhaskara V, Aebersold R, Peters JM. Characterization of a DNA exit gate in the human cohesin ring. *Science (80-)*. 2014;346(6212):968-972. doi:10.1126/science.1256904

Ishiguro KI, Kim J, Fujiyama-Nakamura S, Kato S, Watanabe Y. A new meiosis-specific cohesin complex implicated in the cohesin code for homologous pairing. *EMBO Rep*. 2011;12(3):267-275. doi:10.1038/embor.2011.2

Janssen A, Burg M Van Der, Szuhai K, Kops GJPL, Medema RH. Chromosome Segregation Errors as a Cause of DNA Damage and Structural Chromosome Aberrations Chromosome Segregation Errors as a Cause of DNA Damage and Structural Chromosome Aberrations. *Science (80-)*. 2011;333:1895-1898. doi:10.1126/science.1210214

Kagey MH, Newman JJ, Bilodeau S, Zhan Y, Orlando DA, Van Berkum NL, Ebmeier CC, Goossens J, Rahl PB, Levine SS, Taatjes DJ, Dekker J, Young RA. Mediator and cohesin connect gene expression and chromatin architecture. *Nature*. 2010;467(7314):430-435. doi:10.1038/nature09380

Kawauchi S, Calof AL, Santos R, Lopez-Burks ME, Young CM, Hoang MP, Chua A, Lao T, Lechner MS, Daniel JA, Nussenzweig A, Kitzes L, Yokomori K, Hallgrimsson B, Lander AD. Multiple organ system defects and transcriptional dysregulation in the Nipbl+/- mouse, a model of Cornelia de Lange syndrome. *PLoS Genet*. 2009;5(9):1-17. doi:10.1371/journal.pgen.1000650

Kim JS, Krasieva TB, LaMorte V, Malcolm A, Taylor R, Yokomori K. Specific recruitment of human cohesin to laser-induced DNA damage. *J Biol Chem*. 2002;277(47):45149-45153. doi:10.1074/jbc.M209123200

Kim JS, He X, Orr B, Wutz G, Hill V, Peters JM, Compton DA, Waldman T. Intact Cohesion, Anaphase, and Chromosome Segregation in Human Cells Harboring Tumor-Derived Mutations in STAG2. *PLoS Genet*. 2016;12(2):1-18. doi:10.1371/journal.pgen.1005865

Kitajima TS, Sakuno T, Ishiguro KI, Iemura SI, Natsume T, Kawashima SA, Watanabe Y. Shugoshin collaborates with protein phosphatase 2A to protect cohesin. *Nature*. 2006;441(1):46-52. doi:10.1038/nature04663

Kleyman M, Kabeche L, Compton DA. STAG2 promotes error correction in mitosis by regulating kinetochore-microtubule attachments. *J Cell Sci*. 2014;127(19):4225-4233. doi:10.1242/jcs.151613

Kojic A, Ana C, De Koninck M, Gomez-Lopez G, Rodriguez-Corsino M, Le Dily F, Marti-Renom M, Losada A. Distinct roles of cohesin-SA1 and cohesin-SA2 in 3D chromosome organization. *bioRxiv*. 2017:1-20. doi:10.1101/166264

Kong X, Ball AR, Pham HX, Zeng W, Chen H-Y, Schmiesing JA, Kim J-S, Berns M, Yokomori K. Distinct Functions of Human Cohesin-SA1 and Cohesin-SA2 in Double-Strand Break Repair. *Mol Cell Biol*. 2014;34(4):685-698. doi:10.1128/MCB.01503-13

Ladurner R, Kreidl E, Ivanov MP, Ekker H, Idarraga-Amado MH, Busslinger GA, Wutz G, Cisneros DA, Peters J. Sororin actively maintains sister chromatid cohesion. *EMBO J*. 2016;35(6):635-653. doi:10.15252/embj.201592532

Lafont AL, Song J, Rankin S. Sororin cooperates with the acetyltransferase Eco2 to ensure DNA replication-dependent sister chromatid cohesion. *PNAS*. 2010;107(47):20364-20369. doi:10.1073/pnas.1011069107

Lambrus BG, Holland AJ. A New Mode of Mitotic Surveillance. *Trends Cell Biol*. 2017;27(5):314-321. doi:10.1016/j.tcb.2017.01.004

Lara-Gonzalez P, Taylor SS. Cohesion Fatigue Explains Why Pharmacological Inhibition of the APC/C Induces a Spindle Checkpoint-Dependent Mitotic Arrest. *PLoS One*. 2012;7(11):1-14. doi:10.1371/journal.pone.0049041

Lara-Gonzalez P, Westhorpe FG, Taylor SS. The spindle assembly checkpoint. *Curr Biol*. 2012;22:R966-R980. doi:10.1016/j.cub.2012.10.006

Lee AJX, Endesfelder D, Rowan AJ, Walther A, Birkbak NJ, Futreal PA, Downward J, Szallasi Z, Tomlinson IPM, Howell M, Kschischo M, Swanton C. Chromosomal instability confers intrinsic multidrug resistance. *Cancer Res*. 2011;71(5):1858-1870. doi:10.1158/0008-5472.CAN-10-3604

Ley TJ, Miller C, Ding L, Raphael BJ, Mungal AJ, Robertson AG, Katherine H, Timothy JT, Laird PW, Baty JD, Fulton LL, Fulton R, Heath SE, Kalicki-Veizer J, Kandoth C, Klco JM, Koboldt DC, Kanchi KL, Kulkarni S, Lamprecht TL, Larson DE, Lin L, Lu C, McLellan MD, McMichael JF, Payton J, Schmidt H, Spencer DH, Tomasson MH, Wallis JW, Wartman LD, Watson MA, Welch J, Wendl MC, Ally A, Balasundaram M, Birol I, Butterfield Y, Chiu R, Chu A, Chuah E, Chun HJ, Corbett R, Dhalla N, Guin R, He A, Hirst C, Hirst M, Holt RA, Jones S, Karsan A, Lee D, Li HI, Marra MA, Mayo M, Moore RA, Mungall K, Parker J, Pleasance E, Plettner P, Schein J, Stoll D, Swanson L, Tam A, Thiessen N, Varhol R, Wye N, Zhao Y, Gabriel S, Getz G, Sougnez C, Zou L, Leiserson MDM, Vandin F, Wu HT, Applebaum Fk, Baylin SB, Akbani R, Broom BM, Chen K, Motter TC, Nguyen K, Weinstein JN, Zhang N, Ferguson ML, Adams C, Black A, Bowen J, Gastier-Foster J, Grossman T, Lichtenberg T, Wise L, Davidsen T, Demchok JA, Shaw KRM, Sheth M, Sofia HJ, Yang L, Downing JR, Eley G, Alonso S, Ayala B, Baboud J, Backus M, Barletta SP, Berton DL, Chu AL, Girshik S, Jensen MA, Kahn A, Kothiyal P, Nicholls MC, Pihl TD, Pot DA, Raman R, Sanbhadti RN, Snyder EE, Srinivasan D, Walton J, Wan Y, Wang Z, Issa JJ, Beau ML, Carroll M, Kantarjian H, Kornblau S, Bootwalla MS, Lai PH, Shen H, Van Den Berg DJ , Weisenberger DJ, Link DC, Walter MJ, Ozenberger BA, Mardis ER, Westervelt P, Graubert TA, DiPersio JF, Wilson RK. Genomic and Epigenomic Landscapes of Adult De Novo Acute Myeloid Leukemia. N Engl J Med. 2013;368(22):2059-2074. doi:10.1056/NEJMoa1301689

Li M, Fang X, Baker DJ, Guo L, Gao X, Wei Z, Han S, van Deursen JM, Zhang P. The ATM–p53 pathway suppresses aneuploidy-induced tumorigenesis. *Pnas*. 2010;107(32):14188-14193. doi:10.1073/pnas.1005960107/-/DCSupplemental.www.pnas.org/cgi/doi/10.1073/pnas.1005960107

Li X, Zhang TW, Tang JL, Fa PP, Lu JX, Qi FM, Cai ZM, Liu CX, Sun XJ. Loss of STAG2 causes aneuploidy in normal human bladder cells. *Genet Mol Res*. 2015;14(1):2638-2646. doi:10.4238/2015.March.30.24

Lindsley DL, Sandler L, Baker BS, Carpenter AT, Denell RE, Hall JC, Jacobs PA, Miklos GL, Davis BK, Gethmann RC, Hardy RW, Steven AH, Miller M, Nozawa H, Parry DM, Gould-Somero M. Segmental aneuploidy and the genetic gross structure of the Drosophila genome. *Genetics*. 1972;71(1):157-184.

Liu H, Rankin S, Yu H. Phosphorylation-enabled binding of SGO1-PP2A to cohesin protects sororin and centromeric cohesion during mitosis. *Nat Cell Biol*. 2013;15(1):40-49. doi:10.1038/ncb2637

López-García C, Sansregret L, Domingo E, McGranahan N, Hobor S, Birkbak NJ, Horswell S, Grönroos E, Favero F, Rowan AJ, Matthews N, Begum S, Phillimore B, Burrell R, Oukrif D, Spencer-Dene B, Kovac M, Stamp G, Stewart A, et al. BCL9L Dysfunction Impairs Caspase-2 Expression Permitting Aneuploidy Tolerance in Colorectal Cancer. *Cancer Cell*. 2017;31(1):79-93. doi:10.1016/j.ccell.2016.11.001

Lorke DE. Developmental characteristics of trisomy 19 mice. *Cells Tissues Organs*. 1994;150(3):159-169. doi:10.1159/000147614

Löwenberg B, Downing JR, Burnett AK. Acute Myeloid Leukemia. *N Engl J Med*. 1999;341(14):1051-1062.

Mayer TU, Kapoor TM, Haggarty SJ, King RW, Schreiber SL, Mitchison TJ. Small Molecule Inhibitor of Mitotic Spindle Bipolarity Identified in a Phenotype-Based Screen. *Science (80-)*. 1999;286:971-974. doi:10.1126/science.286.5441.971

Mazumdar C, Shen Y, Xavy S, Zhao F, Reinisch A, Li R, Corces MR, Flynn RA, Buenrostro JD, Chan SM, Thomas D, Koenig JL, Hong WJ, Chang HY, Majeti R. Leukemia-Associated Cohesin Mutants Dominantly Enforce Stem Cell Programs and Impair Human Hematopoietic Progenitor Differentiation. *Cell Stem Cell*. 2015;17(6):675-688. doi:10.1016/j.stem.2015.09.017

McLellan JL, O'Neil NJ, Barrett I, Ferree E, van Pel DM, Ushey K, Sipahimalani P, Bryan J, Rose AM, Hieter P. Synthetic lethality of cohesins with PARPs and replication fork mediators. *PLoS Genet*. 2012;8(3):1-13. doi:10.1371/journal.pgen.1002574

Meena JK, Cerutti A, Beichler C, Morita Y, Bruhn C, Kumar M, Kraus JM, Speicher MR, Wang Z, Kestler HA, Fagagna F d'Adda di, Günes C, Rudolph KL. Telomerase abrogates aneuploidy-induced telomere replication stress, senescence and cell depletion. *EMBO J*. 2017;36(19):2922-2924. doi:10.15252/embj.201797470

Michaelis C, Ciosk R, Nasmyth K. Cohesins: Chromosomal proteins that prevent premature separation of sister chromatids. *Cell*. 1997;91(1):35-45. doi:10.1016/S0092-8674(01)80007-6

Mönnich M, Banks S, Eccles M, Dickinson E, Horsfield J. Expression of cohesin and condensin genes during zebrafish development supports a non-proliferative role for cohesin. *Gene Expr Patterns*. 2009;9(8):586-594. doi:10.1016/j.gep.2009.08.004

Morales C, Losada A. Establishing and dissolving cohesion during the vertebrate cell cycle. *Curr Opin Cell Biol*. 2018;52:51-57. doi:10.1016/j.ceb.2018.01.010

Mullenders J, Aranda-Orgilles B, Lhoumaud P, Keller M, Pae J, Wang K, Kayembe C, Rocha PP, Raviram R, Gong Y, Premsrirut PK, Tsirigos A, Bonneau R, Skok JA, Cimmino L, Hoehn D, Aifantis I. Cohesin loss alters adult hematopoietic stem cell homeostasis, leading to myeloproliferative neoplasms. *J Exp Med*. 2015;212(11):1833-1850. doi:10.1084/jem.20151323

Nagy G, Czipa E, Steiner L, Nagy T, Pongor S, Nagy L, Barta E. Motif oriented high-resolution analysis of ChIP-seq data reveals the topological order of CTCF and cohesin proteins on DNA. *BMC Genomics*. 2016;17(1):1-9. doi:10.1186/s12864-016-2940-7

Nasmyth K. Cohesin: A catenase with separate entry and exit gates? *Nat Cell Biol*. 2011;13(10):1170-1177. doi:10.1038/ncb2349

Nishiyama T, Sykora MM, Veld PJH in ’t, Mechtler K, Peters J. Aurora B and Cdk1 mediate Wapl activation and release of acetylated cohesin from chromosomes by phosphorylating Sororin. *PNAS*. 2013;110(33):13404-13409. doi:10.1073/pnas.1305020110/-/DCSupplemental.www.pnas.org/cgi/doi/10.1073/pnas.1305020110

Niwa O, Tange Y, Kurabayashi A. Growth arrest and chromosome instability in aneuploid yeast. *Yeast*. 2006;23:937-950. doi:10.1002/yea

O’Neil NJ, van Pel DM, Heiter P. Synthetic Lethality and Cancer: Cohesin and PARP at the Replication Fork. *Trends Genet*. 2013;29(5):290-297. doi:10.1109/TMI.2012.2196707.Separate

Ohashi A, Ohori M, Iwai K, Nakayama Y, Nambu T, Morishita D, Kawamoto T, Miyamoto M, Hirayama T, Okaniwa M, Banno H, Ishikawa T, Kandori H, Iwata K. Aneuploidy generates proteotoxic stress and DNA damage concurrently with p53-mediated post-mitotic apoptosis in SAC-impaired cells. *Nat Commun*. 2015;6:1-16. doi:10.1038/ncomms8668

Oromendia AB, Dodgson SE, Amon A. Aneuploidy causes proteotoxic stress in yeast. *Genes Dev*. 2012;26:2696-2708. doi:10.1101/gad.207407.112

Ouyang Z, Zheng G, Tomchick DR, Luo X, Yu H. Structural Basis and IP6 Requirement for Pds5-Dependent Cohesin Dynamics. *Mol Cell*. 2016;62(2):248-259. doi:10.1016/j.molcel.2016.02.033

Passerini V, Ozeri-Galai E, De Pagter MS, Donnelly N, Schmalbrock S, Kloosterman WP, Kerem B, Storchová Z. The presence of extra chromosomes leads to genomic instability. *Nat Commun*. 2016;7:1-12. doi:10.1038/ncomms10754

Pauli A, Althoff F, Oliveira RA, Heidmann S, Schuldiner O, Lehner CF, Dickson BJ, Nasmyth K. Cell-Type-Specific TEV Protease Cleavage Reveals Cohesin Functions in Drosophila Neurons. *Dev Cell*. 2008;14(2):239-251. doi:10.1016/j.devcel.2007.12.009

Pezzi N, Prieto I, Kremer L, Pérez, Jurado LA, Valero C, Del Mazo J, Martínez-A C, Barbero JL. STAG3, a novel gene encoding a protein involved in meiotic chromosome pairing and location of STAG3-related genes flanking the Williams-Beuren syndrome deletion. *FASEB J*. 2000;14(3):581-592. doi:10.1096/fasebj.14.3.581

Plumb JA, Finn PW, Williams RJ, Bandara MJ, Romero MR, Watkins CJ, La Thangue NB, Brown R. Pharmacodynamic response and inhibition of growth of human tumor xenografts by the novel histone deacetylase inhibitor PXD101. *MolCancer Ther*. 2003;2(8):721-728. doi:10.1158/1535-7163.mct-07-2026

Potts PR, Porteus MH, Yu H. Human SMC5/6 complex promotes sister chromatid homologous recombination by recruiting the SMC1/3 cohesin complex to double-strand breaks. *EMBO J*. 2006;25(14):3377-3388. doi:10.1038/sj.emboj.7601218

Revenkova E, Eijpe M, Heyting C, Gross B, Jessberger R. Novel meiosis-specific isoform of mammalian SMC1. *Mol Cell Biol*. 2001;21(20):6984-6998. doi:10.1128/MCB.21.20.6984-6998.2001

Ricke RM, Jeganathan KB, Malureanu L, Harrison AM, Van Deursen JM. Bub1 kinase activity drives error correction and mitotic checkpoint control but not tumor suppression. *J Cell Biol*. 2012;199(6):931-949. doi:10.1083/jcb.201205115

Riggi N, Knoechel B, Gillespie SM, Rheinbay E, Boulay G, Rossetti NE, Boonseng WE, Cook EB, Patel A, Gymrek M, Deshpande V, Ting DT, Hornicek FJ, Nielsen GP, Stamenkovic I, Aryee MJ, Bernstein BE, Rivera MN. EWS-FLI1

utilizes divergent chromatin remodeling mechanisms to directly activate or repress enhancer elements in Ewing sarcoma. *Cancer Cell*. 2014;26(5):668-681. doi:10.1016/j.ccell.2014.10.004.EWS-FLI1

Rocquain J, Gelsi-Boyer V, Adélaïde J, Murati A, Carbuccia N, Vey N, Birnbaum D, Mozziconacci MJ, Chaffanet M. Alteration of cohesin genes in myeloid diseases. *Am J Hematol*. 2010;85(9):717-719. doi:10.1002/ajh.21798

Rogakou EP, Pilch DR, Orr AH, Ivanova VS, Bonner WM. Double-stranded Breaks Induce Histone H2AX phosphorylation on Serine 139. *J Biol Chem*. 1998;273(10):5858-5868. doi:10.1074/jbc.273.10.5858

Rollins RA, Morcillo P, Dorsett D. Nipped-B, a Drosophila Homologue of Chromosomal Adherins, Participates in Activation by Remote Enhancers in the cut and Ultrabithorax Genes. *Genetics*. 1999;152:577-593.

Roper RJ, Reeves RH. Understanding the basis for Down syndrome phenotypes. *PLoS Genet*. 2006;2(3):0231-0236. doi:10.1371/journal.pgen.0020050

Rutledge SD, Douglas TA, Nicholson JM, Vila-Casadesús M, Kantzler CL, Wangsa D, Barroso-Vilares M, Kale SD, Logarinho E, Cimini D. Selective advantage of trisomic human cells cultured in non-standard conditions. *Sci Rep*. 2016;6(March):1-12. doi:10.1038/srep22828

Sansregret L, Patterson JO, Dewhurst S, López-García C, Koch A, McGranahan N, Chao WCH, Barry DJ, Rowan A, Instrell R, Horswell S, Way M, Howell M, Singleton MR, Medema RH, Nurse P, Petronczki M, Swanton C. APC/C dysfunction limits excessive cancer chromosomal instability. *Cancer Discov*. 2017;7(2):218-233. doi:10.1158/2159-8290.CD-16-0645

Santaguida S, Amon A. Aneuploidy triggers a TFEB-mediated lysosomal stress response. *Autophagy*. 2015;11(12):2383-2384. doi:10.1080/15548627.2015.1110670

Santaguida S, Amon A. Short- and long-term effects of chromosome mis-segregation and aneuploidy. *Nat Rev Mol Cell Biol*. 2015;16(8):473-485. doi:10.1038/nrm4025

Santaguida S, Richardson A, Iyer DR, M'Saad O, Zasadil L, Knouse KA, Wong YL, Rhind N, Desai A, Amon A. Chromosome Mis-segregation Generates Cell-Cycle-Arrested Cells with Complex Karyotypes that Are Eliminated by the Immune System. *Dev Cell*. 2017;41(6):638-651.e5. doi:10.1016/j.devcel.2017.05.022

Santaguida S, Tighe A, D'Alise AM, Taylor SS, Musacchio A. Dissecting the role of MPS1 in chromosome biorientation and the spindle checkpoint through the small molecule inhibitor reversine. *J Cell Biol*. 2010;190(1):73-87. doi:10.1083/jcb.201001036

Santaguida S, Vasile E, White E, Amon A. Aneuploidy-induced cellular stresses limit autophagic degradation. *Genes Dev*. 2015;29(19):2010-2021. doi:10.1101/gad.269118.115

Sanyal A, Lajoie BR, Jain G, Dekker J. The long-range interaction landscape of gene promoters. *Nature*. 2012;489(7414):109-113. doi:10.1038/nature11279

Sapkota H, Wasiak E, Gorbsky GJ. Multiple Determinants and Consequences of Cohesion Fatigue in Mammalian Cells. *bioRxiv*. 2017:1-30.

Schmidt D, Schwalie PC, Ross-Innes CS, Hurtado A, Brown GD, Carroll JS, Flicek P, Odom DT. A CTCF-independent role for cohesin in tissue-specific transcription. *Genome Res*. 2010;20(5):578-588. doi:10.1101/gr.100479.109

Sheltzer JM, Blank HM, Pfau SJ, Tange Y, George BM, Humpton TJ, Brito IL, Hiraoka Y, Niwa O, Amon A. Aneuploidy Drives Genomic Instability in Yeast. *Science (80-)*. 2011;333(August):1026-1030. doi:10.1126/science.1206412

Sheltzer JM, Ko JH, Replogle JM, Habibe Burgos NC, Chung ES, Meehl CM, Sayles NM, Passerini V, Storchova Z, Amon A. Single-chromosome Gains Commonly Function as Tumor Suppressors. *Cancer Cell*. 2017;31(2):240-255. doi:10.1016/j.ccell.2016.12.004

Shen Y, Rehman FL, Feng Y, Boshuizen J, Bajrami I, Elliott R, Wang B, Lord CJ, Post LE, Ashworth A. BMN 673, a Novel and Highly Potent PARP1/2 Inhibitor for the Treatment of Human Cancers with DNA Repair Deficiency. *Clin Cancer Res*. 2013;19(18):5003-5015. doi:10.1158/1078-0432.CCR-13-1391

Shintomi K, Hirano T. Releasing cohesin from chromosome arms in early mitosis: Opposing actions of Wapl-Pds5 and Sgo1. *Genes Dev*. 2009;23(18):2224-2236. doi:10.1101/gad.1844309

Skibbens R V, Corson LB, Koshland D, Hieter P. Ctf7p is essential for sister chromatid cohesion and links mitotic chromosome structure to the DNA replication machinery. *Genes Dev*. 1999;13:307-319. doi:10.1101/gad.13.3.307

Solomon DA, Kim JS, Bondaruk J, Shariat SF, Wang ZF, Elkahloun AG, Ozawa T, Gerard J, Zhuang D, Zhang S, Navai N, Siefker-Radtke A, Phillips JJ, Robinson BD, Rubin MA, Volkmer B, Hautmann R, Küfer R, Hogendoorn PCW,

et al. Frequent truncating mutations of STAG2 in bladder cancer. *Nat Genet*. 2013;45(12):1428-1430. doi:10.1038/ng.2800

Solomon DA, Kim T, Diaz-Martinez LA, Fair J, Elkahloun AG, Harris BT, Toretsky JA, Rosenberg SA, Shukla N, Ladanyi M, Samuels Y, James CD, Yu H, Kim JS, Waldman T. Mutational inactivation of STAG2 causes aneuploidy in human cancer. *Science (80-)*. 2011;333(6045):1039-1043. doi:10.1126/science.1203619

Stevens D, Gassmann R, Oegema K, Desai A. Uncoordinated loss of chromatid cohesion is a common outcome of extended metaphase arrest. *PLoS One*. 2011;6(8):1-13. doi:10.1371/journal.pone.0022969

Stingele S, Stoehr G, Peplowska K, Cox J, Mann M, Storchova Z. Global analysis of genome, transcriptome and proteome reveals the response to aneuploidy in human cells. *Mol Syst Biol*. 2012;8(608):1-12. doi:10.1038/msb.2012.40

Ström L, Lindroos HB, Shirahige K, Sjögren C. Postreplicative recruitment of cohesin to double-strand breaks is required for DNA repair. *Mol Cell*. 2004;16(6):1003-1015. doi:10.1016/j.molcel.2004.11.026

Tang YC, Amon A. Gene copy-number alterations: A cost-benefit analysis. *Cell*. 2013;152(3):394-405. doi:10.1016/j.cell.2012.11.043

Tang YC, Williams BR, Siegel JJ, Amon A. Identification of aneuploidy-selective antiproliferation compounds. *Cell*. 2011;144(4):499-512. doi:10.1016/j.cell.2011.01.017

Taylor CF, Platt FM, Hurst CD, Thygesen HH, Knowles MA. Frequent inactivating mutations of STAG2 in bladder cancer are associated with low tumour grade and stage and inversely related to chromosomal copy number changes. *Hum Mol Genet*. 2014;23(8):1964-1974. doi:10.1093/hmg/ddt589

Terret ME, Sherwood R, Rahman S, Qin J, Jallepalli P V. Cohesin acetylation speeds the replication fork. *Nature*. 2009;462(7270):231-234. doi:10.1038/nature08550

Thompson SL, Bakhoum SF, Compton DA. Mechanisms of Chromosomal Instability. *Curr Biol*. 2010;20(6):R285-R295. doi:10.1016/j.cub.2010.01.034

Thompson SL, Compton DA. Proliferation of aneuploid human cells is limited by a p53-dependent mechanism. *J Cell Biol*. 2010;188(3):369-381. doi:10.1083/jcb.200905057

Thompson SL, Compton DA. Proliferation of aneuploid human cells is limited by a p53-dependent mechanism. *J Cell Biol*. 2010;188(3):369-381. doi:10.1083/jcb.200905057

Tirode F, Surdez D, Ma X, Parker M, Le Deley MC, Bahrami A, Zhang Z, Lapouble E, Grossetete-Lalami S, Rusch M, Reynaud S, Rio-Frio T, Hedlund E, Wu G, Chen X, Pierron G, Oberlin O, Zaidi S, Lemmon G, et al. Genomic landscape of ewing sarcoma defines an aggressive subtype with co-association of STAG2 and TP53 mutations. *Cancer Discov*. 2014;4(11):1342-1353. doi:10.1158/2159-8290.CD-14-0622

Tomazou EM, Sheffield NC, Schmidl C, Schuster M, Schönegger A, Datlinger P, Kubicek S, Bock C, Kovar H. Epigenome Mapping Reveals Distinct Modes of Gene Regulation and Widespread Enhancer Reprogramming by the Oncogenic Fusion Protein EWS-FLI1. *Cell Rep*. 2015;10(7):1082-1095. doi:10.1016/j.celrep.2015.01.042

Torres EM, Sokolsky T, Tucker CM, Chan LY, Boselli M, Dunham MJ, Amon A. Effects of Aneuploidy on Cellular Physiology and Cell Division in Haploid Yeast. *Science (80-)*. 2007;317:916-923. doi:10.1126/science.1142210

Tóth A, Ciosk R, Uhlmann F, Galova M, Schleiffer A, Nasmyth K. Yeast Cohesin complex requires a conserved protein , Eco1p (Ctf7), to establish cohesion between sister chromatids during DNA replication. *Genes Dev*. 1999;13:320-333.

Uhlmann F, Lottspelch F, Nasmyth K. Sister-chromatid separation at anaphase onset is promoted by cleavage of the cohesin subunit Scc1. *Nature*. 1999;400(6739):37-42. doi:10.1038/21831

Ünal E, Arbel-Eden A, Sattler U, Shroff R, Lichten M, Haber JE, Koshland D. DNA damage response pathway uses histone modification to assemble a double-strand break-specific cohesin domain. *Mol Cell*. 2004;16(6):991-1002. doi:10.1016/j.molcel.2004.11.027

van der Lelij P, Lieb S, Jude J, Wutz G, Santos CP, Falkenberg K, Schlattl A, Ban J, Schwentner R, Hoffmann T, Kovar H, Real FX, Waldman T, Pearson MA, Kraut N, Peters JM, Zuber J, Petronczki M. Synthetic lethality between the cohesin subunits STAG1 and STAG2 in diverse cancer contexts. *Elife*. 2017;6:1-15. doi:10.7554/eLife.26980

Walther A, Houlston R, Tomlinson I. Association between chromosomal instability and prognosis in colorectal cancer: A meta-analysis. *Gut*. 2008;57(7):941-950. doi:10.1136/gut.2007.135004

Weitzer S, Lehane C, Uhlmann F. A Model for ATP Hydrolysis-Dependent Binding of Cohesin to DNA. *Curr Biol*. 2003;13(22):1930-1940. doi:10.1016/j.cub.2003.10.030

Welch JS, Ley TJ, Link DC, Miller CA, Larson DE, Koboldt DC, Wartman LD, Lamprecht TL, Liu F, Xia J, Kandoth C, Fulton RS, McLellan MD, Dooling DJ, Wallis JW, Chen K, Harris CC, Schmidt HK, Kalicki-Veizer JM, et al. The origin and evolution of mutations in acute myeloid leukemia. *Cell*. 2012;150(2):264-278. doi:10.1016/j.cell.2012.06.023

Wendt KS, Yoshida K, Itoh T, Bando M, Koch B, Schirghuber E, Tsutsumi S, Nagae G, Ishihara K, Mishiro T, Yahata K, Imamoto F, Aburatani H, Nakao M, Imamoto N, Maeshima K, Shirahige K, Peters JM. Cohesin mediates transcriptional insulation by CCCTC-binding factor. *Nature*. 2008;451(7180):796-801. doi:10.1038/nature06634

Williams BR, Prabhu VR, Hunter KE, Glazier CM, Whittaker CA, Housman DE, Amon A. Aneuploidy Affects Proliferation and Spontaneous Immortalization in Mammalian Cells. *Science (80-)*. 2008;322:703-710.

Xu H, Beasley MD, Warren WD, van der Horst GTJ, McKay MJ. Absence of mouse REC8 cohesin promotes synapsis of sister chromatids in meiosis. *Dev Cell*. 2005;8(6):949-961. doi:10.1016/j.devcel.2005.03.018

Zeng X, Sigoillot F, Gaur S, Choi S, Pfaff KL, Oh DC, Hathaway N, Dimova N, Cuny GD, King RW. Pharmacologic Inhibition of the Anaphase-Promoting Complex Induces A Spindle Checkpoint-Dependent Mitotic Arrest in the Absence of Spindle Damage. *Cancer Cell*. 2010;18(4):382-395. doi:10.1016/j.ccr.2010.08.010.Pharmacologic

Zhang N, Ge G, Meyer R, Sethi S, Basu D, Pradhan S, Zhao Y-J, Li X-N, Cai W-W, El-Naggar AK, Baladandayuthapani V, Kittrell FS, Rao PH, Medina D, Pati D. Overexpression of Separase induces aneuploidy and mammary tumorigenesis. *Proc Natl Acad Sci*. 2008;105(35):13033-13038. doi:10.1073/pnas.0801610105

Zhang N, Jiang Y, Mao Q, Demeler B, Tao YJ, Pati D. Characterization of the Interaction between the Cohesin Subunits Rad21 and SA1/2. *PLoS One*. 2013;8(7):1-13. doi:10.1371/journal.pone.0069458

Zhang N, Kuznetsov SG, Sharan SK, Li K, Rao PH, Pati D. A handcuff model for the cohesin complex. *J Cell Biol*. 2008;183(6):1019-1031. doi:10.1083/jcb.200801157

Zhu J, Pavelka N, Bradford WD, Rancati G, Li R. Karyotypic determinants of chromosome instability in Aneuploid budding yeast. *PLoS Genet*. 2012;8(5):1-13. doi:10.1371/journal.pgen.1002719

Zuin J, Dixon JR, van der Reijden MIJA, Ye Z, Kolovos P, Brouwer RWW, van de Corput MPC, van de Werken HJG, Knoch TA, van IJcken WFJ, Grosveld FG, Ren B, Wendt KS. Cohesin and CTCF differentially affect chromatin architecture and gene expression in human cells. *Proc Natl Acad Sci*. 2014;111(3):996-1001. doi:10.1073/pnas.1317788111